Monocyte Covalent Immune Recruiters: Tools to Modulate Synthetic Immune Recognition

Rebecca Turner and Dr. Anthony F. Rullo

Department of Chemistry and Chemical Biology, and Department of Medicine, McMaster University

April 21st, 2022

McMaster University

Abstract

Immune recruiters are small molecule immunotherapeutics which redirect endogenous components of the immune system to target cells to elicit anti-cancer responses. Current immune recruiters made in the Rullo Lab are heterobispecific molecules which bind receptors on cancer cells and ligand-specific antibodies. Upon antibody binding, a proximity-induced covalent reaction with nearby nucleophilic residues installs a targeting ligand onto the protein. The resultant antibody conjugate then facilitates cancer killing through immune cell recruitment. Covalency circumvents limited binding affinity of the ligand•antibody complex, however antibody•immune receptor affinity remains an issue. This thesis presents an alternative immune recruiting strategy through direct engagement of effector immune cells; monocyte covalent immune recruiters (mCIRs). mCIRs utilize a monocyte specific peptide (cp33) to bind CD64, an activating receptor on monocytes. By incorporating a sulfonyl fluoride electrophile onto the *N*-terminus of cp33, selective covalent labelling of CD64 was achieved within 24 h. Furthermore, mCIRs demonstrated enhanced monocyte function relative to antibody recruiting platforms. However, these constructs have demonstrated that the order of addition to the target receptor then to CD64 is critical for bridging the two species. As a result, the effect of covalency on complex simplification and monocyte function has yet to be determined. Despite this, mCIRs represent a covalent immune recruitment strategy with the potential to address shortcomings of antibody-based therapeutics.

Acknowledgements

First and foremost, thank you to Dr. Rullo for giving me the opportunity to work in your lab, and for your guidance with a project that had a seemingly endless number of surprises. This project would have been impossible to navigate without your help.

Thank you to members of the Rullo lab both past and present, Sissi Yang, Akshaya Raajkumar, Sarah Eisinga, Harrison McCann, Eden Kapcan, Benjamin Lake, Nick Serniuck, Fiona Chung, and Eline El-Awad Gonzalez, you made my time in this lab enjoyable and memorable. As well, thanks to Eden Kapcan and Sissi Yang for assisting with the flow cytometry for this project. And thank you to both Ruijia Zhang and Gavin Yuen for your efforts to model cp33 with huCD64.

As well, thank you to my committee, Dr. Berti and Dr. Bujold, for your input and guidance given on this project.

Table of Contents

List of Figures

List of Tables

List of Abbreviations

AZ647	AZDye 647
ARM	Antibody recruiting molecule
ACN	acetonitrile
ADCC	Antibody dependent cellular cytotoxicity
ADCP	Antibody dependent cellular phagocytosis
BLI	Biolayer interferometry
BSA	Bovine serum albumin
cARM	Covalent antibody recruiting molecule
CDR	Complementarity Determining Region
CD16a	Cluster of differentiation 16a
CD64	Cluster of differentiation 64 (often paired with hu or mu prefixes to denote human or murine)
CIR	Covalent immune recruiter
Ct	*C*-terminal
cp33	Cyclic peptide 33
DBCO	Dibenzocyclooctyne
DIC	Diisocarbodiimide
Dmb	Dimethoxy benzyl
DMF	Dimethylformamide
DMSO	Dimethyl sulfoxide
EC_{50}	Effective concentration 50
FA	Formic acid

Fab	Fragment antigen binding
Fc	Fragment crystallizable
FcR	Fc Receptor
FcγRI	Fc Receptor Gamma I
FP	Fluorescence polarization
Fmoc	Fluorenylmethoxycarbonyl
GUL	Glutamate urea lysine
HEK	Human embryonic kidney 293 cells
HPLC	High performance liquid chromatography
IBD	Immune binding domain
IgG	Immunoglobulin G
IFNγ	Interferon gamma
ILD	Immune labelling domain
KB	Kinetics buffer
LCMS	Liquid chromatography-mass spectrometry
mAb	Monoclonal antibody
mCIR	Monocyte covalent immune recruiter
mNCIR	Monocyte noncovalent immune recruiter
mmt	methoxytrityl
NCS	*N*-chlorosuccinimide
Nt	*N*-terminal
PE	Phycoerythrin
PBS	Phosphate buffered saline

PSMA	Prostate specific membrane antigen
RT	Room temperature
SDS PAGE	Sodium dodecyl sulfate poly acrylamide gel electrophoresis
SPPS	Solid phase peptide synthesis
SuFEx	Sulfonyl fluoride exchange
SyAM	Synthetic Antibody Mimics
TBD	Target binding domain
TI_{50}	Ternary inhibition 50
TIPS	Triisopropylsilane
TF_{50}	Ternary formation 50
TFA	Trifluoroacetic acid

1. Introduction

1.1. Cancer – a global and rising burden

Cancer is among the oldest and most consistently reported diseases over the course of human history, with osteocarcomas found in mummies from Ancient Egypt dating to 1600 BCE[1] The oldest known written description of cancer dates to 1500 BCE, where it was described as an untreatable disease with recommendations for palliative care. Today, cancer is one of the largest health burdens globally, and ranks within the top three leading causes of death around the world in virtually every country.[2] Global trends project that cancer will surpass cardiovascular disease as the leading cause of death around the globe within the next 100 years – leading to an increased burden on healthcare systems. In Canada, data suggests that 2 in 5 Canadians will be diagnosed with cancer during their lifetime, and 1 in 4 Canadians will die of it. With the expected increase in cancer incidence rates together with the inherent complexity of cancer, an increased understanding of cancer and treatment approaches are therefore a top priority for health-based scientific research.

1.2. The immune system and its role in cancer treatment

The involvement of the immune system in cancer, from development to treatment, is a growing topic in modern immunology. The cancer immunoediting theory puts forward three steps which describe the role of the immune system in cancer control to tumour development. These steps are denoted as the three E's: elimination, equilibrium, and escape.[3] The elimination step describes the ability of the immune system to recognize and destroy transformed cells. However, this elimination applies a selective pressure which induces cancer cell variants with less immunogenic antigens that are resistant to elimination. This is considered the equilibrium stage

where tumour variants with recognizable neoantigens are eliminated, while less immunogenic tumour cells multiply. Finally, the growth and development of the tumour outperforms the immune system and produces chemical signals which induce mechanisms to escape immune mediated elimination.

Tumours can be broadly characterized into either immunologically inflamed (hot) or noninflamed (cold) phenotypes.[4] Principle characteristics of hot tumours include increased T-cell infiltration, high levels of inflammatory cytokines, and high mutational load. Mutational load refers to the number of mutations per coding area of the genome.[5] Tumours with a higher mutational load, can result in the accumulation of immunogenic neoantigens.[6] Generally, inflamed tumours are associated with better clinical prospects. Cold tumours, however, typically have a lower mutational load, resulting in fewer neoantigens, and have decreased lymphocyte infiltration. As well, noninflamed tumours possess populations of transformed immune cells which perform immunosuppressive and pro-tumour roles, enabling tumour development and growth. This tumour phenotype is typically associated with worse prognoses.

The involvement, or lack thereof, of the immune system in cancer recognition can have a significant impact on patient outcome. The immune system is a complex network of cells and proteins which work together to protect the body from foreign pathogens. There are two main branches of the immune system: the innate and the adaptive system. The innate system is comprised of circulating cells and proteins including monocytes, macrophages, natural killer cells, and complement proteins, which are capable of recognizing generic non-host cells and bodies.[7] The innate immune system has an immediate and rapid response to foreign bodies. The second branch of the immune system is the adaptive immune system. This arm of the immune system

mounts highly specific responses against foreign antigens. The adaptive immune system is responsible for long-term responses to pathogens and is primarily comprised of B and T-cells. B-cells are responsible for antibody production, which help to alert and enforce immune recognition in the body, while T cells have antigen receptors expressed on their surface for direct recognition. These two systems work together synergistically to provide protection against a host of infections and diseases.

For this project there are two components of the immune system which are critical to understand: antibodies, and monocytes and macrophages. Antibodies are proteins produced by B-cells to recognize and neutralize foreign antigens. Antibodies opsonize foreign surfaces which can lead to pathogen neutralization (e.g., with viruses), or recruitment of other immune components such as phagocytes (e.g., with diseased or dying cells).[8] Cells recruited to opsonized surfaces eliminate the pathogen through processes such as antibody dependent cellular cytotoxicity (ADCC) and antibody dependent cellular phagocytosis (ADCP). The ability of antibodies to both recognize antigens and interact with immune cells is enabled by their bifunctional nature. Antibodies possess two distinct functional regions; the antigen binding fragment (Fab), and the fragment crystallizable region (Fc) (Figure 1.1).

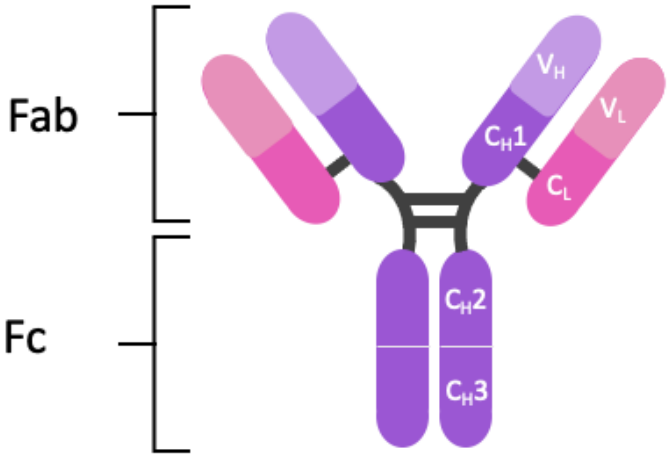

Figure 1.1 Antibody structure
Antibodies are composed of two identical heavy (purple) and light chains (pink). Each heavy chain consists of one variable region (V_H) and three constant ones (C_H1-3). Light chains are significantly shorter and consist only of one variable and one constant region (C_L C_H).

The Fab region is comprised of two variable and two constant regions. The complementarity determining region (CDR) is found within the variable region of the Fab and is responsible for antigen recognition. The hypervariability of the CDR enables libraries of antibodies to be generated against an infinite number of antigens and is the key to effective immune recognition and responses against pathogens. Many antibodies can bind to a single antigen but target different epitopes, or regions of the antigen. In comparison to the Fab, the Fc region is composed of four identical constant chains and is highly conserved within antibody each isotype. The Fc region is responsible for mediating antibody effector functions; that is, processes which are induced but not carried out directly by antibodies, such as ADCC and ADCP. The Fc region of antibodies binds to corresponding Fc receptors (FcRs) on the surface of immune cells to trigger an immune response against a bound antigen.[9] The affinity of antibodies for various FcRs is highly influenced by the glycosylation of the Fc region.[10] For immune recruiting purposes immunoglobulin G (IgG) is the most relevant antibody isotype as its Fc region binds to activating

FcRs on potent immune cells such as FcγR1, also called CD64, which is expressed on the surface of monocytes and macrophages to trigger ADCP.

The recruitment of effector immune cells like monocytes and macrophages is an essential part of pathogen elimination in the body. In homeostatic conditions, monocytes are one of the most abundant leukocytes, making up 5-12% of the circulating population of white blood cells.[11] Monocytes play a significant role in pathogen defense: they are key to modulating inflammatory conditions through cytokine production; they facilitate the clearance of apoptotic cells; and can phagocytose target cells and microbes through ADCP.[12] When monocytes exit circulation and enter tissues, they develop into macrophages. Macrophages retain the functional plasticity of monocytes, having roles in angiogenesis, inflammation, *and* anti-inflammation, as well as phagocytosis. A macrophage's function is heavily influenced by environment-specific factors and signals, which can occasionally be disadvantageous. Many cancers are associated with the influx of monocytes; however, the tumour microenvironment encourages the development of tumour associated macrophages. These populations of macrophages typically have aggressive pro-cancer roles in tumour angiogenesis, metastasis, and immune suppression.[13] Despite their broad repertoire of functions, all monocytes and macrophages constitutively express CD64, a high affinity FcR for IgG, with $K_D \leq 10$ nM.[9] Stimulating CD64 is an effective method for encouraging ADCP of a target antigen, and even tumour associated macrophages have been shown to retain the capacity to perform anti-cancer responses through FcR engagement.[13]

1.2.1. Immunotherapeutics

Chemotherapy and radiation are two of the most frequently employed cancer treatments. These two regimens can be accompanied by severe side effects and systemic toxicity issues. In

comparison, immunotherapy has become a pillar of modern cancer treatment as it is a more targeted approach which maintains potency and has fewer side effects. Immunotherapeutics are a broad group of compounds which aim to harness the innate ability of the immune system to recognize and eliminate targets. The concept of immunotherapy dates back to the 1890s when William B. Coley found that tumours injected with toxic cocktails of bacteria would undergo spontaneous regression without surgery.[14] However, due to the potentially septic response of patients, this practice fell out of use during the mid 1900s. Modern immunotherapeutics use rigorously tested biological agents such as monoclonal antibodies (mAbs) and T-cells, which are re-engineered to target cancer cells.

Monoclonal Antibodies

Since their introduction in the 1980s, mAbs have become a regular component of treatment cocktails, with 30 out of 79 approved mAbs by the United States Food and Drug Administration designated as cancer treatments.[15] mAbs have engineered specificity for cancer antigens. These proteins are produced from B-cells that are clones of a single parent cell and thus share the same affinity for the same epitope of an antigen. In contrast, polyclonal antibodies recognize numerous epitopes for a single antigen. Like all IgG antibodies, mAbs possess a Fab region which determines specificity and an Fc region which can engage effector functions. mAbs have an array of therapeutic mechanisms including blocking receptor-ligand interactions, triggering apoptosis, and notably the induction of ADCP and ADCC.[16] Their high specificity for a target antigen combined along with their numerous modes of action have made mAbs the gold standard for immunotherapeutics. However, their large size (~ 150 kDa) prevents efficient diffusion of these proteins into solid tumours, and administration must be done via intravenous injection which

requires large doses. Moreover, the high affinity of mAbs for their target antigen can often lead to saturating target binding on the periphery of the tumour, which further prevents even distribution of the therapeutic into the solid tumour.[17] Additionally, the immune system often develops anti-mAb antibodies which reduce mAb function and can cause toxicity issues. While mAbs have been established as a critical tool to fight cancer, further research and development into mAbs and similar constructs is required.

1.3. Small Molecule Approaches to Immunotherapeutics

Traditional immunotherapeutic approaches are either protein biologics or cell based. While mAbs are the most utilized immunotherapeutic, their *in vivo* efficacy is constrained by the above factors as well as their affinity for FcRs like CD16a (K_D 10-100 μM), an FcR involved in stimulating ADCC.[17] Cell-to-cell variations in glycosylation of the mAb Fc during production can further decrease the affinity of the mAb for this receptor.[9,17] Recently there has been an increased interest in small bifunctional molecule approaches to immune recruitment. Antibody recruiting molecules (ARMs) offer a unique approach to target pathogenic species while harnessing the host immune system. ARMs are bifunctional, heterospecific small molecules which simultaneously bind a target antigen and an endogenous serum antibody. ARM approaches have been utilized to target pathogens such as viruses, infected cells, cancerous cells, and various bacteria.[18–20] ARMs possess a target binding domain (TBD), specific for a pathogen antigen and an immune binding domain (IBD). The IBD is a ligand which is recognized by endogenous antibodies in the general population, such as 2,4-dinitrophenyl.[21] Bound antibodies are then redirected to target cells via the TBD of the bound ARM. TBDs are targeting ligands which bind over expressed receptors on target cells such as prostate specific membrane antigen (PSMA) on prostate cancer cells. Surfaces

covered in recruited antibodies can then interact with FcRs on effector cells and induce targeted cell killing. ARMs enable a series of non-covalent interactions between the target receptor, endogenous antibody, and ultimately an effector immune cell. These multicomponent complexes lead to targeted cancer cell elimination.

The Rullo Lab has reported covalent immune recruiters (CIRs) as a new approach to probe the importance of affinity and pharmacokinetics in synthetic immune activation. Like ARMs, CIRs are small molecules which act as a guide for the immune system. Current CIRs include covalent ARMs (cARMs). These small molecules also have similar structures as ARMs but contain a third domain: an immune labelling domain (ILD). The ILD is an electrophilic centre placed within the cARM, situated near the IBD to enable a proximity-driven covalent reaction with nearby nucleophiles on the bound antibody.[21] This results in an antibody which is covalently modified with a tumour targeting ligand which serves to redirect the endogenous antibody to target cells. These cARMs simplify the ARM mediated immune complexes by removing the equilibrium between the ABD and the antibody. cARMs produced in the Rullo Lab have demonstrated that the covalent approach to immune recruitment leads to enhanced immune responses to target cells.[22] However, both ARMs and cARMs are fundamentally limited by their intrinsic mechanism of action for immune complex formation.

1.4. Ternary Complexes

The anti-tumour efficacy of ARMs and cARMs is dependent in large part on their ternary complex mechanism of action. The number, stability, and lifetime of ternary complexes formed by immune recruiters is hypothesized to govern efficacy in a manner not currently well understood.[19,21] Ternary complexes are formed between two terminal species (A and C) which are

bridged by a third binding partner (B), to form complexes of ABC (Figure 1.2A).[23] These complexes can be thought of as the result of two binary complexes.[23] Binary complexes involve the interaction of two species (A and B), which form the complex AB upon binding. On a logarithmic scale binary models produce sigmoidal binding curves, defined by a single inflection point and a plateau at the maximum concentration of the binary species. In comparison, ternary species are modeled by a signature parabolic curve, which is really the product of the two AB and BC binary curves. Ternary models have 2 inflection points, representing the concentration of B which produces 50% of maximum ternary complex formation (TF_{50}) and the concentration of B producing 50% of the maximum ternary inhibition, (TI_{50}) (Figure 1.2B).

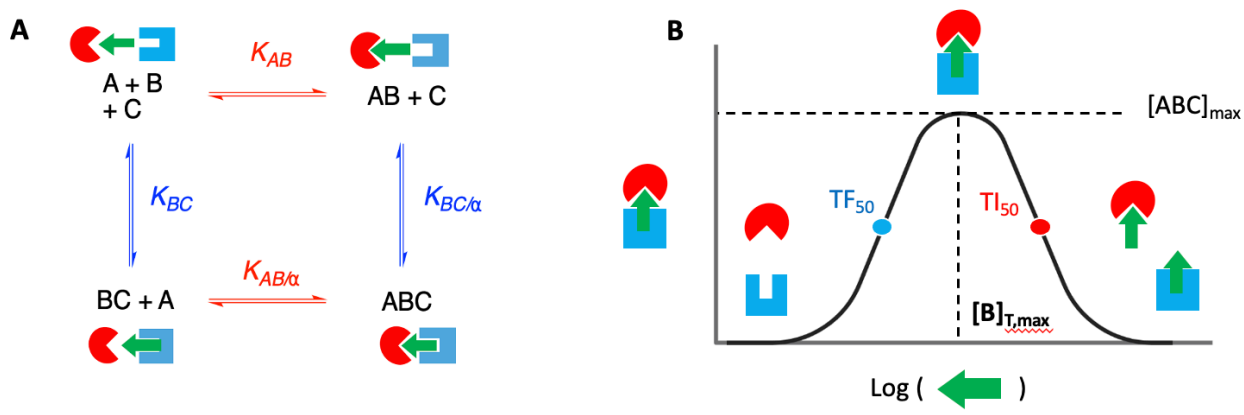

Figure 1.2. Ternary complexation mechanism
A) Possible binding pathways for ternary complexes. A and C are terminal species, bridged by B. The alpha factor represents the cooperativity factor, where the binding of A or C influences the affinity of B for the other terminal binding partner. This paper has only discussed non-cooperative binding, where alpha is equal to 1. **B)** Representative ternary binding curve. At $[B]_{t,max}$ the maximum amount of ABC is formed. Beyond $[B]_{t,max}$ ternary complexing is inhibited.

Furthermore, ternary binding models have a brief plateau at which the maximum amount of ternary complex $[ABC]_{max}$ is formed. The concentration of B at which $[ABC]_{max}$ is produced is referred to as $[B]_{t,max}$. At concentrations above $[B]_{t,max}$, the formation of ABC is inhibited and favours the formation of individual AB and BC binary species. This phenomenon is universally

seen among ternary binding species and is referred to as autoinhibition. The height of the plateau of $[ABC]_{max.}$is influenced by the binding affinities of B for A and C, but also by the cooperativity of the system. Relative to non-cooperative systems, positively cooperative systems will have higher plateaus reflecting greater ABC formation, while negatively cooperative systems will have lower plateaus, restricting the amount of ABC formation. The overall stability of these complexes (and concentration of ABC) is influenced by the affinity and concentrations of composite parts and is central to ARM and cARM function.

1.4.1. ARM Mediated Ternary Complexes

Ternary complexes formed by ARMs refer to complexes between the antibody, the ARM, and the target receptor. ARM efficacy has been reported to be dependent on the number of ternary complexes which can form between those species. Concentrations of endogenous antibody that can be recruited can be the limiting factor for *in vivo* ternary complex formation if concentrations are below the K_D of the IBD.[21] Additionally, their low molecular weight is associated with a rapid clearance rate, with a half-life on the order of hours, driving ternary complex dissociation. Due to the autoinhibitory nature of ternary species, administering more ARM is not a viable approach to increasing ternary complexation. To have anti-cancer activity, the Fc region of a bound antibody must bind an FcR on an effector immune cell. This in turn leads to the formation of a minimal quaternary complex between the target, ARM, antibody, and immune cell. The formation of these complexes is even more difficult to maximize in therapeutic settings, and limited by the same factors outlined above, which further curtail the efficacy of ARMs.

1.4.2. cARM Ternary Complexes and the ILD Simplification Strategy

Due to the challenges presented by ARMs, cARMs were developed in the Rullo Lab to simplify quaternary complexes and overcome limitations due to low concentrations of endogenous antibody.[21] Relative to functional ARM immune complexes, cARM mediated ones are simplified quaternary complexes, which comprise a cARM-labelled-antibody, bridging an effector immune cell receptor with a target cell receptor/tumour antigen. This resulting immune complex resembles a ternary complex, formed between three binding species. By covalently labelling the bound antibody, it removes the equilibrium between the cARM and antibody, and irreversibly modifies the antibody with the TBD. Current cARMs have used acyl-imidazole chemistry as the ILD.

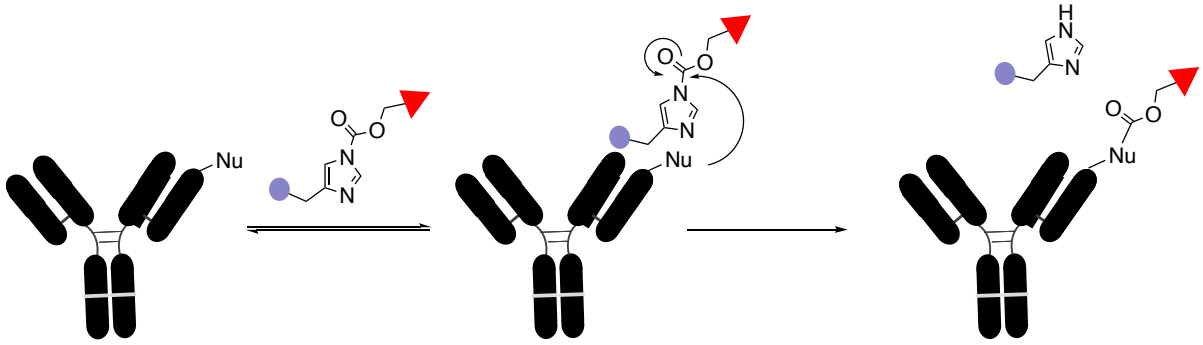

Figure 1.3. Acyl imidazole mediated labelling of target antibody
Nearby nucleophiles at the antigen binding site on the antibody react with the acyl imidazole of cARM scaffolds producing an antibody functionally modified with a tumour targeting ligand. The purple circle represents the IBD, while the red triangle represents the TBD.

Acyl imidazoles are sensitive to nucleophilic attack primarily by lysine residues upon sustained proximity, with reported rate constants from $10^{1\text{-}3}$ $M^{-1}s^{-1}$, providing a fast labelling rate for *in vitro* and potential *in vivo* purposes. [21,24,25] The acyl-imidazole is grafted into the linker, near the IBD. Binding of the IBD to the antibody positions the ILD close to a lysine residue on the antibody, accelerating the reaction between the nucleophile and the acyl imidazole. This thus

enables transfer of the TBD from the cARM to the antibody, resulting in an antibody labelled with a tumour-specific ligand (Figure 1.3). Following the covalent reaction at the acyl-imidazole, the IBD dissociates from the antibody. The cARM-antibody conjugate can engage in ternary binding complexes with recruited effector immune cells and the target cell. In antibody recruiting assays using flow cytometry, the Rullo Lab has shown that cARMs are able to recruit more antibodies and induce greater amounts of ADCP than ARMs, demonstrating the benefits of covalently stabilizing immune complexes.[22]

Despite their potential to enhance target cell elimination, cARM ternary complexes are fundamentally constrained by the innate affinity between the antibody's Fc and corresponding FcRs on immune cells. Moreover, the acyl-imidazole labelling chemistry has two distinct limitations. The first being that acyl-imidazoles primarily react with lysine residues thereby limiting the number of potential protein targets due to the narrow nucleophilic reactivity profile. The second, this chemistry is hydrolytically labile and prone to breaking down in solution prior to protein labelling. Premature hydrolysis of the ILD generates inhibitory fragments that compete with intact cARM for antibody and target binding sites.

1.5. Sulfonyl fluoride exchange chemistry as a new ILD chemistry

Due to the limitations of acyl-imidazole chemistry, next generation CIRs are being developed to incorporate sulfonyl fluoride exchange (SuFEx) chemistry in place of acyl imidazoles. SuFEx based probes have been increasingly used for covalent inhibitor applications since their re-emergence in the late 2000s.[26,27] This chemistry is based on the R-SO_2F functional group, associated with a unique reactivity profile due to the properties of the F—S(VI) bond.[28,29]

Sulfonyl fluorides and their derivatives are more stable to reduction than other sulfonyl halides and result in exclusively sulfonylated products with no fluorinated by-products (Figure 1.4)

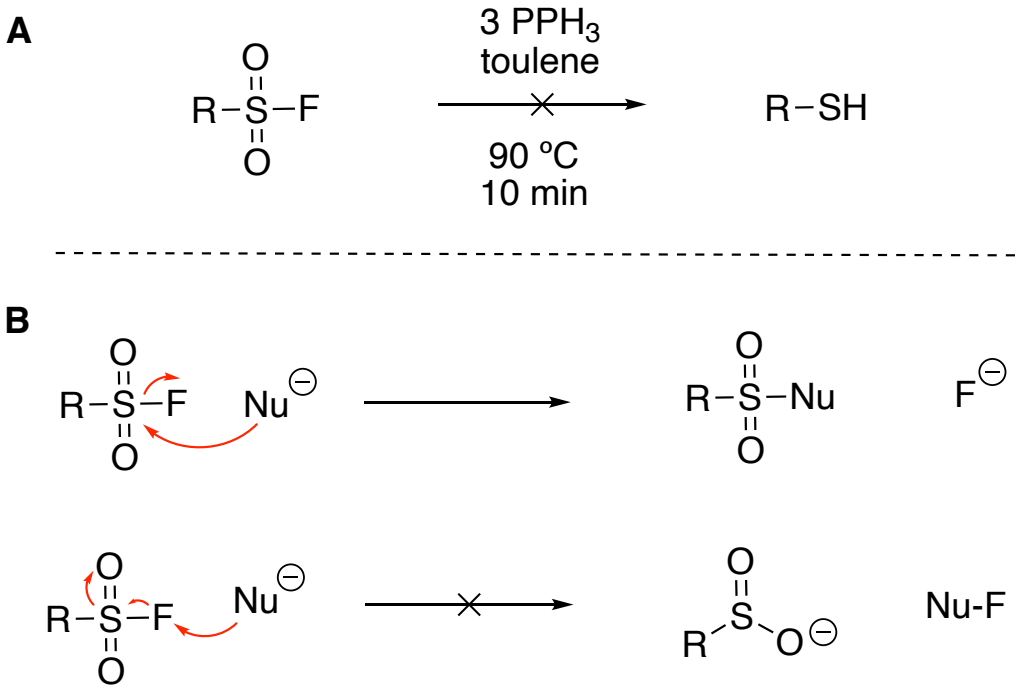

Figure 1.4. Sulfonyl fluorides are robust to reduction and produce no fluorinated by- products
A) Sulfonyl fluorides are resistant to reduction by agents capable of reducing other sulfonyl halides to the resulting thiol. B) Nucleophilic attack of the S(IV) center occurs exclusively at the sulphur centre and does not result in any fluorinated by-products.

The R-SO_2F group is also more stable to non-specific nucleophilic attack than other sulfonyl halides used in protein labelling. As such, R-SO_2F ligands are better suited for selective labelling applications.

The features of sulfonyl fluorides are dependent on the stabilization that the fluoride ion receives during the substitution process. Nearby proton donors in solution activate the S-F bond and stabilize the fluoride anion, which promotes nucleophilic substitution in aqueous conditions.[30] However, the exact mechanisms of SuFEx chemistry have yet to be elucidated. Recently, computational studies modeling alkyl sulfonyl fluorides reacting with primary amines suggest the

chemistry proceeds by a non-synchronous one-step mechanism.[31] However, this mechanism has not yet been shown to be applicable with different nucleophiles and with other SuFEx chemistries. Moreover, modelling results from this approach were heavily influenced by the formation of hydrogen fluoride, which is not considered to be a significant product of SuFEx reactions. Generally, R-SO_2F groups provide a useful electrophilic center for rapid substitution upon sustained proximity to nucleophiles such as Tyr, Lys, Ser, Thr, His, and Cys.[27,32]

Another frequently employed SuFEx functional group is the aryl fluorosulfate (R-OSO_2F). These compounds are proposed to balance the reactivity of sulfonyl fluorides with greater aqueous stability and specificity.[27] Aryl fluorosulfates have context dependent reactivity but are generally known to react with Tyr and Lys, and given the right microenvironment reactions with Ser are also possible. These fluorosulfates are known to be even more stable towards hydrolysis than sulfonyl fluorides. As well, they have also been shown to be unreactive in the presence of amino acids and other reactive natural products in solution, highlighting the importance of residence time and specific binding for SuFEx reactivity.[27] Importantly, all forms of SuFEx chemistry have been shown to be unreactive to both copper and strain promoted click reactions which are utilized to assemble CIR scaffolds.[28] Based on these properties, SuFEx moieties are an attractive approach for new ILD chemistry.

1.6. Designing mCIRs

Based on the inherent limitations of cARMs discussed above, coupled with the known limiting affinity of antibodies for FcR, we sought to develop next generation CIRs that aim to directly engage immune cells. This thesis is focused on the development of CIRs that directly engage the FcR on effector immune cells and bypass the need for antibody recruitment. My goal

was to specifically develop CIRs that engage CD64 (FcyR1) on monocytes and macrophages (mCIRs).

1.6.1. SyAMs and the cp33 peptide – literature precedence for monocyte recruitment

Important considerations for the IBD of mCIRs was a ligand specific to monocytes and capable of inducing effector functions. We selected a peptide called cyclic peptide 33 (cp33) for the IBD of mCIRs as this peptide was shown to mimic the interaction between the Fc region of IgG1 and CD64 (Figure 1.5). [33]

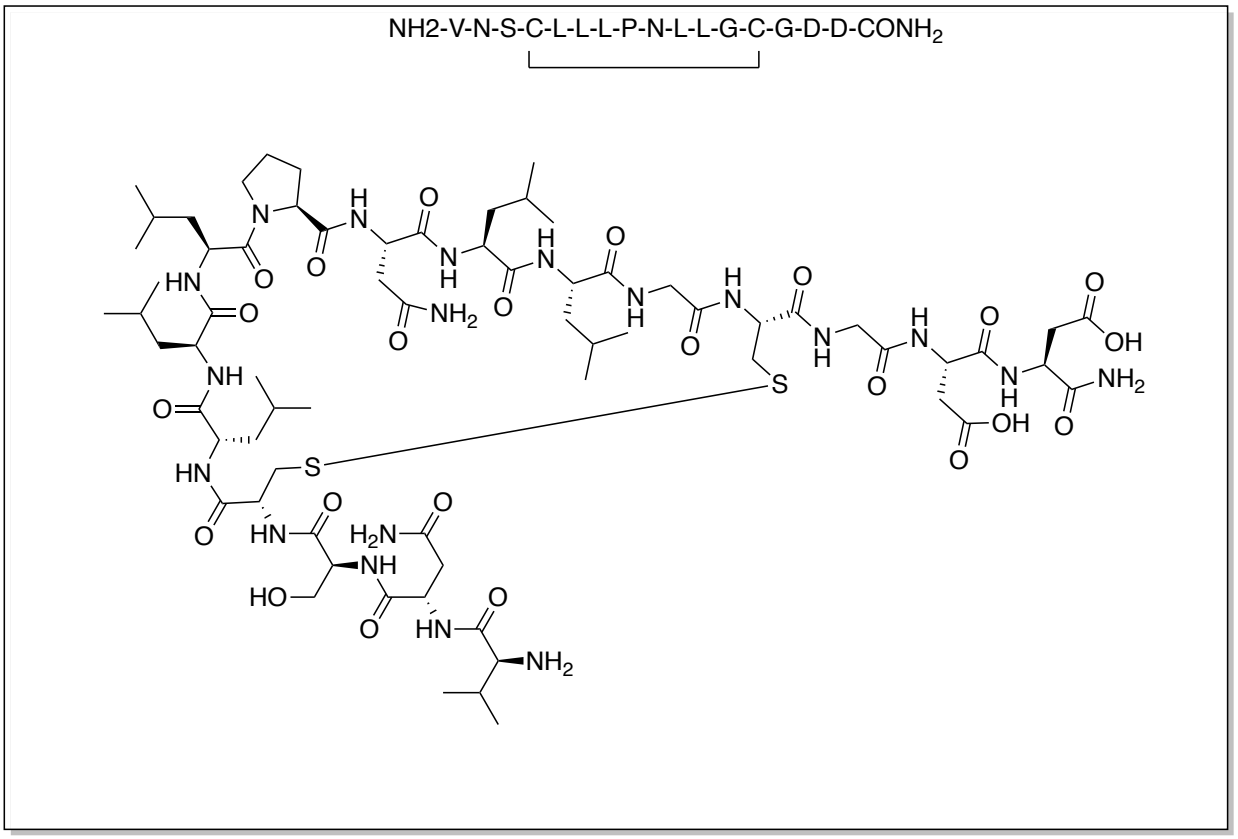

Figure 1.5. cp33 sequence and structure

cp33 is 16 amino acids long and cyclized via a single disulfide bond. It is reported to bind CD64 competitively with IgG1, supporting a shared binding site. When synthesized as a homodimer, the bivalent structure was capable of inducing monocyte activation (EC_{50} = 2 μM). cp33 was incorporated into immune recruiting molecules called synthetic antibody mimics (SyAMs), to engage both CD64 on monocytes and tumour antigens on cancer cells. [34] In the context of SyAMs, the cp33 peptide was found to have a K_D of 250 nM for CD64. Based on literature success of this peptide, it was chosen to be the IBD for mCIRs.

Peptide Synthesis

Because cp33 is a synthetic peptide that requires the installation of a carefully positioned tumour binding ligand and an appropriately placed strategic electrophile, peptide synthesis is a critical part of this thesis. Peptides have become an essential part of modern pharmaceutical products. Strategies to achieve successful and reliable peptide synthesis have been revolutionized through solid phase peptide synthesis (SPPS). SPPS enables the stepwise elongation of a peptide chain through the attachment of the peptide to an insoluble solid support resin. In this way, reagents can be added to the resin in excess to maximize the efficiency of coupling two amino acids together, and the remaining reagent can be washed away. The steps of a single coupling cycle are as follows:

1. Deprotection of the fluorenylmethoxycarbonyl (Fmoc) protecting group on the N^{α} of the growing peptide chain

2. Activation of the incoming amino acid through an activator (diisocarbodimide, (DIC)) and an activator base (oxyma) and

3. Wash with either DMF or NMP, which are commonly used solvents in SPPS, to remove excess reagents.

The N^{α} deprotection uses a mild base to remove the Fmoc protecting group. Due to the electron withdrawing nature of the fluorene ring system, the proton on the β-carbon is highly acidic. As a result, only a mild base is needed to selectively remove the Fmoc protecting group (Figure 1.6)

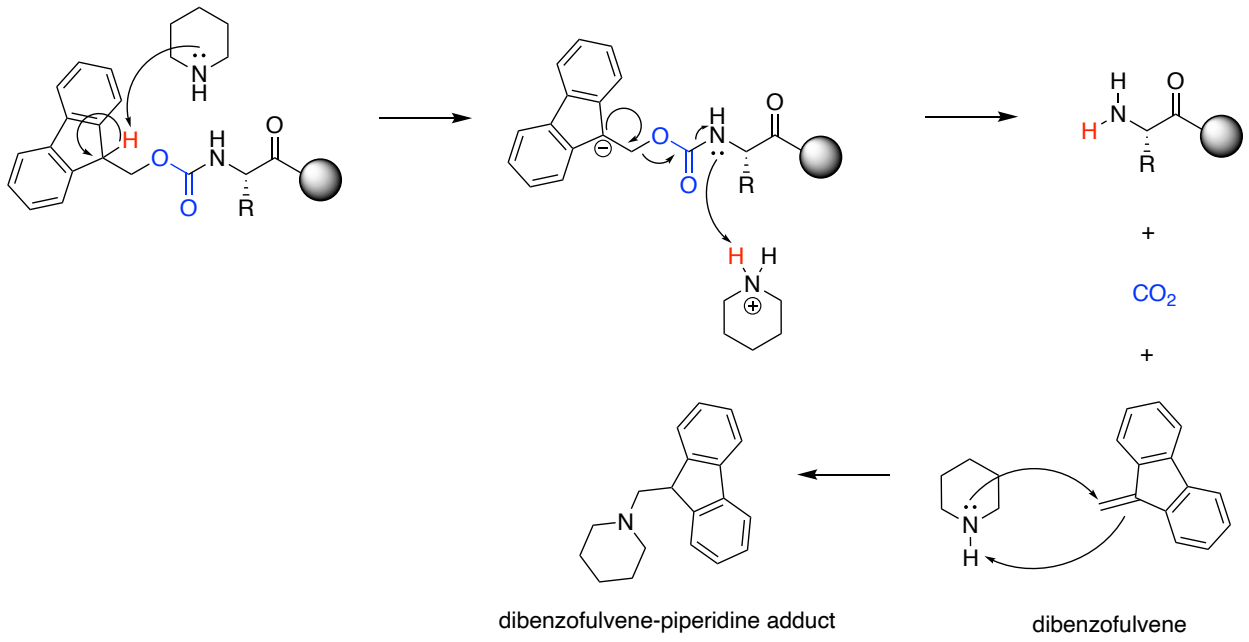

Figure 1.6. Piperidine driven Fmoc deprotection

The piperidine generates a carbanion which is stabilized by the resulting cationic piperidine. The activated ester (blue) acts an electron accepting system, and results in the generation of CO_2 and dibenzofulvene, and a growing peptide chain with a reactive primary amine. Dibenzofulvene is a reactive structure that can alkylate the growing peptide if not quenched by excess piperidine.

Following deprotection of the primary amine on the growing peptide, the in-coming amino acid is added to the reaction vessel and activated using a carbodiimide (DIC) to form an *O*-acylisourea.[35] *O*-acylisoureas are highly reactive structures, and while they can react with primary amines, they are prone to rearrangement to an inactive *N*-acylurea structure, preventing amino acid coupling. To avoid this, an activator base (ethyl 2-cyano-2-(hydroxyimino)acetate (oxyma)) is added following DIC activation to form an active ester. This active ester forms rapidly, out competing *N*-acylurea formation (Figure 1.7).

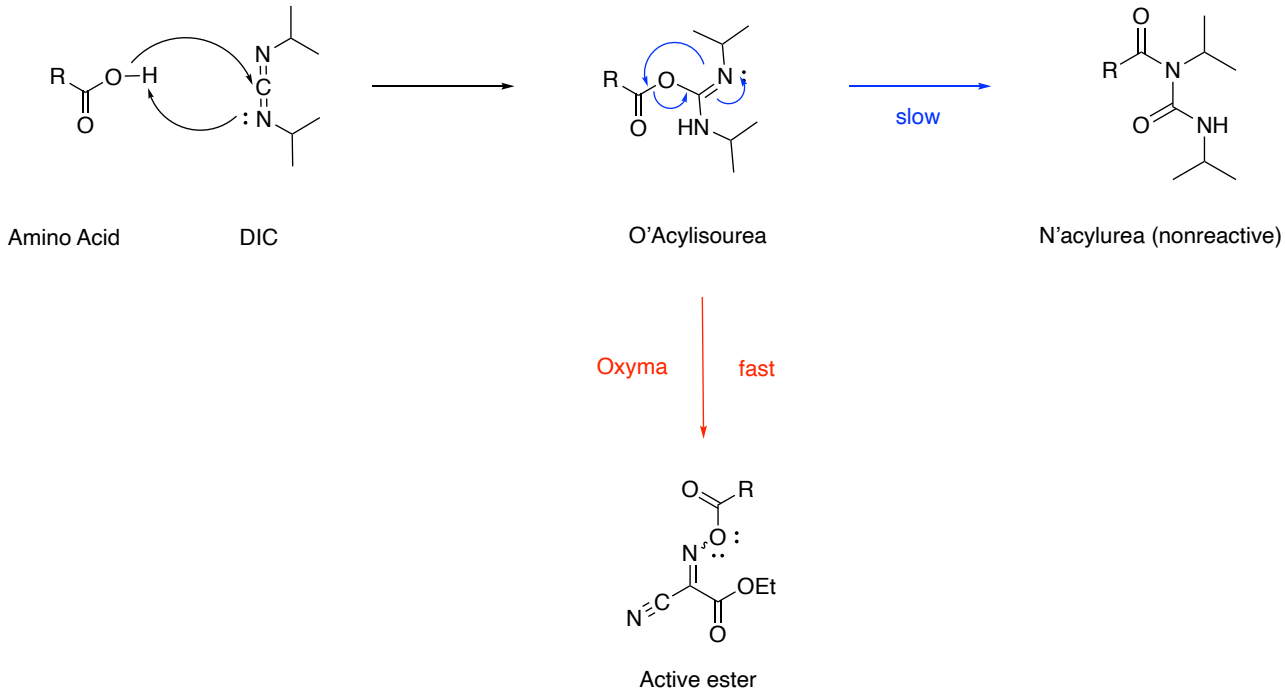

Figure 1.7. Addition of oxyma prevents *N*-acylurea formation

While the active ester is less reactive than the *O*-acylisourea, it prevents unwanted side reactions and ultimately results in increased peptide yields.[36,37] The primary amine on the growing peptide chain is then capable of reacting with the activated ester of the in-coming amino acid, forming a new amide bond (Figure 1.8).

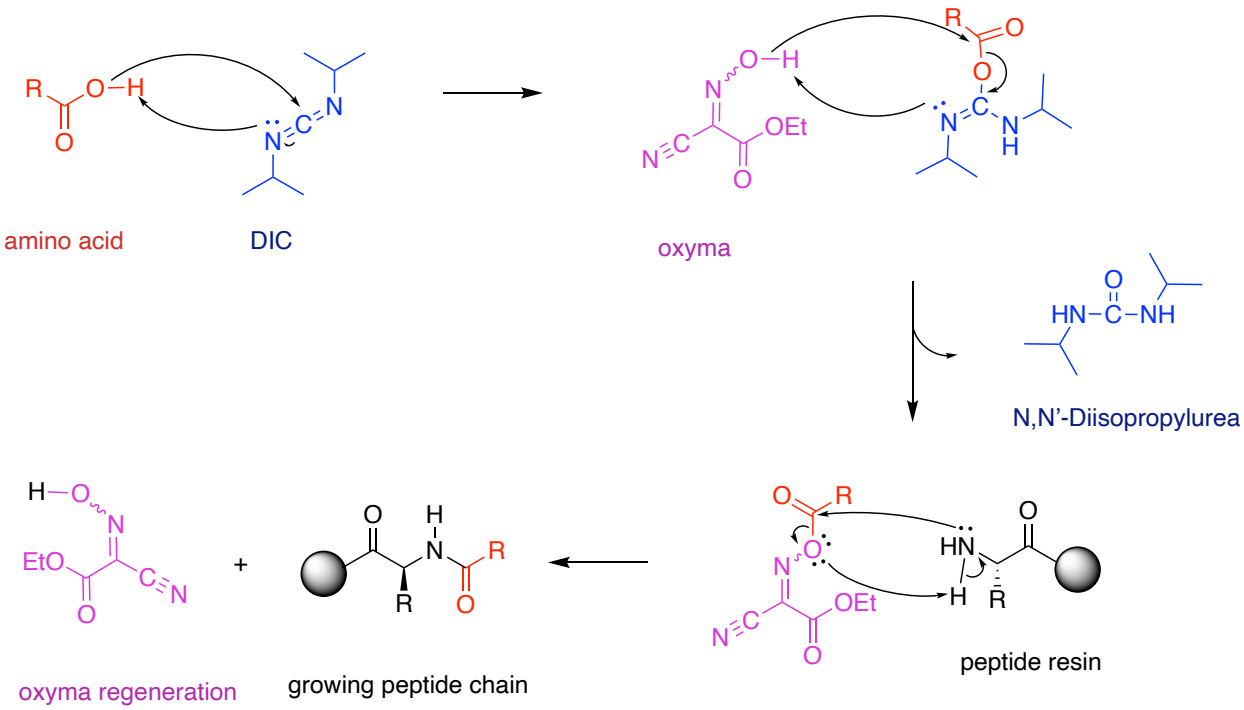

Figure 1.8. DIC and Oxyma mediated peptide coupling mechanism

Certain peptides, such as the Asp-Gly sequence within cp33, are susceptible to aspartimide formation. Aspartimide is an unwanted side-product which has a propensity to form between Asp and other residues, but especially with Gly due to the exposed backbone nitrogen. This reaction is base catalyzed and leads to intramolecular cyclization between the backbone nitrogen and the protected carboxylic acid of the aspartic acid (Figure 1.9).

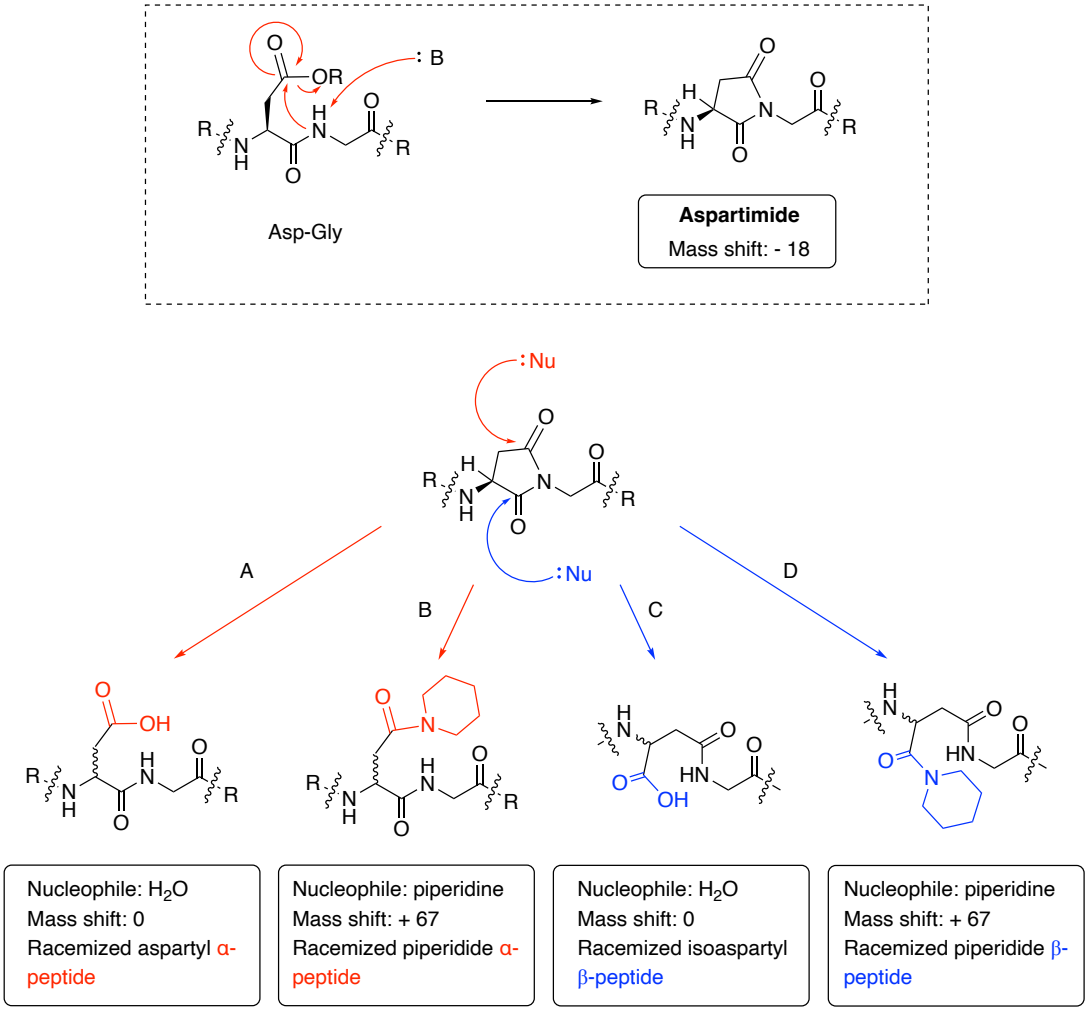

Figure 1.9. Aspartimide formation between Asp and Gly and possible side-products.

This ring can then be opened in 4 different ways leading to both detectable piperidide (+67 mass shift) products, or the more troublesome racemized side-products which has no detectable mass shift, and potentially results in backbone modifications (Figure 1.10). The promotion of racemized products is due to the acidic nature of the H^{α} (in blue), which is removed by base in solution, resulting in enantiomeric aspartimide products.[38]

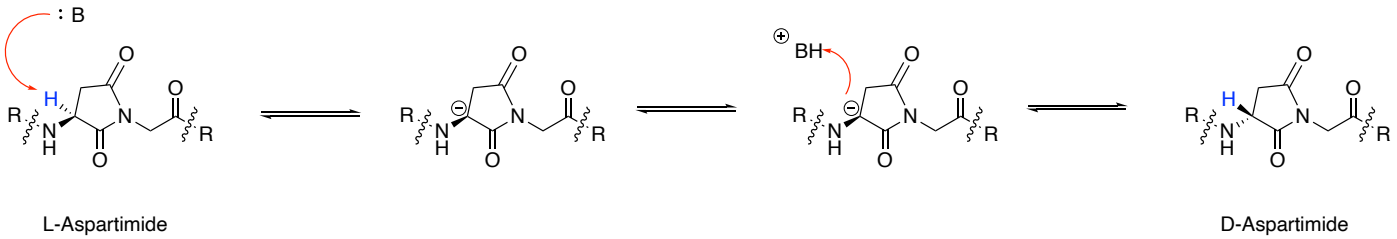

Figure 1.10. Racemization of aspartimide

The percentage of piperidide and aspartimide by-products increases with the number of Fmoc-removal cycles, and in DMF, β-peptides are preferentially formed.[39] The presence and amount of aspartimide which forms is dependent on a series of factors, including the temperature of coupling, the chosen resin and solvent, as well as the sequence of the peptide itself. Approaches to reduce aspartimide formation include the use of bulky-sterically hindered protecting groups such as 2,3-dimethyoxybenzyl (Dmb). The inclusion of 0.1 M oxyma in the deprotection solution can also help to suppress the base-catalyzed reaction. The ability for oxyma to suppress this side reaction is thought to stem from the acidic pK_a (4.6) which competes with the acidic hydrogen within the amide backbone. As such, similar strategies employing both an Asp (OtBu)-(Dmb)Gly fragment and oxyma in the deprotection were utilized in this project.

The process of peptide synthesis finishes by cleaving the peptide off the solid support, and globally deprotecting the side chains of the amino acids. The linkage between the peptide and the resin is acid sensitive, and most protecting groups for peptide synthesis are made to be acid labile and base insensitive; creating a process which enables repeated exposure to base while minimizing product loss and by-product formation. Standard cocktails for peptide cleavage include 95% TFA to remove protecting groups and cleave the peptide from the resin. During cleavage, some amino acids possess reactive protecting groups which can generate carbonium ions. For that reason,

scavengers such as tri-isopropyl silane (TIPS), H_2O, and phenol are frequently added to the cocktail in low amounts (~2.5% each).

1.7. Biolayer Interferometry

BLI, biolayer interferometry, is an optical technique to monitor molecular interactions where a protein or small molecule is immobilized on the surface of a probe which measures the interference patterns of white light.[40,41] There are two surfaces for BLI probes (1) an internal reference surface and (2) the external sample surface which can be coated with different proteins of interest. Changes in optical thickness at the surface of the probe correlates with changes in a shift of the measured light wavelength (nm shift). As such, analytes of interest associate with the complementary ligand immobilized on the probe, this technique enables us to monitor real-time binding rates. Additionally, available probes utilize known strong biomolecular interactions such as that between biotin and streptavidin, or between protein G and the Fc of IgG to immobilize proteins to the surface of the probe. However, because BLI detection is directly proportionate to the weight and structure of the compound both immobilized and associated, the amount of measurable signal can change depending on the assay format and ligand character.

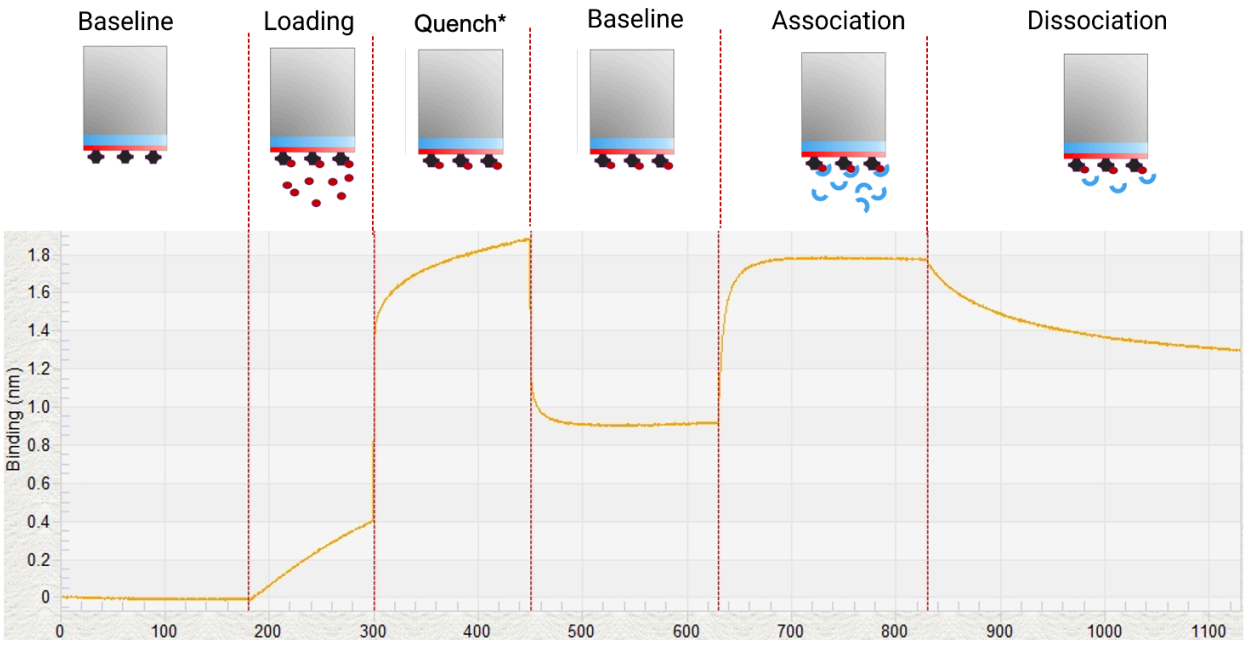

Figure 1.11. Steps of a BLI assay
Illustrative steps of a BLI assay along with the corresponding sensogram. Different steps are denoted by the red-dashed line and correspond to the label above. Figure made by author using raw data from the Octet Red.

There are five basic steps to kinetic BLI assays: baselining, loading, quenching, association, and dissociation (Figure 1.11). Baselining a probe in 1 x kinetics buffer (KB) (phosphate buffered saline (PBS), 0.01% bovine serum albumin (BSA), 0.002% Tween 20) establishes the basal nm shift for the probe in a given state (with or without something on the surface). Loading is the process of immobilizing a protein/construct to the surface of the probe. Quenching is performed in a solution of 5% skim milk powder and helps to occupy non-specific binding sites to ensure the response seen is due to specific binding. Association steps involve the dipping of probes into a solution with the analyte of interest, and dissociation steps are performed by dipping probe with associated analyte into a well with buffer. These 5 steps comprise the fundamentals of BLI and when repeated with analytes of different concentration, these allow a

kinetic profile to be constructed for a given compound and target as they generate a series of association and dissociation curves from which the k_{on} and k_{off} values can be calculated.

1.8. Overall Objectives

The goal of this thesis was to synthesize an mCIR capable of covalently engaging CD64 on monocytes and recruiting these immune cells to destroy cancer calls. We hypothesized that the direct engagement of immune cells and simplification of synthetic immune complexes would produce greater effector functions. To test this hypothesis, we synthesized a series of CD64-binding covalent (via SuFEx) and non-covalent peptides and studied binding and covalent labelling kinetics and selectivity. To covalently engage CD64 we built on literature precedence of SyAM binding via the cp33 peptide. Lead covalent peptides were engineered to contain a prostate specific tumour antigen (PSMA) binding ligand (glutamate urea lysine (GUL)) to generate the final mCIR which we tested in functional cell-based assays.

2. cp33 development and mutant peptides

2.1. Objectives

The first goal of this project was to synthesize and characterize the original cp33 peptide to use as a reference for future mCIR activity. This peptide was hypothesized to have a high specificity and moderate affinity (~ 250 nM) for human CD64 (huCD64) based on the reported K_D from literature.[34] BLI experiments to test this hypothesis were designed with immobilized cp33 dipped into a solution of huCD64. Following characterization of the base peptide, a series of mutant cp33 sequences were to be synthesized. These peptides were to incorporate a tyrosine

residue at various positions in their sequence to predict whether future inclusion of a tyrosine-SuFEx moiety at those positions would eliminate affinity for huCD64. To test Tyr position viability, BLI assays were designed with immobilized mutant peptide dipped into solutions of soluble protein to ensure retention of huCD64 binding affinity and specificity.

2.2. cp33 – synthesis and characterization of the base sequence

2.2.1. Peptide Synthesis

The first peptide made for this project was the based off the literature sequence of cp33 (Figure 2.1). However, the sequence made in the lab contained 2 inverse amino acids (DG) relative to the original structure due to the usage of a commercial pre-coupled DG fragment, which is only available in a single orientation. As well, an azido lysine residue was incorporated at the *N*-terminus to provide an accessible click handle for modification with DBCO-linkers containing various functional ligands such as biotin or GUL. The peptide was successfully identified in the crude pellet post synthesis on liquid chromatography mass spectrometry (LCMS) and worked up by high performance liquid chromatography (HPLC). Crude pellet mass was ~ 100 mg, but yields for pure peptide were low, with less than a 1 mg of product per 25 mg of crude pellet purified. It was suspected that most product loss was occurring between resuspending the crude pellet and HPLC work up. The crude pellet had poor solubilization likely due to the hydrophobic nature of most of the pellet. The most effective solvent system for solubilizing the bulk of the pellet was DMF/ACN/H_2O added in a 2:1:2 ratio prior to injection on the HPLC. Pure cp33 was resuspended in dimethylsulfoxide (DMSO) and diluted in PBS to get a final solution of 5% DMSO. This peptide was then clicked to DBCO-PEG4-biotin to test on BLI.

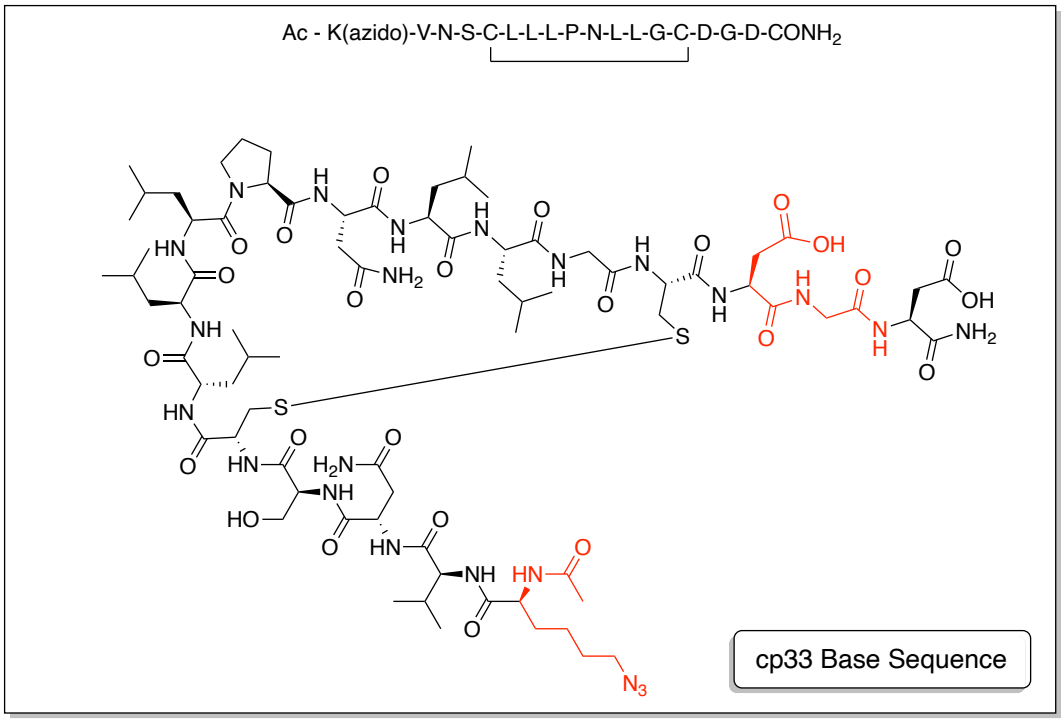

Figure 2.1. cp33 base sequence and structure
Portions of the structure which differ from the original cp33 peptide in literature are denoted in red.

2.2.2. Peptide Binding Behaviour

cp33 was tested on BLI for its affinity to huCD64, and for cross-reactivity with similar proteins. This peptide had a K_D of 52.5 nM, with minimal off target binding to muCD64 and CD16a (Figure 2.2).

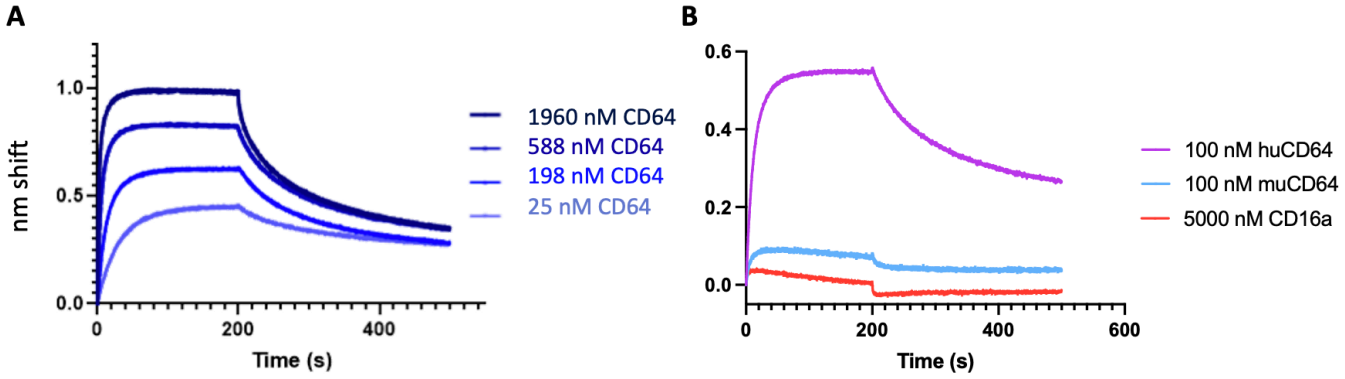

Figure 2.2. cp33 affinity and specificity
A) BLI curves generated for the affinity of cp33 for huCD64. Loading solution of 50 nM of cp33-PEG4 biotin was used with streptavidin probes and associated with increasing concentrations of huCD64. **B)** specificity of cp33 for huCD64, muCD64, and huCD16a shows minimal off-target binding.

2.2.3. SyAM Peptide

The SyAM paper which also utilized cp33, connected the peptide to their scaffold via the *C*-terminus in comparison to the one made above which was attached at the *N*-terminus.[34] As well, the peptide used in the SyAM paper had the Asp-Gly sequence in the correct order. To test if the changes we had made to cp33 were strongly influencing the binding properties we synthesized a SyAM-like peptide within the lab. This peptide had the azido-lysine residue placed at the C-terminus and did not incorporate the DG fragment. The SyAM peptide was successfully made within the lab but was associated with a lower yield than the previous peptide, likely because of the requirement to use lower coupling temperatures during synthesis to avoid aspartimide formation. Testing on BLI showed this peptide had similar characteristics to the cp33 peptide made in the lab, but it had a faster dissociation rate with a K_D of ~ 249 nM (Figure 2.3). Because there was no clear benefit in using this peptide sequence, it was not pursued as a primary structure for this project.

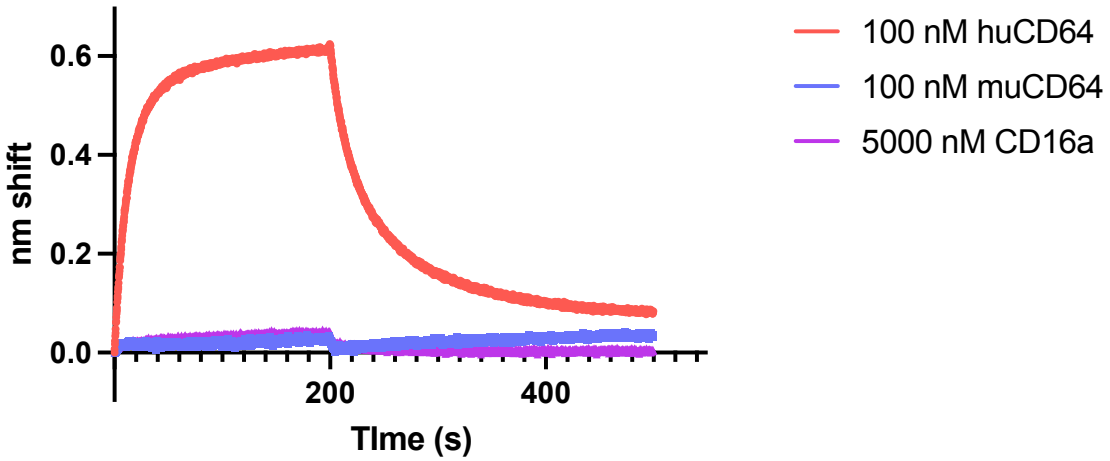

Figure 2.3. SyAM peptide affinity and specificity
Loading solution of 50 nM SyAM peptide associated with indicated concentrations of proteins of interest. This peptide had nearly identical binding properties as the original cp33 sequence tested prior with specific binding to huCD64.

2.3. Non-covalent cp33 tyrosine variants

2.3.1. Synthesis of cp33 variants

To probe potential positions to incorporate the electrophilic fluorosulfate SuFEx group, three sequences of cp33 with a Tyr addition/substitution were synthesized. We had envisioned the fluorosulfate could be most efficiently installed as an Fmoc protected tyrosine amino acid analogue, where SO_2F is linked via the phenolic hydroxyl group of tyrosine. Prior to incorporating the covalent chemistry, these Tyr based mutants were made to ensure that the inclusion of a new amino acid would not disrupt binding of cp33 to huCD64. Synthesized variants included a Tyr residue at the *C*-terminus (cp33-Ct-Y) ahead of the peptide sequence, a Tyr at the *N*-terminus following the *N*-terminal valine (cp33-Nt-Y), and a Tyr placed internally in place of the Gly13 residue (cp33-G13Y) (Figure 2.4). All peptides were successfully synthesized as confirmed by LCMS and purified on HPLC. These peptides also had poor yields with < 1 mg of peptide isolated per 25 mg of crude pellet purified.

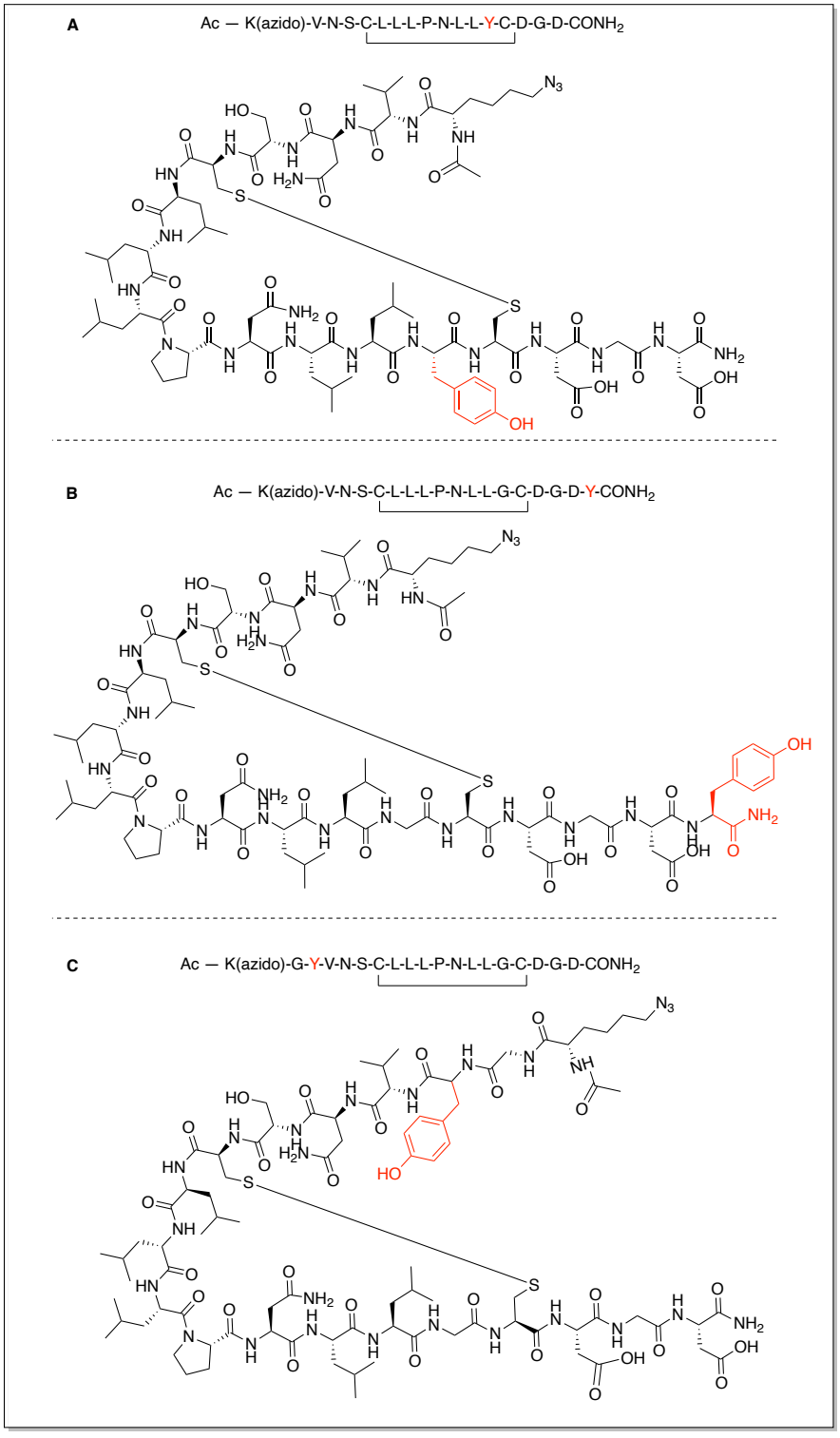

Figure 2.4. cp33-Tyr variant structures

Structures of the different cp33 Tyr variants, components in red are portions which differ from the base sequence cp33 **A)** cp33 G13Y structure **B)** cp33 Ct-Tyr **C)** cp33 Nt-Tyr

2.3.2. Characterization of cp33 Tyr variants on BLI

Of the three cp33 variants, only cp33-Ct-Y and cp33-Nt-Y had measurable affinity constants (K_D = 2.96 nM and 19.0 nM respectively) (Figure 2.5 and Figure 2.6). As well, these two peptides had no measurable binding to other closely related proteins. The cp33 G13Y construct had no detectable binding to huCD64 or to the other proteins (Figure 2.7). cp33-Nt-Y was the most promising structure and was selected as the non-covalent control for future experiments and is hereinafter referred to as the monocyte non-covalent immune recruiter (mNCIR) when modified with functional ligands, including biotin, fluorescein, AZDye 647 ((AZ647), an alexafluor 647 analogue), and GUL.

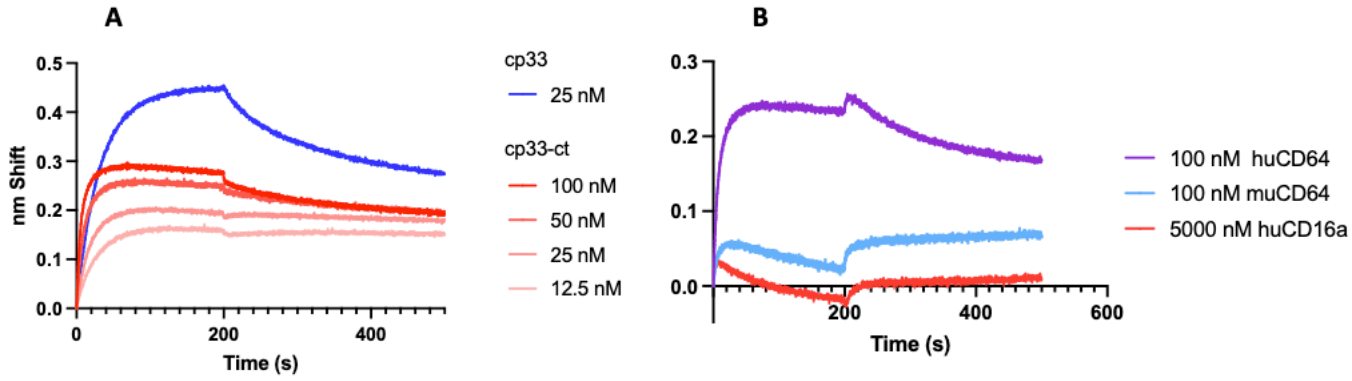

Figure 2.5. Affinity and specificity of cp33-Ct-Y for huCD64

A) The binding affinity of cp33-ct-Y for huCD64. Note that the binding curves for cp33-Ct-Y had abnormally low amplitudes and the unusually flat dissociation curves. **B)** the cp33-Ct-Y construct also had no detectable binding to other proteins.

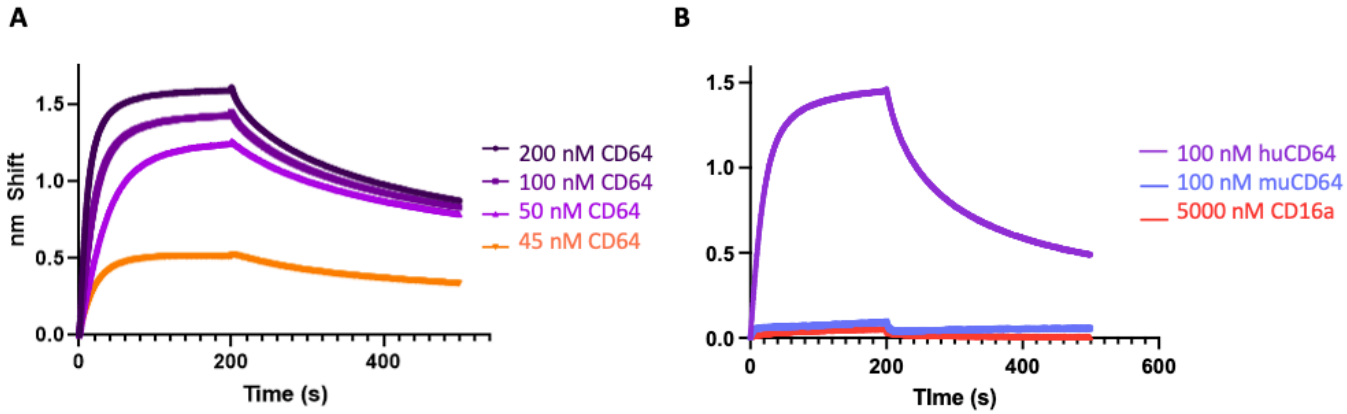

Figure 2.6. Affinity and specificity of cp33 Nt Y for huCD64

A) cp33-Nt-Y affinity for huCD64 as assessed on BLI. The affinity of this construct is greater than that of the original construct shown in here in orange as a control. The K_D was 19.0 nM. **B**)Specificity of cp33-Nt-Y for huCD64, muCD64, and CD16a. There was no detectable binding to any protein other than huCD64.

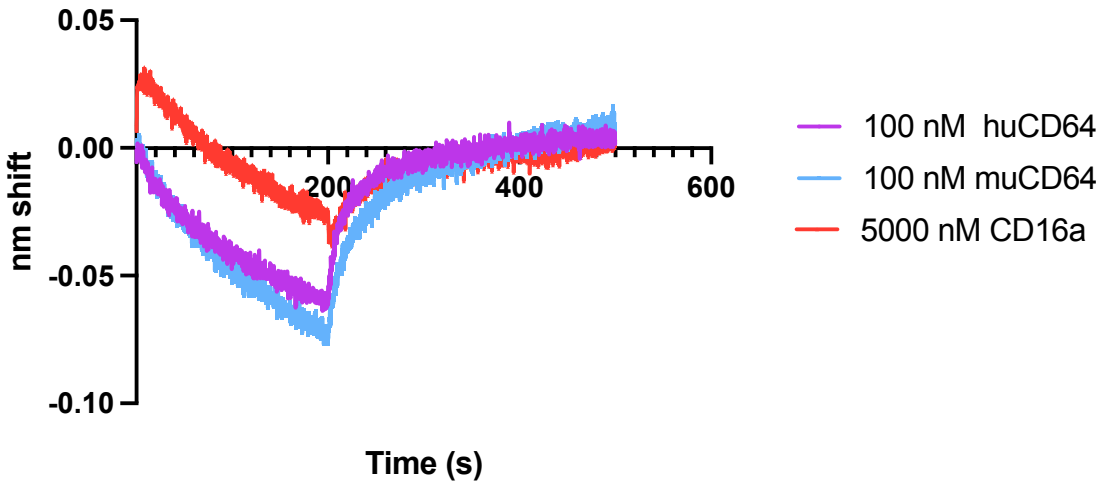

Figure 2.7. cp33 G13Y lacks binding to huCD64, muCD64, and CD16a

BLI sensograms for cp33-G13Y had no detectable binding to any of the protein including huCD64.

2.3.1. cp33 L7YL8N mutant

In an effort to increase peptide solubility, an undergraduate student in the Rullo Lab, Gavin Yuen, modelled peptide mutations which suggested that mutations at Leu 7 and Leu 8 could increase peptide solubility. The peptide was mutated to Tyr at position 7 and Asn at position 8 (Figure 2.8).

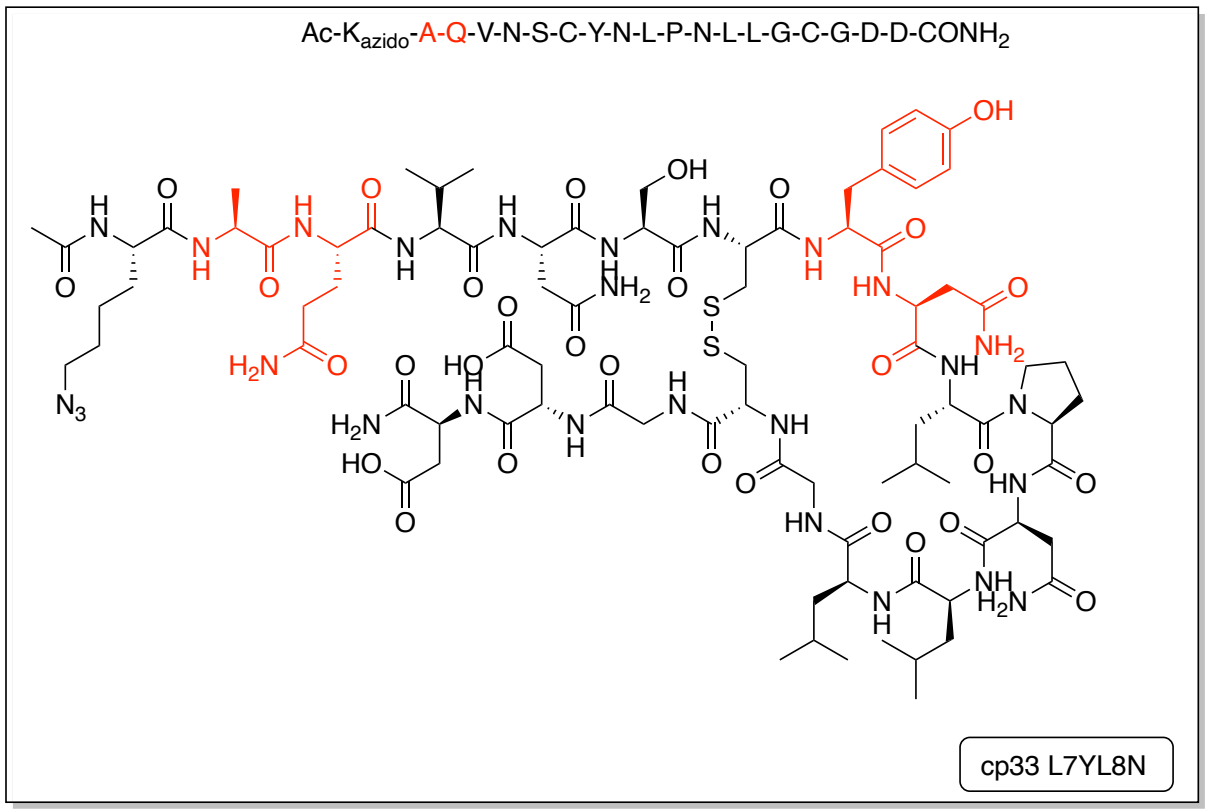

Figure 2.8. cp33 L7YL8N structure and sequence
Parts of the peptide denoted in red differ from the base cp33 sequence first made in the lab.

Synthesis of this peptide was successful, and the crude pellet dissolved easily in DMF and H_2O, without the need for can, unlike other peptides. Yields post HPLC were similar to other peptides, but the peptide solubilized in PBS more easily than previous peptides. Following click

reactions to PEG4 biotin, this construct demonstrated a comparable binding affinity to huCD64 as cp33 with a K_D of 57.6 nM (Figure 2.9).

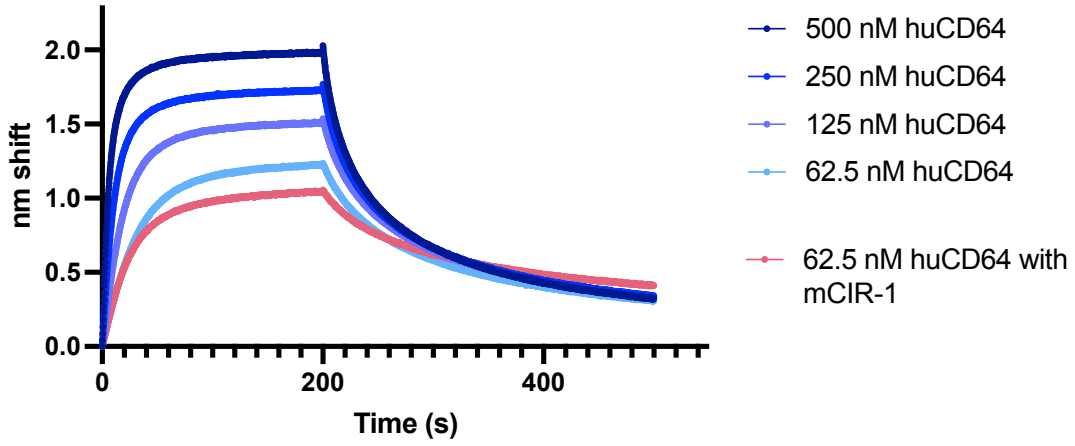

Figure 2.9. Binding affinity of cp33 L7YL8N to huCD64
cp33 L7YL8N (50 nM loading solution) sensograms (blue) closely resembled that of the mCIR1-biotin, discussed below, (50 nM loading solution) control sensograms (red).

2.4. Discussion

2.4.1. Peptide Synthesis

Based on literature success of the peptide cp33, it was thought this peptide would be a viable IBD to begin establishing a model system for immune cell recruitment. However, cp33 proved to be a challenging peptide to synthesize. The base sequence for cp33 consists of 43.75% hydrophobic amino acids, with the remainder being neutral (43.75%) or acidic (12.5%). The hydrophobicity of this peptide made it difficult to synthesize due to the repeated hydrophobic amino acids in the core of the peptide, which decreases coupling efficiencies and can hinder peptide yields.

While cp33 could be synthesized, small changes made in the peptide sequence in efforts to improve peptide yield or to probe covalent chemistry locations often compromised SPPS yield (Table 2). Many of the peptide variants were made in attempt to probe reactivity, alter linker length or location, or change the solubility of the peptide. Ultimately, of the 21 different peptide variations we tried to synthesize, only 10 of the peptides were able to be made *and* were stable enough to enable characterization.

A series of attempts to increase peptide yield post synthesis were done using high swell rink amide resin. The solid phase support beads used in peptide synthesis are solvated by the DMF (or DCM) and expand relative to dry beads. Due to the use of heat and excess reagents in SPPS, the kinetics of peptide coupling are diffusion controlled. Higher swelling resins are associated with better diffusion into the resin-matrix, with more efficient couplings and higher conversion to product. However, even when cp33 synthesis was carried using a low-loading high swelling resin there was no discernable difference in yield between the alternative approach with regular swelling resin.

One SPPS protocol which did result in a noticeable difference in product yield was the utilization of the DG fragment. The DG unit helps to prevent aspartamide formation by having a precoupled Asp (OtBu) residue coupled to a Gly (Dmb) residue. The Dmb protecting group is a bulky protecting group coupled to the amine group of glycine, which helps to sterically prevent aspartimide formation between the Asp and Gly residues. Without the DG unit, following coupling of the 2nd residue (Asp) all couplings afterwards required reduced temperature (40 ˚C vs 90 ˚C) and extended coupling times (10 min vs 2 min). This led to lower yields with a greater number of incomplete products observed on LCMS.

Furthermore, another aspect which complicated peptide synthesis was the disulfide bond between the two Cys residues. Disulfide bond formation is recommended to be performed on bead using methoxyl trityl (mmt) Cys residues for orthogonal deprotection from the rest of the peptide, and then cyclize using *N*-chlorosuccinimide (NCS). However, cyclization was not always successful as seen by LCMS monitoring post synthesis. LCMS chromatograms frequently appeared with both the target peptide mass, and the target mass +2, indicative of free thiols. Uncyclized peptide could often be purified away from the cyclized peptide during HPLC, which manifested as a loss in final product. Attempts to oxidize the cysteine residues in solution using DMSO oxidation and dichloroacetone stapling resulted in either A) di and tri peptide formation, linked to one another through disulfide bridges or B) unsuccessful cyclization with no identifiable product via LCMS.

2.4.2. Characterization of non-covalent scaffolds

Because the original paper did not report a K_D for cp33, our first aim was to characterize the base cp33 peptide. The K_D for this peptide, as determined through BLI, was around 52 nM. This was especially interesting because the SyAM paper reported a K_D for cp33 of 249 nM.[34] To investigate the potential discrepancy between the literature reported value and our value obtained from BLI we also synthesized a SyAM peptide to make a direct comparison. It was suspected that the binding differences were a result of our decision to place the azido lysine residue at the *N*-terminus and the use of the DG fragment. To resemble the peptide made in literature, our SyAM peptide was synthesized with the azido lysine residue placed at the *C*-terminus for linker attachment and with the Asp-Gly sequence in the correct order. When the SyAM peptide was clicked to PEG4-biotin and characterized on BLI, it had a K_D of ~ 285 nM. The similarity between

the results of the SyAM peptide BLI and its literature reported K_D value provided us with confidence that the K_D obtained for our cp33 base sequence is its true affinity for huCD64.

Furthermore, we chose to test the specificity of cp33 using proteins which considered that the peptide was designed to mimic the interactions between IgG1's Fc and huCD64. The Fc region of human IgG has cross reactivity with muCD64, and CD16a is a structurally related low-affinity FcR to huCD64 that also binds the Fc region of IgG.[42,43] For those reasons, we chose to test the specificity of cp33 against muCD64 and CD16a at 100 nM and 5 μM respectively. The base sequence of cp33 showed no binding to CD16a and minimal binding to muCD64, demonstrating comparable specificity reported in the original cp33 paper.

Variants of cp33 were synthesized with Tyr residues at various locations to probe potential positions for SuFEx chemistry. Of the mutants tested on BLI only cp33 G13Y was unable to bind to huCD64. This is presumably because the mutation to tyrosine added a bulky R-group which resulted in a steric clash, either within the peptide or between it and huCD64, rendering it incapable of binding. Between the Nt and Ct Tyr peptides, cp33-Nt-Y had better sensograms relative to the Ct one. While the Ct-Y peptide was fit by Prism to have a lower K_D than both the original cp33 and Nt-Y peptide, this is likely in part due to the low amplitude of the entire experiment. A noticeable trend in all BLI experiments is that when less protein associates with the immobilized ligand on the probe, less is seen dissociating from the probe as well. This is likely resulting in artificially lowered K_D values due to apparent infinitesimally slow dissociation rates. Because the cp33 peptide and the Ct-Y mutant are nearly identical in mass, and ligand modification, the low amplitude relative to the original likely reflects a decreased capacity for cp33-Ct-Y to bind huCD64. The K_D for the Nt-Y mutant from BLI demonstrated that it was a tight binding peptide

and was an excellent candidate for mCIR structures. This structure was chosen as our mNCIR for future experiments, providing a comparative peptide to monitor the effect of covalency in the mCIR system.

The L7YL8N peptide was another successful non-covalent structure. It was designed to increase the solubility of the peptide, to isolate more peptide through the synthesis process and encourage better behaviour post HPLC reconstitution. Despite better solubility of the crude pellet relative to other cp33 peptides, this did not translate to an increase in yield post HPLC. However, the pure material solubilized easier in PBS without the need for DMSO or to let the solution stand, a common practice for solubilizing lyophilized peptides and proteins. The increased solubility is attributed to the removal of two adjacent leucine residues in the core of the peptide. In addition to its increased solubility, this peptide had a similar affinity to the original sequence and demonstrated that this location of Tyr still enabled binding of the peptide to huCD64 while providing a potential location to test internal SuFEx chemistry. Ultimately, using the non-covalent peptide constructs as a basis for SuFEx placement, only 2 peptides were viable candidates: an *N*-terminally placed SuFEx moiety and an internal SuFEx moiety resembling the L7YL8N peptide.

3. mCIR-1; cp33 Nt Fluorosulfate peptide development and fluorosulfate incorporation

3.1. Objectives

Following the success of cp33-Nt-Y, the replacement of the tyrosine residue with a Tyr-SuFEx one was a top priority. Following incorporation of the SuFEx chemistry, the characterization of the peptides capacity to bind huCD64 needed to be assessed along with its non-

covalent binding specificity. Furthermore, it was paramount to establish whether this chemistry could enable labelling of huCD64 and its rate of covalent modification. Based on previous behaviour of cp33-Nt-Y, this Nt-fluorosulfate containing peptide was hypothesized to have similar non-covalent binding properties from affinity to specificity. Furthermore, based on literature success of fluorosulfate labelling, this peptide was initially hypothesized to have complete labelling within 48 h of incubation with huCD64. To test these hypotheses, this peptide was characterized using BLI to probe non-covalent interactions, and with SDS PAGE using a mCIR1-fluor/AZ647 to identify protein labelling and characterize its kinetic profile.

3.2. Results

3.2.1. Synthesis of cp33-Nt-Fluorosulfate

Encouraged by its CD64 binding properties, we installed a fluorosulfate at the *N*-terminal position of cp33 (Figure 3.1). This peptide was modified with an Fmoc-Tyr-fluorosulfate derivative obtained from Enamine. Following purification, ~ 1.5 mg of product was isolated from the crude pellet. This peptide dissolved well in PBS post lyophilization and did not require any additives to increase solubility. This peptide was then clicked to DBCO-PEG4-biotin, DBCO-PEG8-fluorescein/DBCO-AZ647, and DBCO-PEG8-GUL for BLI, fluorescent studies, and ternary complex assays respectively. Following modifications with functional ligands this construct is referred to as mCIR1-biotin, mCIR1-AZ647/fluor, or mCIR1-GUL.

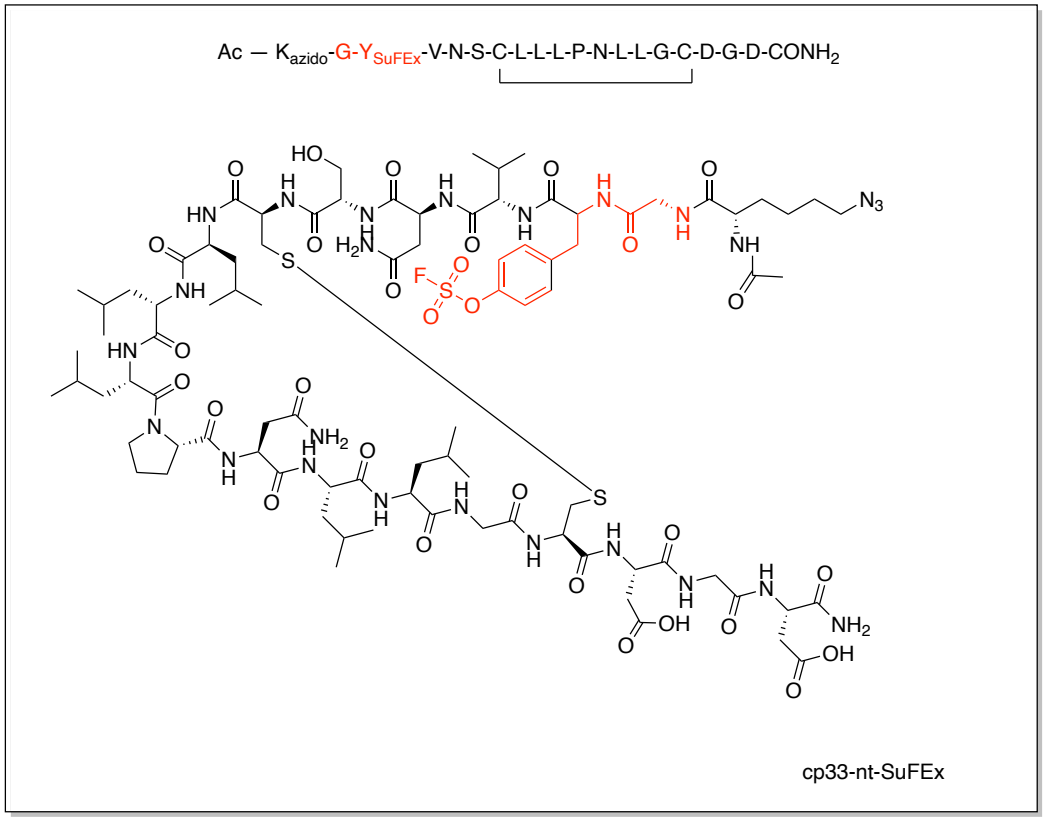

Figure 3.1. cp33-Nt-fluorosulfate
Structure of cp33-Nt-fluorosulfate made using commercial Fmoc-Tyr-fluorosulfate-OH building block. Portions of the structure highlighted in red differ from the base sequence of cp33 characterized in the lab.

3.2.2. Binding and labelling specificity of mCIR-1

Initial testing of the cp33-Nt-fluorosulfate was done using the fluorescent mCIR1-AZ647 and was probing whether this peptide could covalently label huCD64. This was tested using an SDS PAGE experiment by incubating 1.6 µM mCIR1-AZ647 with 0.8 µM huCD64, muCD64, or CD16a for 8 h at RT. Successful labelling was qualified as a double positive where a fluorescent band, indicative of mCIR1-AZ647, and a Coomassie stained band, indicative of a protein, overlapped with one another. The only protein which presented with a double positive following

labelling was huCD64 (Figure 3.2). The huCD64 bands appear as 2 separate bands within the same lane due to differences in glycosylation.

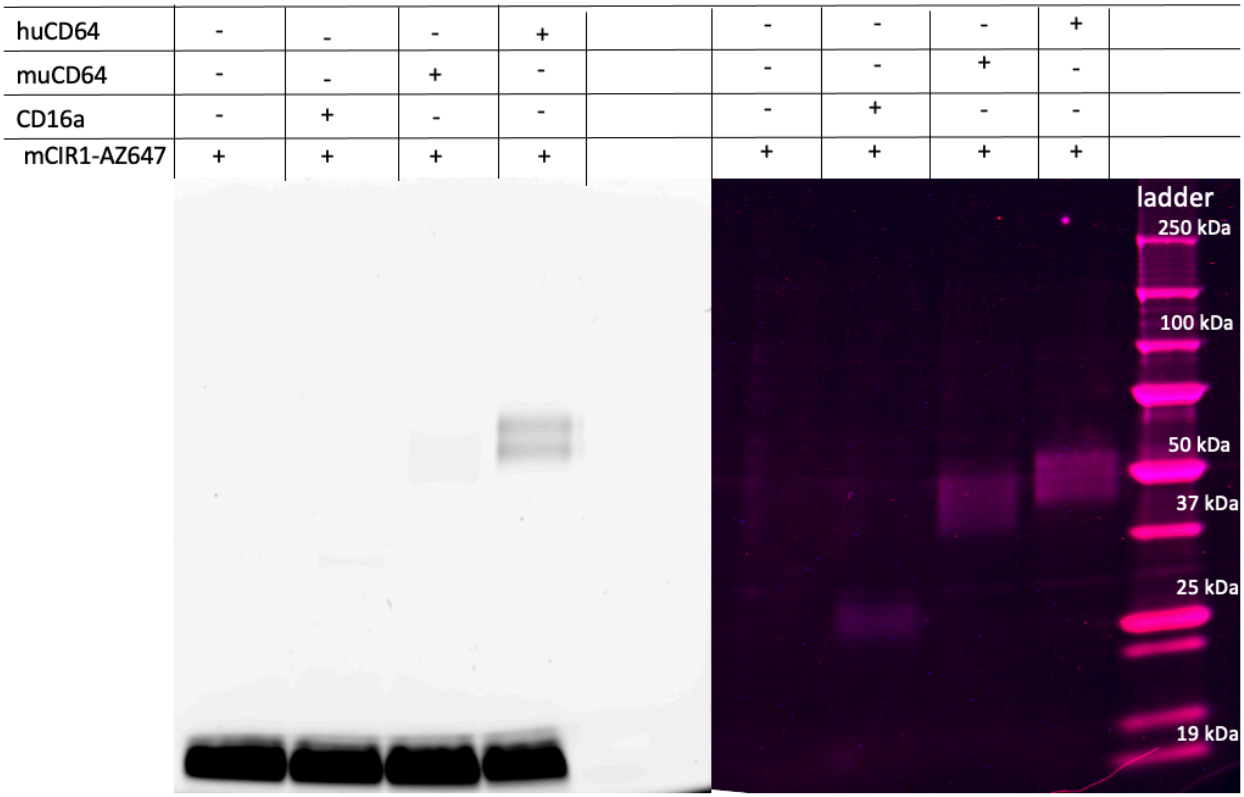

Figure 3.2. Specific labelling of huCD64 by cp33-Nt-fluorosulfate
A 4-20% acrylamide reducing gel imaged using a Coomassie channel (right) and AZ647 channel (left). All constructs were incubated in a 1:1 ratio at 1 μM. The Coomassie channel was used to identify the proteins loaded onto the gel. The gel on the left is the AZ647 channel to identify where the mCIR appeared in the gels. The only bands which overlap between the two different imaging channels are huCD64 bands. The bright bands at the bottom of the gel are the flowthrough bands of excess peptide.

Following successful labelling, the binding specificity and affinity of mCIR1-biotin were assessed by BLI. BLI sensograms showed that this peptide had a K_D similar to the original construct (49.3 nM) and was not found to bind significantly to either muCD64 or CD16a.

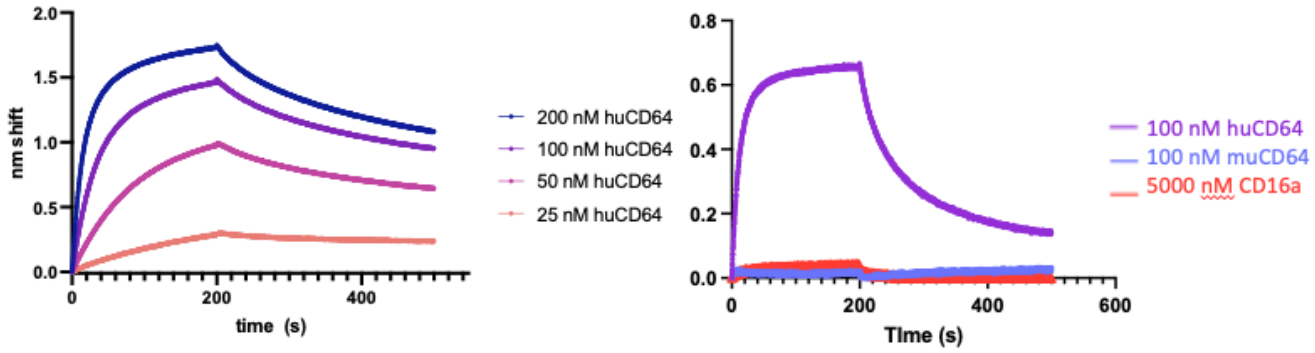

Figure 3.3. mCIR1-biotin affinity and specificity for huCD64
A) mCIR1-biotin (50 nM loading) affinity for huCD64 as assessed on BLI. The affinity of this construct is greater than that of the original construct shown in here in orange as a control. The K_D was 19.0 nM. **B**) Specificity of mCIR1-biotin for huCD64, muCD64, and CD16a. There was no detectable binding to any protein other than huCD64

Fluorescence polarization (FP) experiments using mCIR-1 fluorescein were also conducted to test affinity and to probe covalent labelling of huCD64. Initial experiments used concentrations of huCD64 which were found to be far greater than the K_D of the molecule and had saturated the protein at most concentration points (Figure 8.1). The FP parameters were modified to test lower concentrations of huCD64 and were carried out at 2 time points; one following a 15 min incubation, long enough to establish an equilibrium, and then a second 24 h following incubation (Figure 3.4).

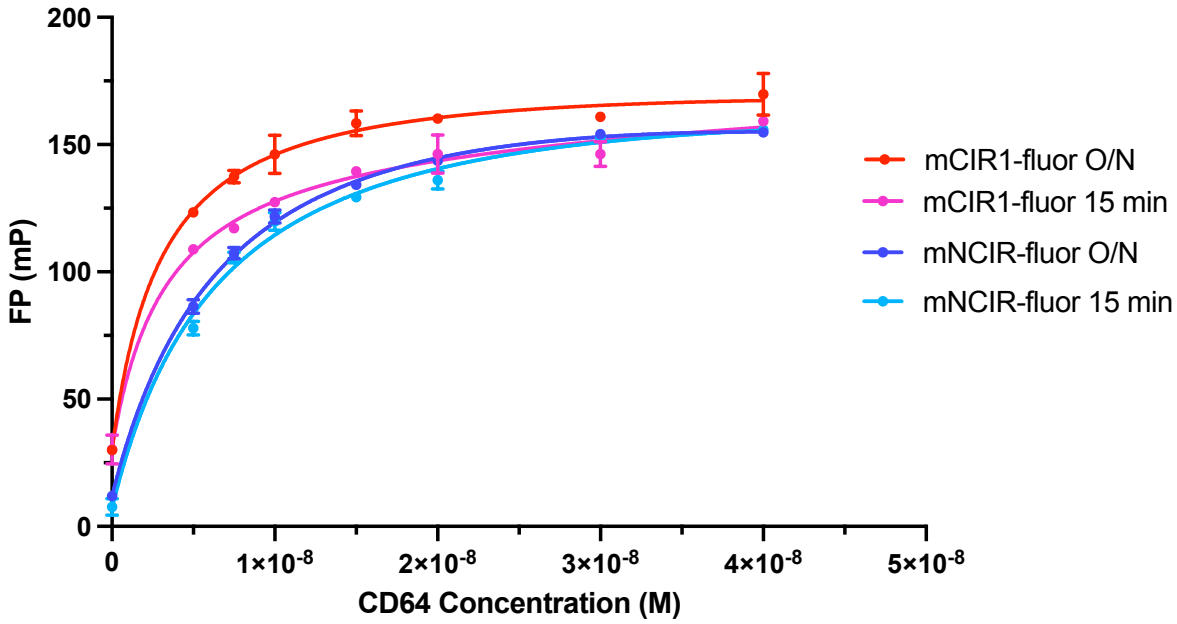

Figure 3.4. Raw data for m(N)CIR-fluor FP experiment probing labelling and binding affinity
Using 5 nM mCIR1-fluor and mNCIR-fluor incubated with 5-40nM huCD64 incubated at RT either overnight (O/N) or for 15 min as indicated.

The mNCIR data converted to fraction bound was identical between the two time points as expected as the system was in equilibrium at both time points (Figure 3.5).

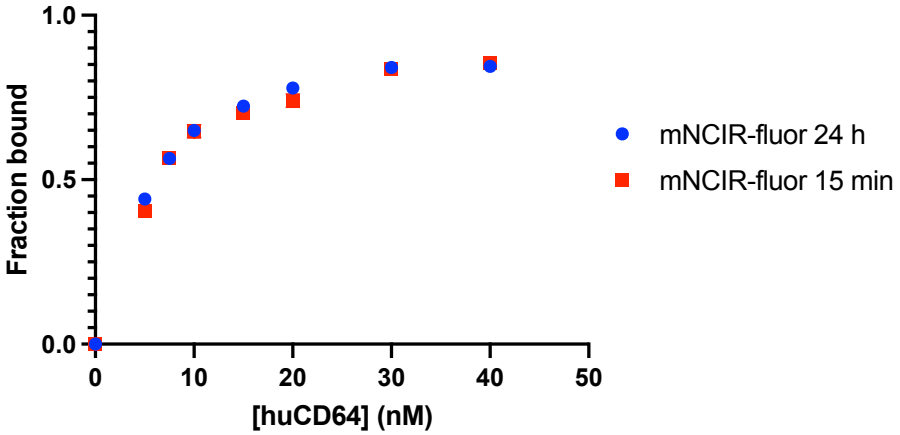

Figure 3.5. mNCIR FP 15 min vs 24 h
FP results from mNCIR fluorescein incubations with increasing concentrations of huCD64. Data points for 15 min incubations and 24 h incubations are identical to one another as the system was in equilibrium.

In comparison to the mNCIR-fluor, following the 24 h incubation period there was a noticeable upwards shift in the data, indicative of covalent labelling (Figure 3.6). However, no quantifiable data for labelling was obtained from this experiment and so this approach was not used to further characterize the mCIRs. While this approach was unable to provide insight into covalent labelling, FP confirmed that this peptide was a tight binding peptide with a low nM binding affinity, ≤ 5 nM.

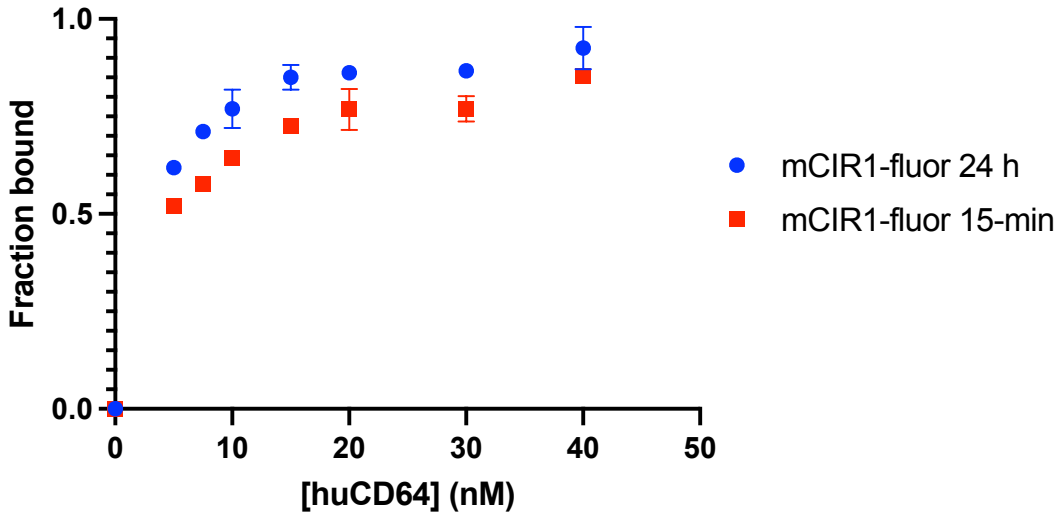

Figure 3.6. mCIR1-fluor FP with huCD64 15 min vs 24 h
FP results from mCIR1-fluor incubated with increasing concentrations of huCD64. The distinct upwards shift in data between the 15 min incubation vs the 24 h incubation indicates covalent labelling of huCD64.

3.2.2.1. Kinetics mCIR-1 labelling of huCD64

Experiments to characterize the covalent labelling of huCD64 by the fluorosulfate moiety of mCIR1-fluor were carried out using SDS PAGE. Prior to beginning labelling studies, the fluorosulfate's stability in solution was monitored over a 2-day period to ensure the peptide and the chemistry was not going to rapidly degrade in solution.

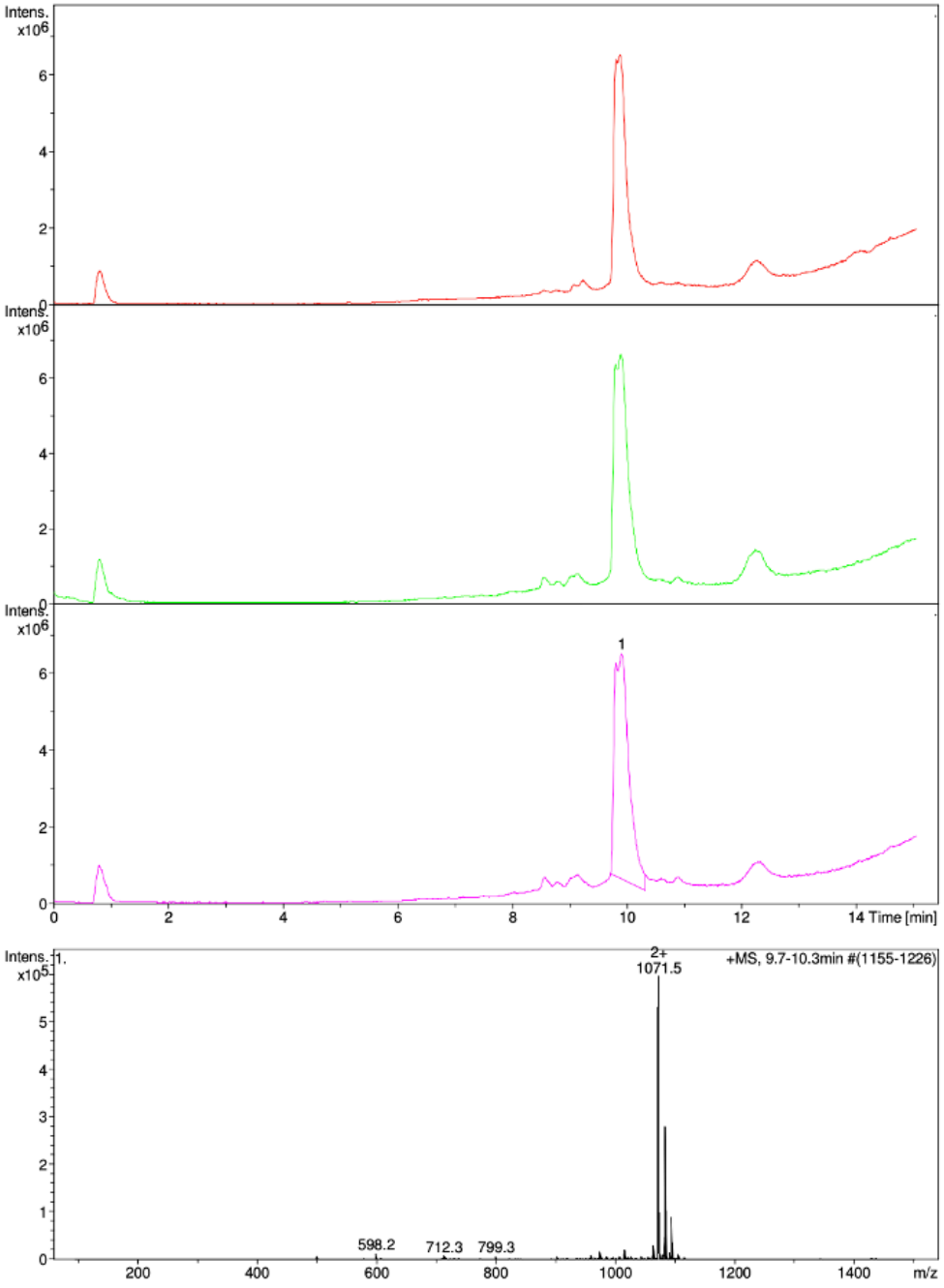

Figure 3.7. LCMS stability of cp33-Nt-fluorosulfate at RT for 48 h

Top three spectra are the total ion chromatograms at 0 h (top, red), 24 h (second, green) and 48 h (third, pink). The mass spectra at the bottom corresponds to the base peak of each chromatogram. There was no significant degradation of the fluorosulfate of cp33-Nt-fluorosulfate in solution.

These studies were carried out by LCMS and found that for at least 2 days at RT the peptide and its chemistry remained intact. To gauge the rate of covalent labelling, mCIR1-fluor and huCD64 were incubated together at a fixed concentration for increasing amounts of time at RT before being run on SDS PAGE. Initial results at 1:1 ratios of peptide to protein revealed that the reaction was still in the linear region (Figure 3.8).

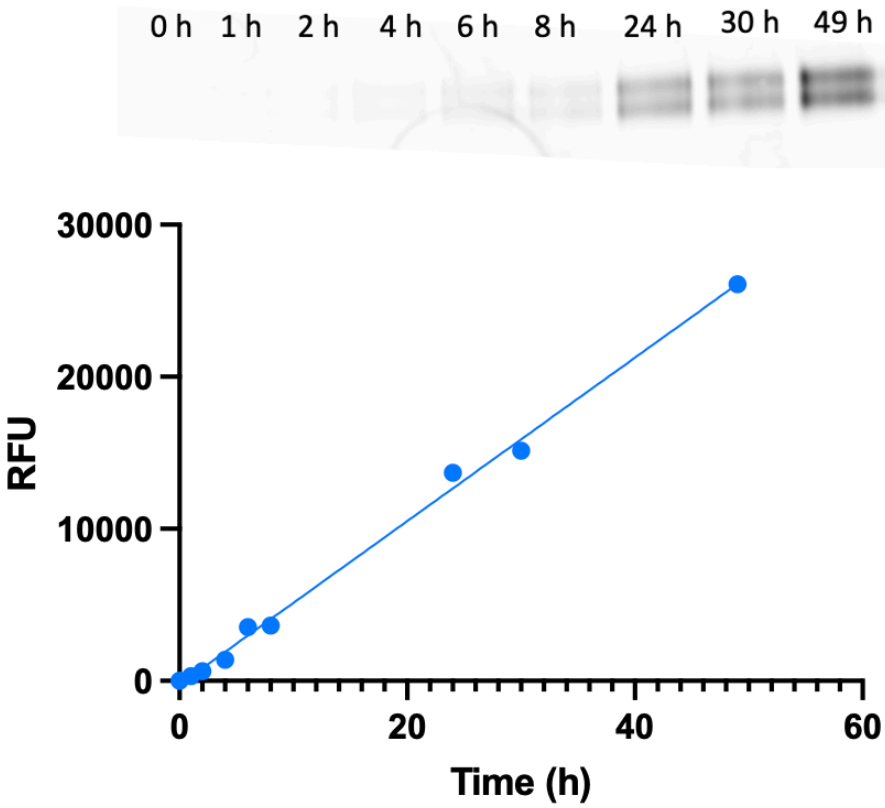

Figure 3.8. mCIR1-fluor 1:1 Kinetics Gel at RT
Fluorescent gel using 1 μM mCIR1-fluor and 1 μM huCD64 incubated at room temperature. This reaction had no observable plateau and is in the linear portion of the reaction curve still. The intensity from pixels was assessed in ImageJ and then normalized to the time zero point. The data was plotted in prism and fitted using a simple linear regression model and has an R^2 of 0.9963.

The unexpectedly slow rate demonstrated by mCIR1-fluor prompted an investigation into its cause. It was hypothesized that there was a percentage of peptide that was conformationally

inactive, so the concentration of functional peptide was lower than assumed. To test this, increasing ratios of mCIR1-fluor relative to huCD64 were incubated at RT and run on SDS PAGE. Ratios of mCIR1-fluor to huCD64 ranged from 2:1, to 40:1. To compare different gels, all pixel intensities were normalized to the darkest band within an incubation series and then plotted together for visualization (Figure 3.9). Despite using up to 40x excess mCIR1-fluor, there was no change in apparent rate between any of the incubations.

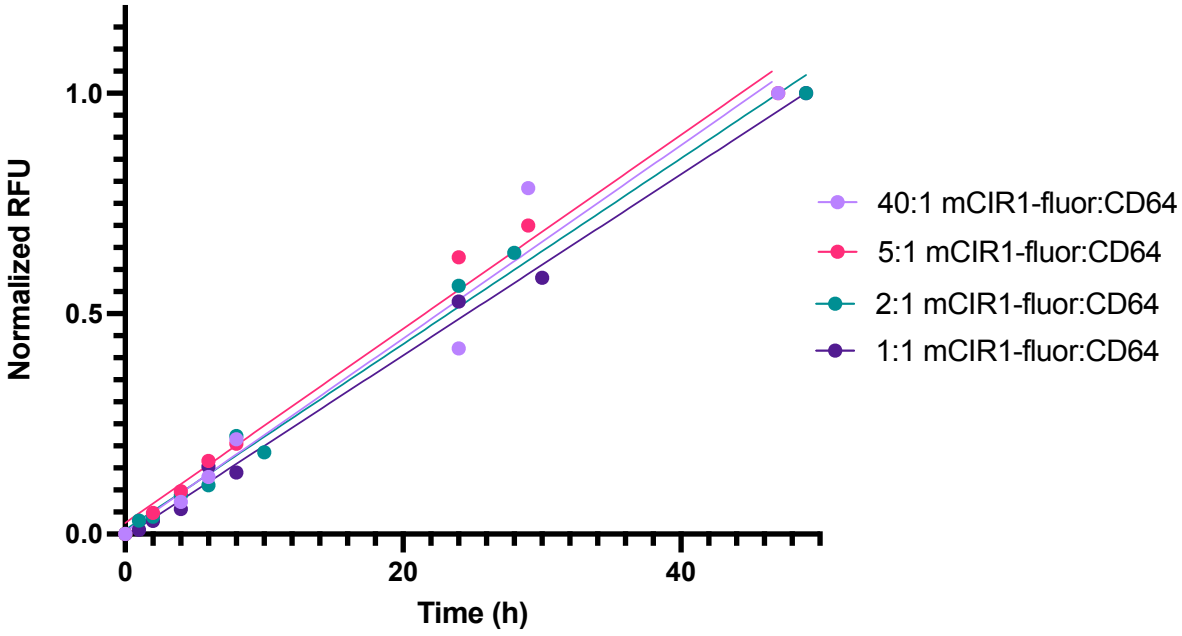

Figure 3.9. Relative rates of all RT mCIR-1 SDS PAGE experiments
Increasing concentration ratio of mCIR:huCD64 had no effect on the observed rate even as high as 40:1. To compare the rates between different gels, the fluorescence from each band was normalized to the brightest band at 49 or 48 h depending on the experiment. R^2 values ranged from 0.959 – 0.995

Despite the slow kinetics observed with the fluorosulfate equipped peptide, its capacity to bind and label huCD64 encouraged its progression to flow cytometry labelling experiments. mCIR1-biotin was tested for its ability to label huCD64 expressed on the surface of human U937 monocytes (Figure 3.10). This experiment used phycoerythrin (PE) (a bright red-orange

fluorophore) labelled streptavidin binding to mCIR1-biotin localized to huCD64 on the surface of the monocytes as a read out for successful binding/labelling. Below the K_D of the m(N)CIRs, mCIR1-biotin significantly outperformed its non-covalent counterpart. Only at 80 nM did the non-covalent and covalent constructs have comparable performance levels. Overall, at 80 nM >95% of monocytes were positive for PE fluorescence, indicative of the mCIR bound to huCD64. Using a fluorescent anti-CD64 antibody, the total amount of CD64 was quantified, and enabled the estimation of total labelled huCD64 by the fluorosulfate of mCIR1-biotin. Using this approach, it was found that at 80 nM following 24 h of incubation ~ 10% of all receptors were labelled.

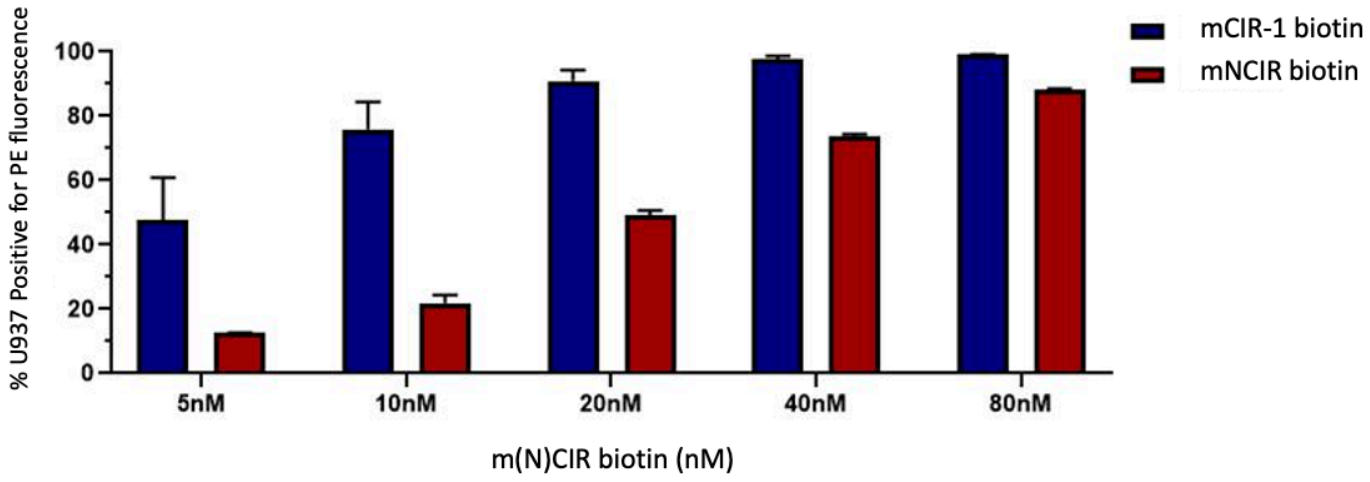

Figure 3.10. Labelling of huCD64 on U937 monocytes at 37 ˚C by the fluorosulfate of mCIR1-biotin

Data from flow cytometry experiment ran by Eden Kapcan for this project. Blue bars are the mCIR1-biotin while red bars are mNCIR-biotin. By 80 nM for both constructs, 90% of the monocytes were positive for the presence of streptavidin-PE.

The results from flow cytometry provided a quantifiable value of huCD64 labelling by mCIR1-biotin by 24 h at 37 ˚C. Another SDS-PAGE experiment using mCIR1-fluor was performed using a 1:1 ratio of peptide:huCD64 (1 μM) and incubated at 37 ˚C for up to 49 h. Based on the flow cytometry data, the intensity at 24 h was assumed to be 10% labelled. The data was

then converted to fraction labelled and fit using first order kinetics to get a k_{obs} of 1.05×10^{-7} s^{-1} (Figure 3.11).

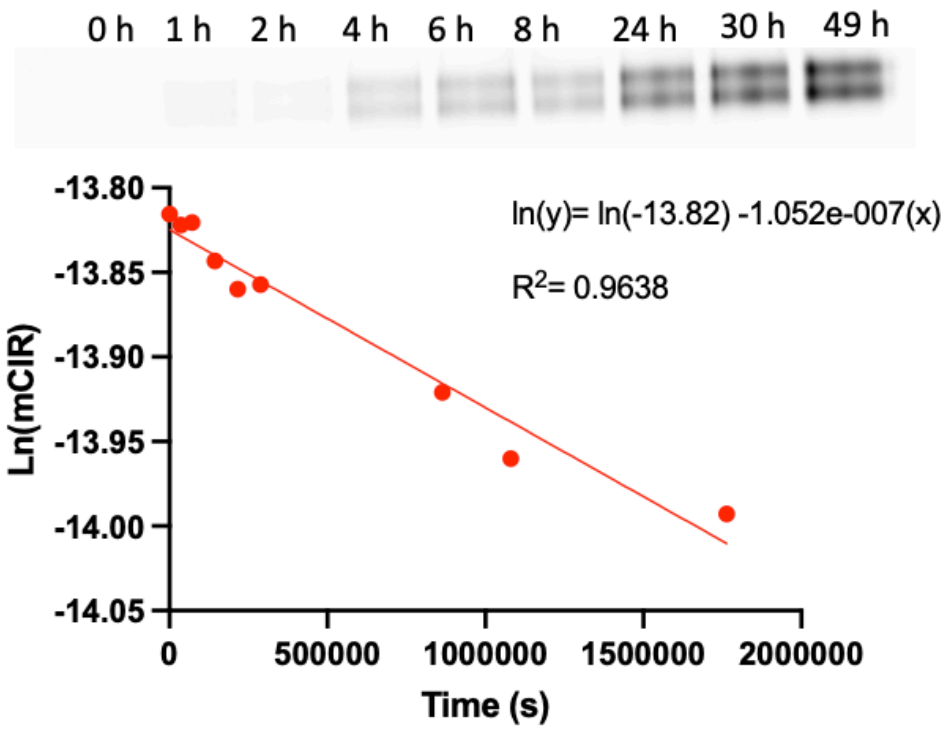

Figure 3.11. Labelling of huCD64 at 37 ˚C by mCIR1-fluor
1:1 huCD64 and mCIR1-fluor incubated together at 37 °C for up to 49 h. No sign of reaction plateauing on the gel (above graph) but data was fit by defining the 24 h point as 10% labelled. Data points were then fit using first order kinetics to provide a k_{obs} of 1.05 x 10^{-7} s^{-1}.

3.2.1. cp33 L7Y$_{SuFEx}$L8N mutant

Because the reactivity of fluorosulfates can be influenced by changes in location/orientation relative to the target nucleophile, it was also a goal of ours to screen internally placed covalent chemistry positions. Using the L7YL8N peptide as its basis, we chose to substitute the Tyr at position 7 for the Tyr fluorosulfate. This peptide was successfully made with yields consistent with other peptides. While the covalent construct reconstituted well in PBS, it was not as instantaneous as the non-covalent version. SDS PAGE experiments using mCIR1-AZ647,

mCIR2-AZ647 (cp33 equipped with an *N*-terminal sulfonyl fluoride, discussed below), and L7Y$_{SuFEx}$L8N clicked to AZ647 were conducted to assess relative rate of the new covalent construct given similar conditions to the other mCIRs after 20 h of incubation (Figure 3.12). The internal mutation of cp33 had little labelling of huCD64 relative to mCIR1-AZ647 and was not pursued further.

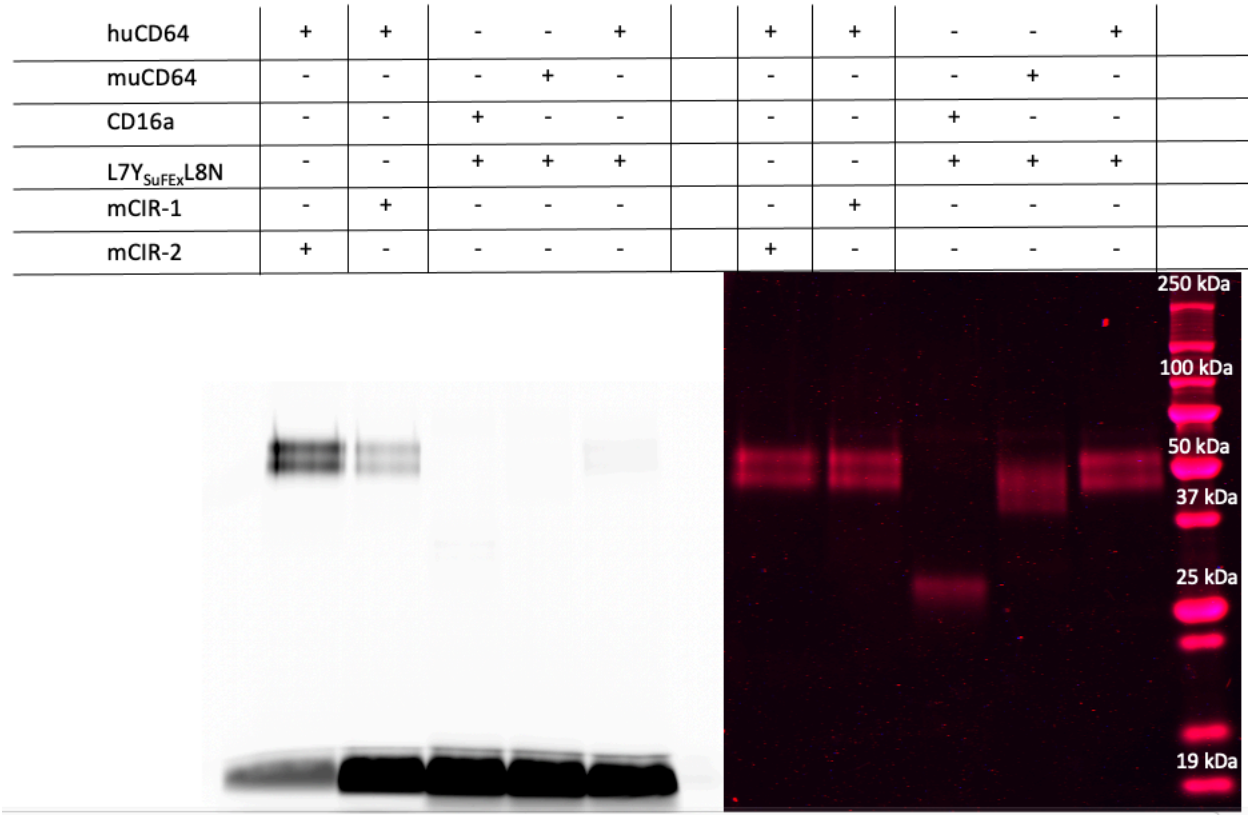

Figure 3.12. Relative labelling of L7Y$_{SuFEx}$L8N to mCIR1-AZ647 and mCIR2-AZ647
This gel was imaged in two channels, AZ647 (left) and a Coomassie channel (right). Labelling by L7Y$_{SuFEx}$L8N was selective for huCD64, but significantly slower mCIR1-AZ647 and mCIR2-A647. Bright bands at the bottom of the gel in the AZ647channel are peptide that did not label the protein.

3.2.2. Peptide Handling Investigations

Early into this project it was noted that there were differences in BLI loading amplitudes between aliquots of a single m(N)CIR batch. As well, at the same time the lack of observed labelling by mCIR1-fluor was hypothesized to be due to issues with peptide solubility/conformation as other peptides in the Rullo Lab equipped with the same chemistry achieved full labelling within 48 h. Because of these two simultaneous deviations in expected peptide behaviour, a series of side investigations into peptide handling were conducted. From LCMS monitoring of the peptides, it was confirmed they were not covalently labelling one another, or forming covalent disulfide crosslinks between peptides. As a result, 2 major components of peptide stability were investigated: the effect of freeze thaw cycles and the effect of solvent on peptide behaviour. Peptide conformation and stability is known to be influenced by solvent choice while freeze thaw cycles can lead to peptide aggregation and subsequent deactivation.[44] The effect of solvent on mCIR1-fluor labelling of huCD64 was first investigated due to the potential for conformational changes to obstruct protein labelling. To investigate whether solvent was having a significant effect on protein labelling a series of SDS PAGE experiments using mCIR1-fluor were performed. The peptide was dissolved in either PBS, 1x KB, 1:9 MeOH:PBS, and incubated in a 2:1 ratio with huCD64 for 4 and 23 h. The fluorescence of all labelled bands was normalized to the total amount of fluorescence found for that solvent system (labelled band/(flowthrough band + labelled band)) (Figure 3.13).

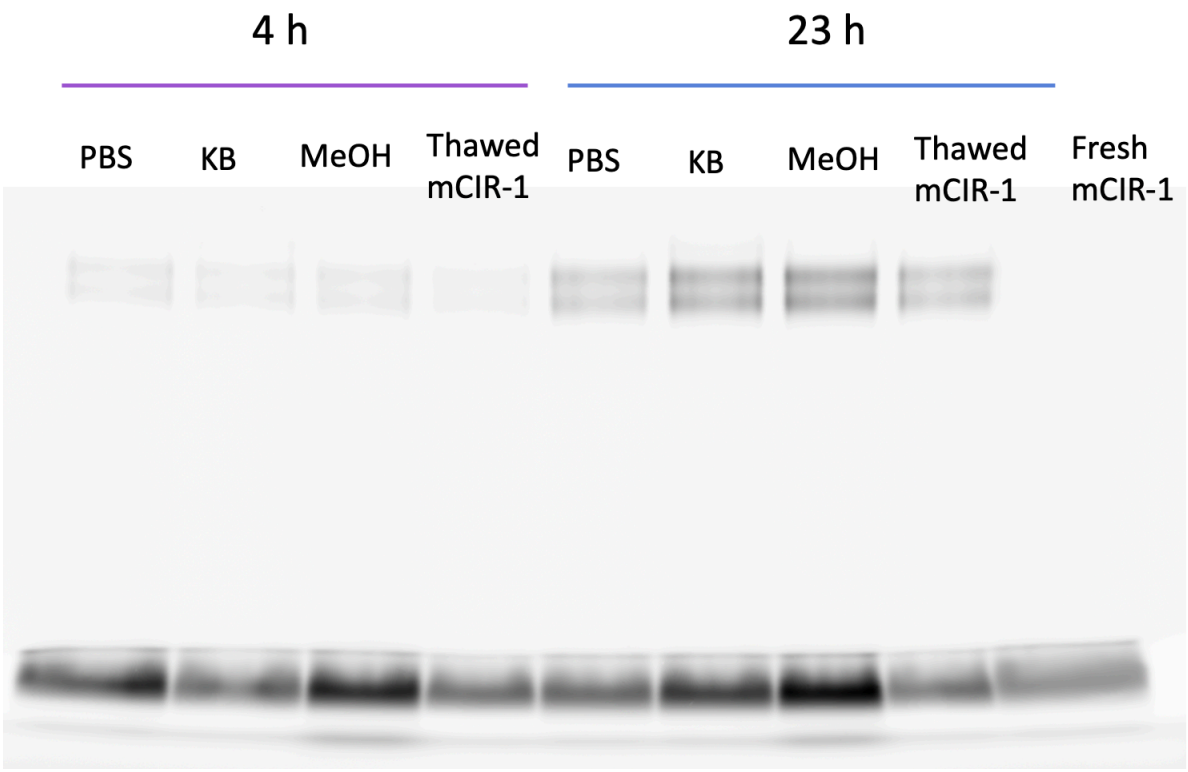

Figure 3.13. Effect of solvent on huCD64 labelling by mCIR1-fluor
Fluorescent gel to test the effect of solvent on the ability of our mCIR1-fluor to label huCD64. Tested peptides were dissolved in either PBS, 1x KB, MeOH, or were an older thawed stock of mCIR1-fluor and incubated with huCD64 for 4 or 23 h.

Using this approach, 1x KB had the greatest amount of protein labelled in comparison to the other solvents. Notably, the stock of thawed mCIR1-fluor also dissolved in PBS had comparable labelling relative to peptides which had not been thawed post suspension. Additionally, LCMS studies of the peptide in MeOH showed that with extended periods of time in MeOH exacerbated peptide degradation. Upon more than 5 days of storage in the fridge, a second peak appeared in the UV trace and in the total ion chromatogram with a mass shift corresponding to the substitution of the fluorine for a methyl group. After a week and a half, the peptide precipitated out of solution.

The effect of freeze thaw cycles on peptide binding behaviour was then evaluated using BLI and FP. For BLI, solvent systems of 1:9 DMSO:PBS, 1:9 ACN:H_2O, and PBS. mCIR1-biotin was either flash frozen or kept at RT following suspension and dilution in these buffers, and then loaded onto BLI to test its ability to bind 40 nM huCD64 in solution (Figure 3.14). PBS was the most consistent solvent between frozen and non-frozen aliquots, but the K_D across all solvent systems and freeze thaw cycles were similar, ranging from 12.3 to 19.8 nM.

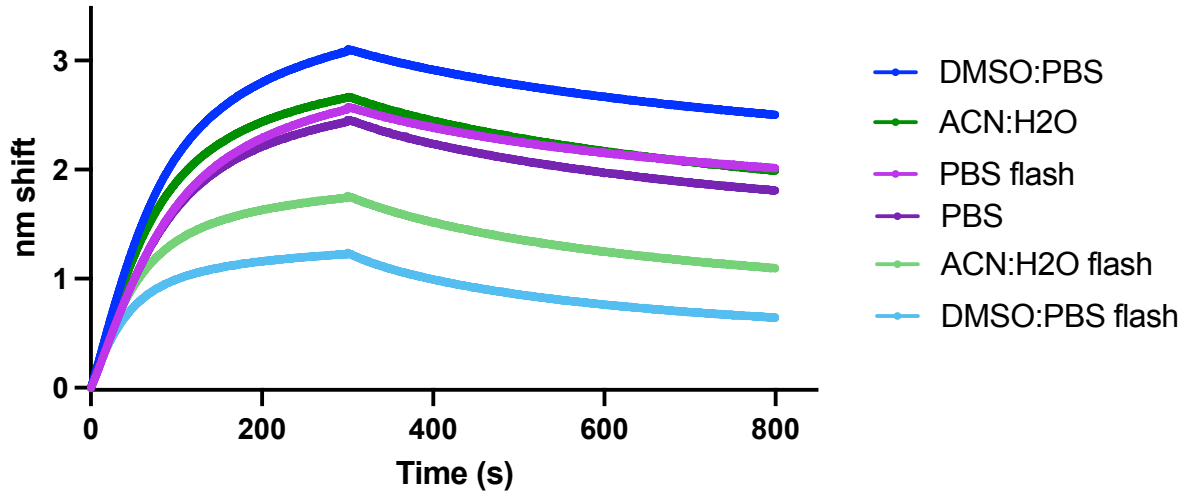

Figure 3.14. Flash frozen vs thawed mCIR1-biotin association on BLI
mCIR1-biotin (50 nM loading solution) associated with 40 nM huCD64. The solvent system which was most consistent between fresh and flash frozen stocks was PBS. Note that by inherent assay design for BLI, all the stocks were dissolved in the solvent systems outlined above and then diluted ~ 100 x into 1x KB and run on BLI.

The last experiment performed was FP, testing mCIR1-fluor and mNCIR-fluor behaviour in PBS or 1x KB with or without the addition of 0.5% Tween 20. For FP of peptides alone, typical values are around 60 mP or below. This was true for the control peptide (produced by Harrison

McCann) and for our mNCIR-fluor. However, mCIR1-fluor, both the thawed and never-frozen samples, had unusually high FP readings ranging from 83.0-90.8 mP (Table 1).

Table 1. FP values from solvent, Tween 20, and freezing investigation

	mCIR1-fluor – thawed	mCIR1-fluor never frozen	mNCIR-fluor - thawed	Control peptide - thawed
PBS	89.5 mP	90.8 mP	63.3 mP	46.3 mP
1x KB	83.6 mP	83.0 mP	/	/
1x KB + 0.5% Tween20	85.1 mP	94.6 mP	77.6 mP	/

Based on these experiments, the peptide handling procedures were modified so that peptides were frozen a minimal number of times before they were used and had 1x KB added prior to freezing at -80 ˚C for extended storage.

3.3. Discussion

The fluorosulfate of mCIR1 constructs was the first covalent structure made and characterized in the lab. The fluorosulfate moiety is associated with greater aqueous stability and selectivity than sulfonyl fluorides. The non-covalent interactions of mCIR1-biotin were indistinguishable from the mNCIR-biotin, with similar K_D values from BLI and FP. Interestingly, the K_D acquired from FP was < 5 nM for mCIR1-fluor and for the mNICR-fluor, which is lower than BLI suggested. FP studies used PEG8 linkers instead of the PEG4 linkers that were utilized for BLI. A similar trend was seen for BLI replicates with the SyAM peptide in which the PEG4 construct had a K_D ~285 nM while the PEG8 version had a K_D ~142 nM. This trend of decreasing K_D values with increasing PEG length between cp33 constructs suggests that the linker length is an important consideration in cp33 containing scaffolds.

While the non-covalent properties of mCIR1 constructs maintained the peptides' high specificity and affinity, the observed labelling rate of huCD64 by mCIR1-fluor/mCIR1-A647 was too slow to for our purposes, with no sign of reaction completion up to 49 h post incubation with huCD64. The slow labelling rate was at first suspected to be a result of peptide deactivation, lowering the effective concentration of mCIR1-fluor in solution. SDS PAGE experiments performed using up to 40x excess mCIR1-fluor relative to huCD64 did not demonstrate any increase in labelling rate with increasing concentration. This suggests that the observed labelling of huCD64 by mCIR1-fluor was inherently slow rate for reasons unrelated to potential deactivation. It is established in the literature that the reactivity of fluorosulfates is highly dependent on their microenvironment, therefore a chemistry which produced a rapid reaction with one protein is subject to sluggish rates with another.[27] This is supported by the fact that other peptides functionalized with this chemistry in the Rullo Lab have demonstrated full labelling of their target protein within 48 h. Literature suggested that changes in placement within the sequence, even small ones, could produce large differences in the observed rate. However, nearly all attempts to shift the location of the Tyr_{SuFEx} residue were not tolerated by the peptide and resulted in syntheses with no product, save the L7YL8N peptide. The internal Tyr residue which did not disrupt binding of the non-covalent peptide was replaced with the Tyr SuFEx residue from Enamine. However, this placement was associated with an even slower reaction rate and therefore did not present any benefits. Ultimately, the slow rate observed by the fluorosulfate of mCIR1 constructs at concentrations far greater than its K_D underscored the importance of either new chemistry placement or the need for a new type of chemistry, and due to issues with the former, testing new chemistry was a top priority going forward.

3.3.1. Peptide handling discussion

There were two primary routes investigated in peptide handling: the effect of solvent and the effect of freeze thaw cycles. These were assessed in the SDS PAGE experiment designed to see if solvent influenced labelling of huCD64.

When first looking at the gel, the CD64 labelled bands corresponding to MeOH suspension appear artificially brighter than the surrounding bands. However, this is suspected to be due to the MeOH influencing the fluorescence profile of fluorescein. The flowthrough bands of the peptide in MeOH were also considerably brighter than surrounding ones despite having the same amount of peptide added to each incubation. When the fluorescence of the labelled huCD64 was normalized to the total amount of fluorescence for that lane, it did not translate to a greater amount of labelled huCD64, suggesting it was the brightness was an artifact from the solvent. As well, this solvent system stopped being considered after LCMS data suggested the MeOH was promoting degradation. The fluorine appeared to be replaced by a methyl group, and eventually resulted in peptide precipitating out of solution. Furthermore, the labelled huCD64 bands on this gel corresponding to the PBS incubations for fresh and thawed mCIR1-fluor have similar intensities. Because of differences in peptide amplitude on BLI depending on if the peptide has been frozen or not, it was originally assumed freeze-thaw cycles would also influence covalent labelling of huCD64. However, the intensities of those two bands suggest that the peptide possesses the same labelling capacity despite freeze-thaw cycles.

The BLI experiment using different solvent systems provided insight on the effect of freeze-thaws on non-covalent peptide behaviour. While the amplitude between the frozen and non-frozen stocks differed, mostly for DMSO and ACN, none of the resulting K_D*'s* fit for this data

were significantly different from one another. This could be because these solvent systems were non-ideal for the peptide and during the freeze thaw cycle, there was binding of the peptide to the Eppendorf tube due to the low concentration of the aliquot, which resulted in a functional stock of a lower concentration than assumed, resulting in lower amplitudes but similar affinities. As well, the PBS flash freeze and the PBS stock which was never frozen are nearly identical in amplitude and in K_D. This data suggested that using PBS as our primary buffer was the correct choice and was continued to be utilized for future peptide synthesis and storage.

Finally, we also wanted to use FP to gauge peptide behaviour in solution. Standard values for peptide FP in the absence of proteins is ~ 60 mP or less. Using PBS alone, our mNCIR-fluor and a control peptide both possessed values in that range, while mCIR1-fluor was consistently above the 60 mP threshold regardless of freeze-thaw cycles. Two approaches were then tried in an attempted to reduce the FP; the inclusion of 1x KB which has both a small amount of Tween 20 (0.002%) and BSA in solution as well as the addition of KB with 0.5% Tween 20. BSA is a common additive for protein storage as it helps prevent protein loss to the vessel and it was suspected that the addition of KB to the storage conditions would help minimize peptide loss and destabilization. The Tween 20 was added because it was hypothesized that the high FP value was a result of the peptide self-associating. Because it is a mild detergent, it was originally thought that Tween 20 would disrupt non-covalent interactions between peptides. Of these two approaches, the addition of 1x KB helped to maintain consistency between freeze-thaw and unfrozen samples but the FP values were still above the 60 mP threshold. Interestingly, the addition of Tween 20 had no influence on interactions in solution prior to freezing and seemed to exacerbate peptide-peptide interactions following a freeze-thaw cycle.

All these experiments together provided us with a route for universal peptide handling and storage. PBS was used as the primary solvent for resuspension post synthesis, followed by the addition of 1x KB after click modifications. As well, because of concerns with peptide-peptide association with freeze thaw cycles, all freezing of peptides was minimized to once post HPLC prior to lyophilization, and then again only after the click reactions were completed and the structure was verified.

4. mCIR-2; cp33-nt-sulfonyl fluoride peptide development

4.1. Objectives

Because of the slow rate observed with the fluorosuflate of mCIR1 constructs, testing an alternative chemistry was a top priority. The sulfonyl fluoride is a more electrophilic SuFEx group and was hypothesized to therefore have faster labelling of huCD64 relative to the fluorosulfate. To test this, a 3-(fluorosulfonyl) benzoic acid capping reagent was incorporated into the N-terminus of the cp33 peptide. To validate this peptide, it was critical to assess non-covalent binding behaviour, relative labelling rates, and finally whether it could label monocytes. These experiments were to be carried out using BLI, SDS PAGE, and flow cytometry, analogous to the characterization techniques employed for the previous fluorosulfate peptide.

4.2. Results

4.2.1. Synthesis of cp33-Nt-Sulfonyl Fluoride

cp33-Nt-sulfonyl fluoride was made in an identical fashion to cp33-Nt-fluorosulfate, except this peptide was modified with 3-(fluorosulfonyl) benzoic acid as a capping reagent in place

of acetic anhydride (Figure 4.1). This peptide also had a low yield post HPLC work up of ~ 1.5 mg for the entire ~ 100 mg crude pellet that was worked up. Post lyophilization cp33-Nt-sulfonyl fluoride was easily resuspended in PBS. Following click reactions with DBCO-AZ647, DBCO-PEG4-biotin, and DBCO-PEG8-GUL this construct is referred to as mCIR2-AZ647, mCIR2-biotin, or mCIR2-GUL.

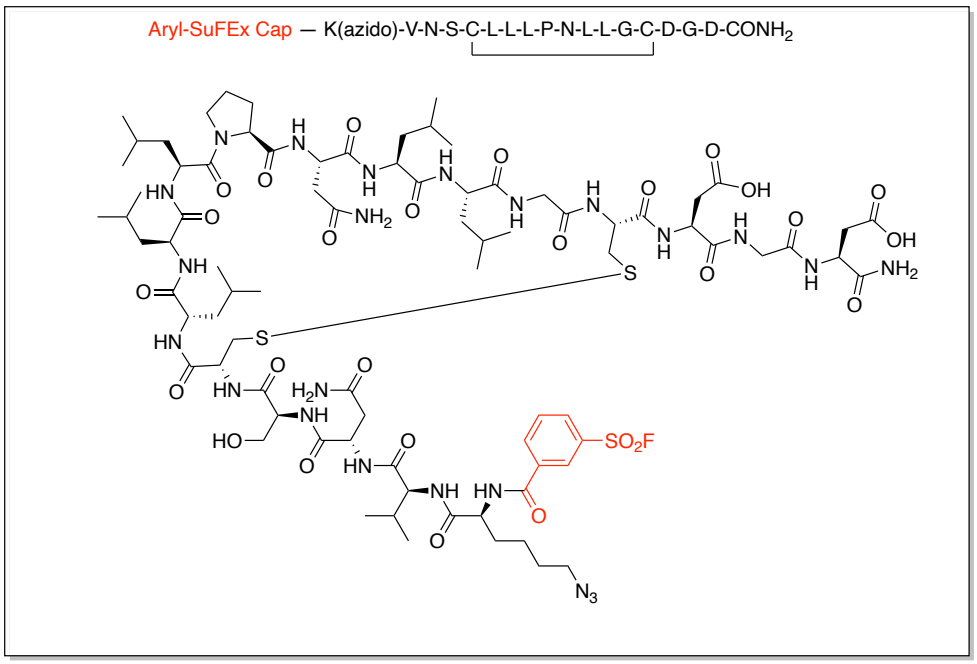

Figure 4.1. cp33-Nt-sulfonyl fluoride
Differences from the base sequence are highlighted in red. The peptide was capped with the benzoic acid sulfonyl fluoride derivative ("Aryl SuFEx cap") instead of the traditional acetic anhydride.

4.2.2. mCIR2 Binding Specificity

To first test if the peptide tolerated the positional shift in chemistry, binding to huCD64 was tested on BLI. The affinity of mCIR2-biotin for huCD64 was not disturbed (K_D = 20.3 nM) with no off-target interactions with CD16a or muCD64 (Figure 4.2).

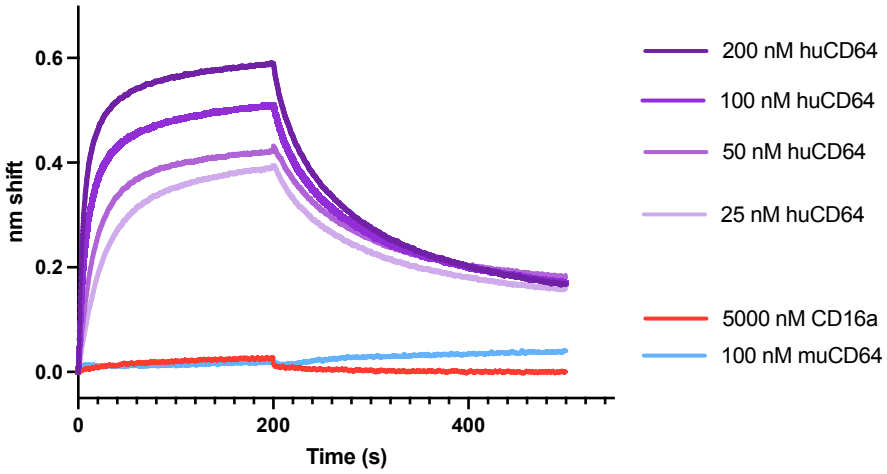

Figure 4.2. mCIR2-biotin affinity and specificity for huCD64 BLI
mCIR2- biotin (50 nM loading solution) associated with the huCD64, muCD64, or CD16a as indicated The peptide had a similar K_D for huCD64 previous constructs (20.3 nM) with negligible off-target binding.

4.2.3. Covalent Labelling of huCD64

mCIR2-AZ647 was tested for its labelling speed relative to mCIR-1. For this, the two mCIRs clicked to AZ647were incubated with huCD64 for 4 h and run on a SDS PAGE. When comparing pixel intensity for the labelled proteins, the sulfonyl fluoride of mCIR2-AZ647 is ~ 10x brighter than the fluorosulfate of mCIR1-AZ647 suggesting that the rate of covalent labelling was faster (Figure 4.3).

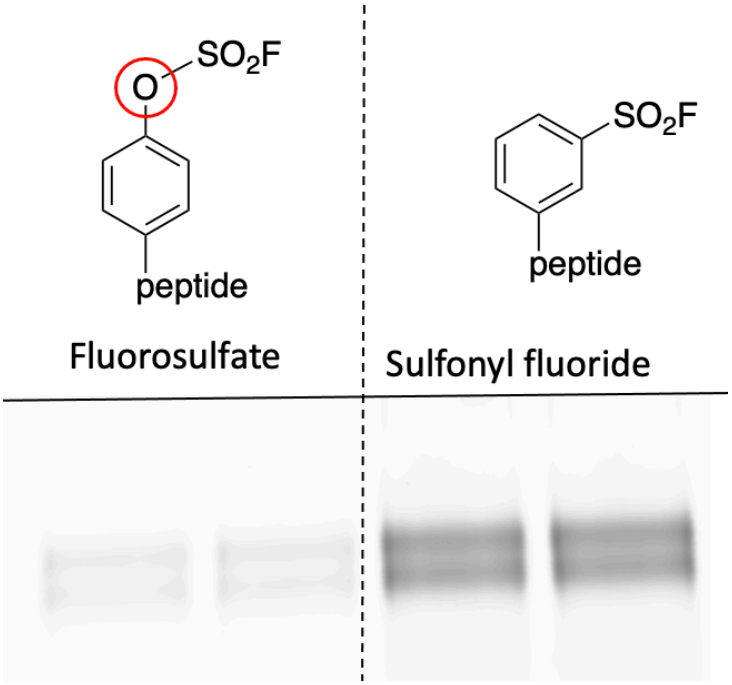

Figure 4.3. Comparative labelling of huCD64 by mCIR1-AZ647 vs mCIR2-AZ647
Image of the SDS PAGE gel with mCIR-1 and mCIR-2 clicked to fluorescein incubated with huCD64. Labelling by the sulfonyl fluoride chemistry (right) was 10x faster than labelling seen with the fluorosulfate.

Prior to conducting a full kinetic profile with mCIR2-AZ647, the stability of the base peptide cp33-Nt-sulfonyl fluoride was monitored in solution over the course of 2 days (Figure 4.4). Because the AZ647 handle does not ionize well on LCMS, the unmodified cp33-Nt-sulfonyl fluoride peptide was used to monitor stability.

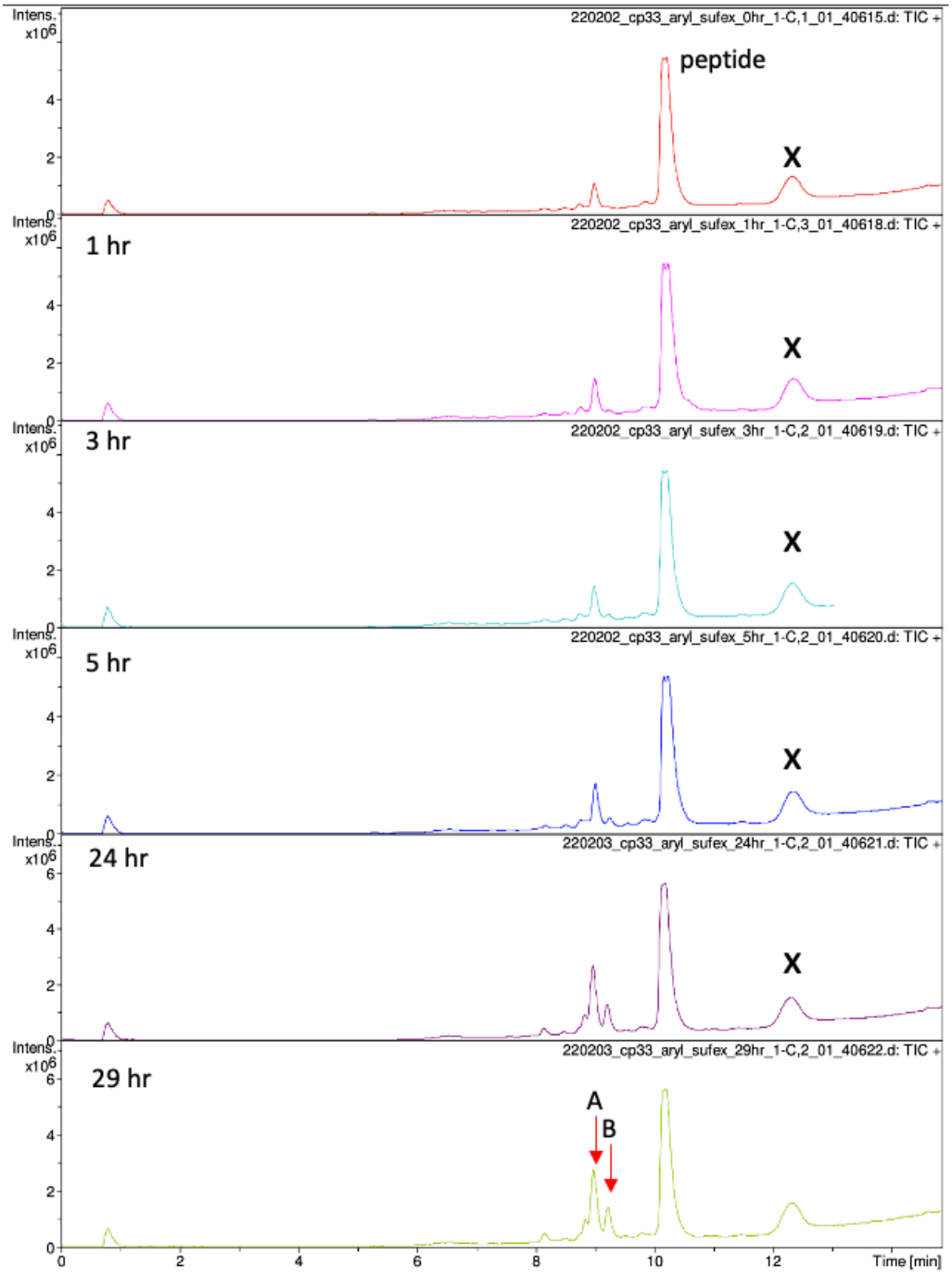

Figure 4.4. cp33-Nt-sulfonyl fluoride LCMS stability up to 29 h shown
Total ion chromatograms for 0 – 29 h mCIR-2 in H_2O. Peaks A and B are the degraded product of the main peptide peak. While ionization peaks resembling 50% the height of the base peak, the UV chromatograms (not shown) for the same peaks are < 10% the height of the base UV peak. Peaks denoted by X are column contaminants.

To establish the full kinetic profile of mCIR2-AZ647 a time-based SDS PAGE experiment with this construct with huCD64 was conducted. This experiment was carried out in 2:1 conditions (mCIR:protein) (Figure 4.5). The labelling of huCD64 by mCIR2-AZ647 plateaued by 24 h and enabled direct quantification of fraction labelled, to yield a k_{obs} of 3.37×10^{-5} s^{-1}.

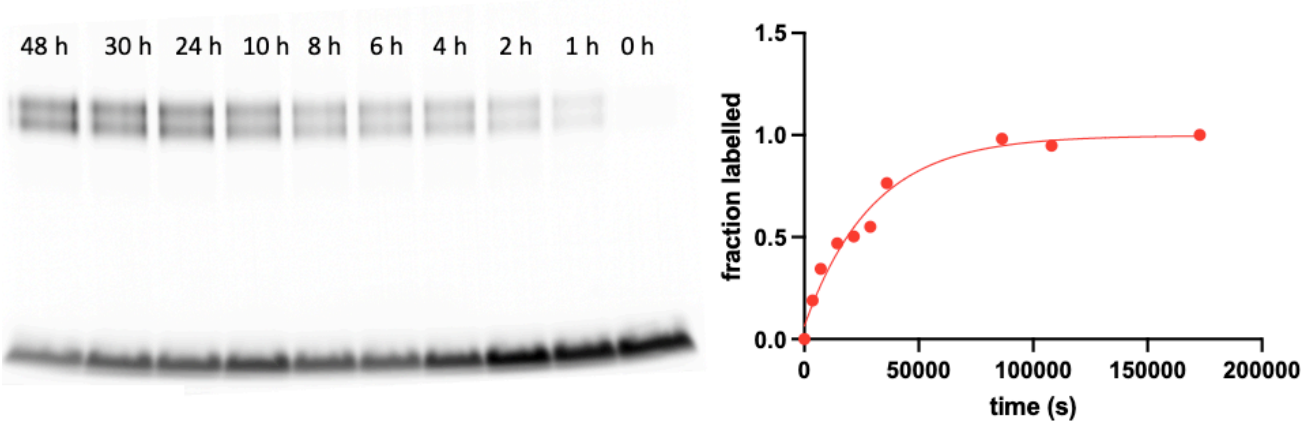

Figure 4.5. mCIR2-AZ647 kinetic SDS PAGE experiment
The 4-20% acrylamide reducing gel on the left. Top bands on the gel correspond to labelled huCD64 by mCIR2-AZ647, while the bands on the bottom of the gel are excess mCIR2-AZ647 that were unreacted. Figure on the right is a graphical illustration of the data on the left. Band intensities were converted to fraction labelled and then fit to obtain a k_{obs} value.

Furthermore, a gel to assess labelling specificity confirmed that following 3 h of incubation (which achieved ~ 50% labelling of huCD64), muCD64 had a small amount of labelling, with no detectable labelling of CD16a (Figure 4.6).

huCD64	-	-	+
muCD64	-	+	-
CD16a	+	-	-
mCIR-2	+	+	+

Figure 4.6. mCIR2-AZ647 specificity fluorescent gel
AZ647 imaged using the Cy5 channel. Dark bands at the bottom of the gel are unreacted mCIR2-AZ647. Only significant labelling of huCD64 was detected, with some background labelling of muCD64.

Labelling of monocytes by mNCIR-AZ647, mCIR1-AZ647, and mCIR2-AZ647 were repeated using both IFNγ activated and non-activated monocytes at 2-12 h time points (Figure 4.7). IFNγ activated cells had notably greater binding/labelling by the m(N)CIRs, with mCIR2-AZ647 having a comparable performance to the control antibody.

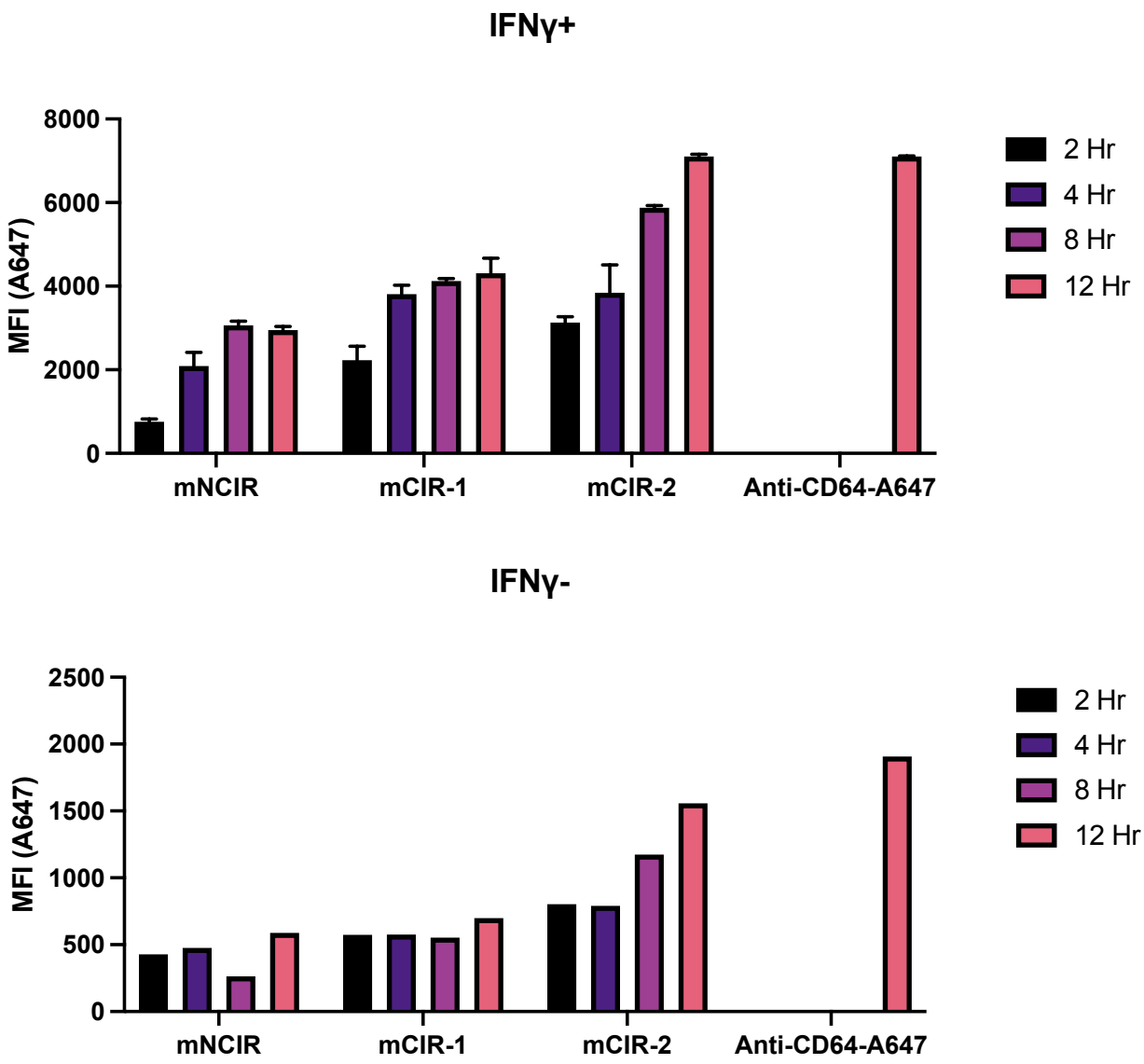

Figure 4.7. Labelling of U937 monocyte (IFNγ +/-) by m(N)CIRs
Top graph illustrates labelling/binding of huCD64 on U937 monocytes either IFNγ activated (+) (top) or non-activated (-) (bottom) at 4 ˚C, using mNCIR-AZ647, mCIR1-A647, and mCIR2-A647. Time dependent increase with mCIR2-AZ647 eventually equals anti-huCD64-A647 (alexafluor 647) indicating reaction completion.

4.2.4. cp33 L7YL8N sulfonyl fluoride

The L7YL8N with the terminal sulfonyl fluoride was unable to be successfully synthesized. This sequence was prone to aspartimide formation, even with the use of the DG fragment. As well,

it had significantly lower solubility further increasing the difficulty of synthesizing and isolating this peptide.

4.2.5. Ternary Complex Formation by m(N)CIRs

First attempts to evaluate ternary complexation were done on flow cytometry using U937 monocytes and HEK PSMA(+) cells, using the mNCIR-GUL and mCIR1-GUL. This experimental approach was unsuccessful with no identifiable ADCP occurring for the m(N)CIR systems, while a positive control using a previously established cARM system successfully induced ADCP.

ADCP induction depends on a series of factors beyond just ternary complexation. For that reason, BLI investigations into ternary complexation were conducted instead using solubilized versions of the proteins to simplify ternary complex parameters. BLI ternary complexes utilized huCD64 and PSMA either immobilized on the probe through a biotin tag or preincubated with an m(N)CIR in solution. This experiment format was first carried out using the mNCIR-GUL preincubated with PSMA with huCD64 immobilized on the probe and saw a distinct concentration dependent association of mCIR•PSMA onto the probe (Figure 4.8).

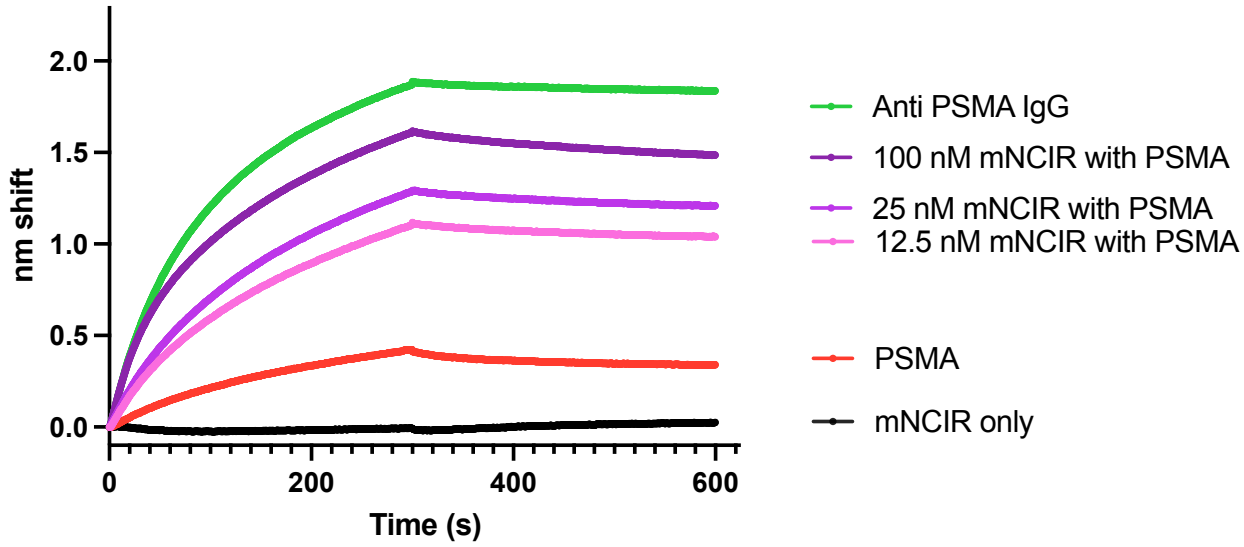

Figure 4.8. Ternary complex with mNCIR-GUL preincubated with PSMA and biotinylated huCD64 on the probe

Biotinylated huCD64 (50 nM) loaded onto streptavidin probes, associated with 100-12.5 nM mNCIR-GUL preincubated with 200 nM of biotinylated PSMA. Probes were quenched with biotin before being dipped into the incubated solutions, but there were still streptavidin sites free indicated by the background loading rate of PSMA onto the probe. However, background loading is lower than the association with any construct, The Anti-PSMA IgG line at the top of the graph was the positive control and suggested the assay format could enable ternary complex formation. The mNCIR-only well had the mNCIR construct alone with no PSMA. The binding of the construct to the immobilized huCD64 is undetectable in this system assay format due to the small size of the mNCIR-GUL.

However, when this format was reversed with biotinylated PSMA immobilized on the probe and huCD64 preincubated with the mNCIR-GUL, there was a distinct decrease in the amount of mNCIR-GUL•huCD64 that was able to load onto the probe (Figure 4.9).

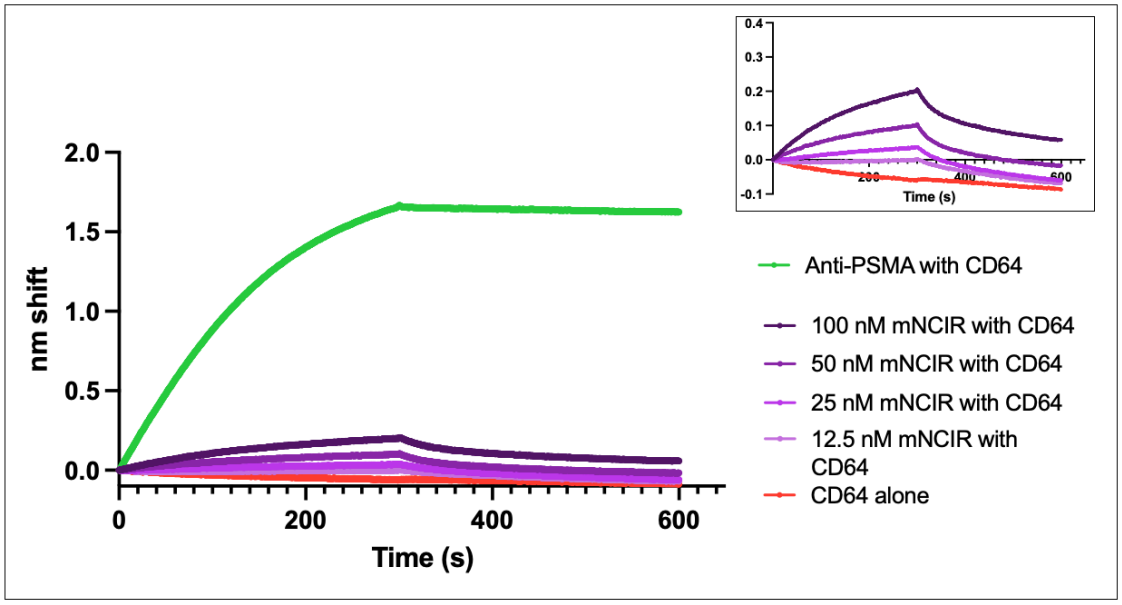

Figure 4.9. mNCIR-GUL preincubated with huCD64 and biotinylated PSMA on the probe
50 nM of biotinylated PSMA was loaded onto the probe, and 50 nM of huCD64 was incubated with 12.5-100 nM mNCIR-GUL. Ternary complexation on the surface of the probe was greatly reduced in comparison to the inverse format, however, the success of the positive control indicates this assay format was functional.

Analogous experiments conducted with mCIR1-GUL also demonstrated that preincubation with PSMA lead to a better signal than with huCD64 (Figure 4.10).

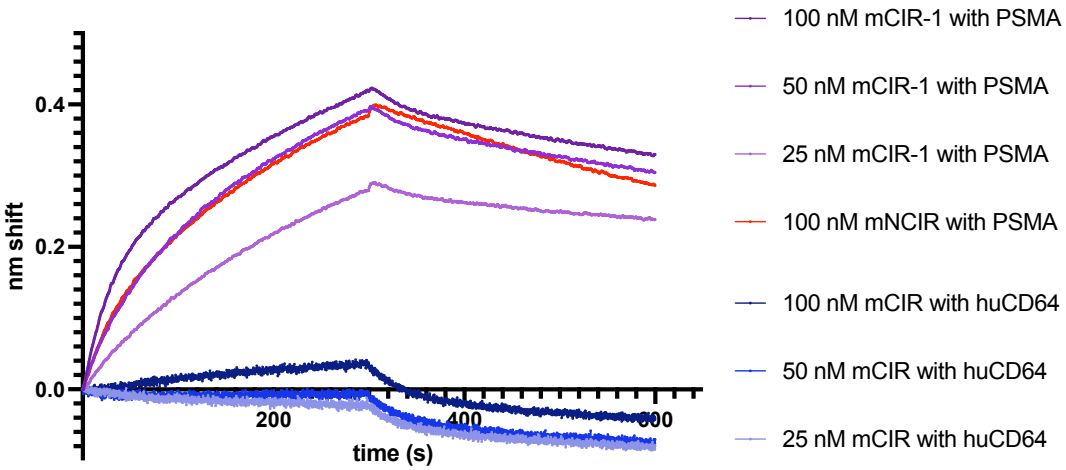

Figure 4.10. mCIR1-GUL BLI ternary complex with PSMA preincubation
Differences in BLI sensograms when mCIR1-GUL is preincubated with PSMA (purple) versus with huCD64 (blue). Significantly more complexation was seen when preincubation

was carried out with PSMA than huCD64, suggesting that order of addition for the mCIR is important.

Moreover, the same pattern was seen with mCIR2-GUL, where preincubation with PSMA resulted in stronger signal, indicative of greater complexation with the protein on the probe (Figure 4.11).

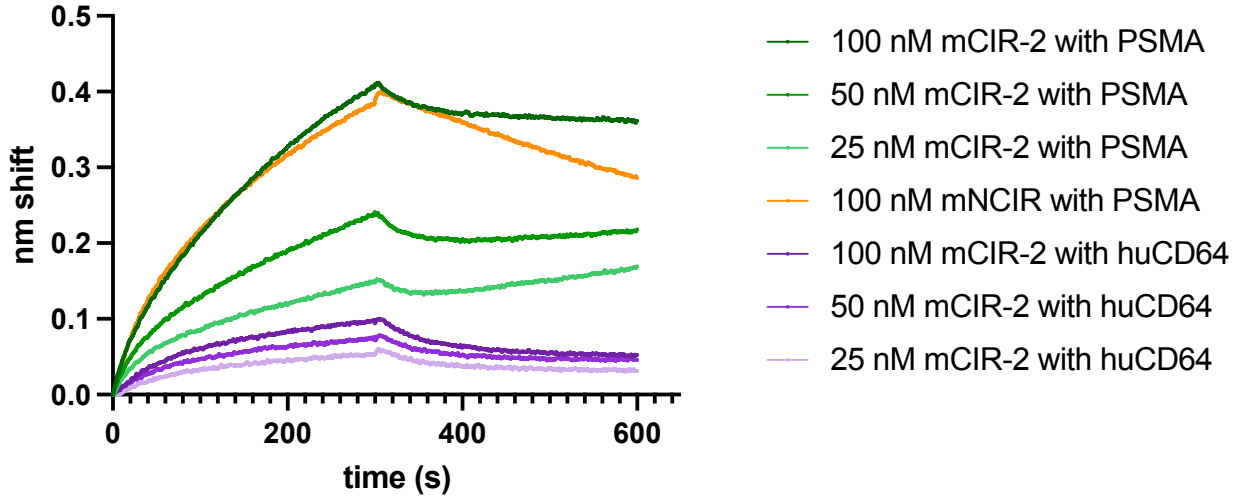

Figure 4.11. mCIR2-GUL BLI ternary complex
Differences in BLI sensograms when mCIR2-GUL is preincubated with PSMA (green) versus with huCD64 (purple). The mNCIR preincubated with PSMA was used as a positive control (orange). Significantly more complexation was seen when preincubation was carried out with PSMA than huCD64, following the same pattern seen for mCIR1-GUL and the mNCIR-GUL.

Based on the consistent behaviour between m(N)CIRs on BLI, another ADCP assay was carried out with a focus on the order of addition of reagents. ADCP assays using fluorescent streptavidin beads were carried out using mCIR1-biotin and the mNCIR. At the time the cp33-Nt-sulfonyl fluoride peptide needed to be resynthesized so no mCIR2 constructs were included in this experiment. The flow experiment was run by Eden Kapcan in the Rullo Lab. From these experiments, it was found that the mCIR induced ~ 46 % ADCP while the mNCIR-biotin induced ~ 8.5 % ADCP (Figure 4.12). Of particular interest is the fact that when this same experiment had

been conducted previously with preincubation of the m(N)CIR with monocytes first, the m(N)CIRs failed to elicit any ADCP in that format.

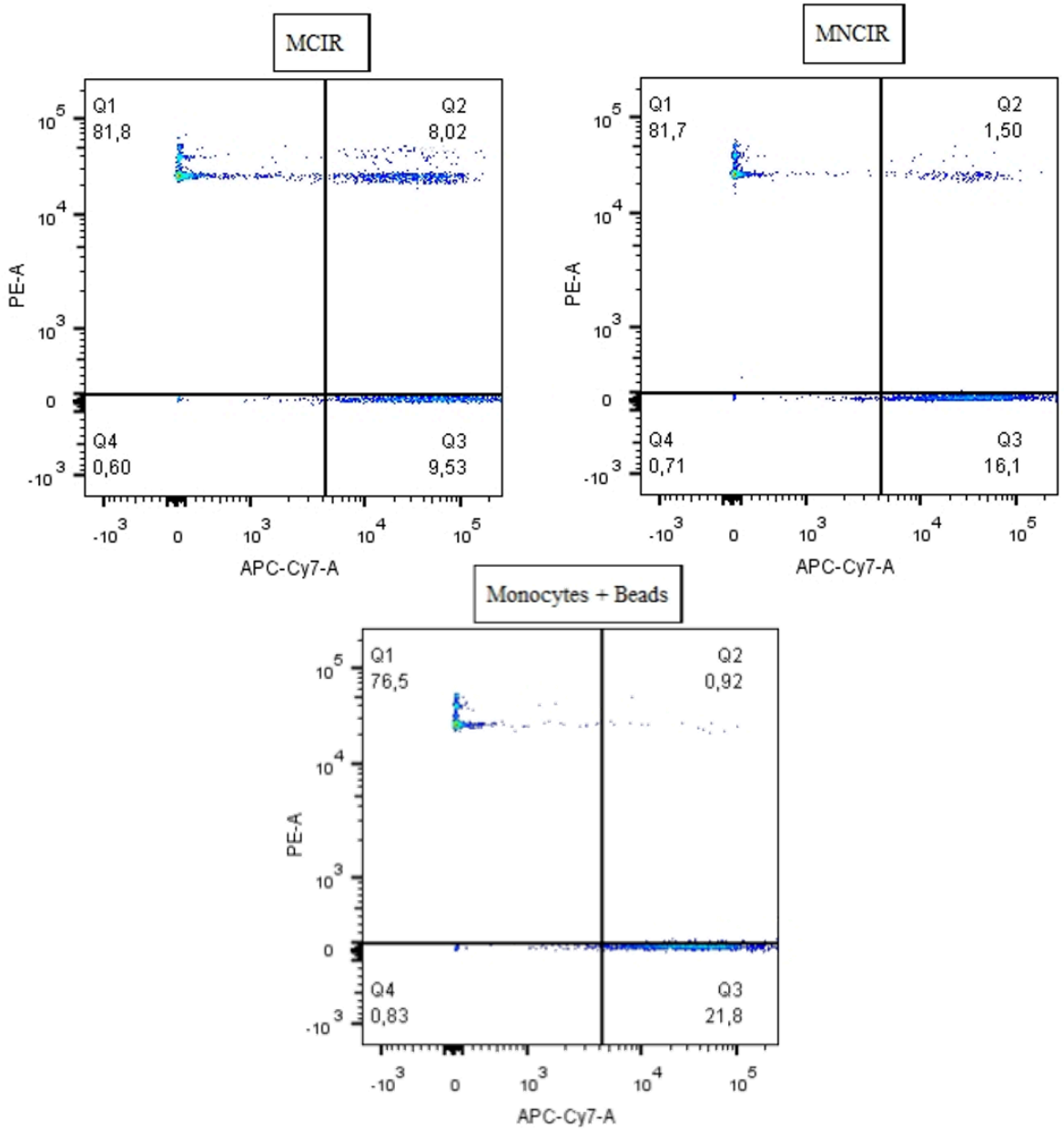

Figure 4.12. ADCP assay using Streptavidin-Beads Preincubated with mCIR1-biotin (MCIR) and mNCIR-biotin (MNCIR)

Events in quadrant 1 indicate beads, events in quadrant 3 correlate to monocytes, and events in quadrant 2 indicate a double positive for PE fluorescence and DiD stained cells indicating successful phagocytosis.

This ADCP experiment was repeated using mCIR1-biotin, mCIR2-biotin, and the mNCIR-biotin but this experiment was designed to also probe the effect of covalent labelling. To do this, the constructs were preincubated with fluorescent streptavidin beads and either placed on ice for 8 h with the monocytes, to enable labelling, or were added to the cells just prior to being put at 37 ˚C for 1 h to enable ADCP. Notably, the incubations on ice did not have fetal bovine serum added to them due to the high amount of BSA in the medium. As well, this experiment utilized a cARM-antibody treatment as the positive control because this system has been previously validated in the Rullo Lab.

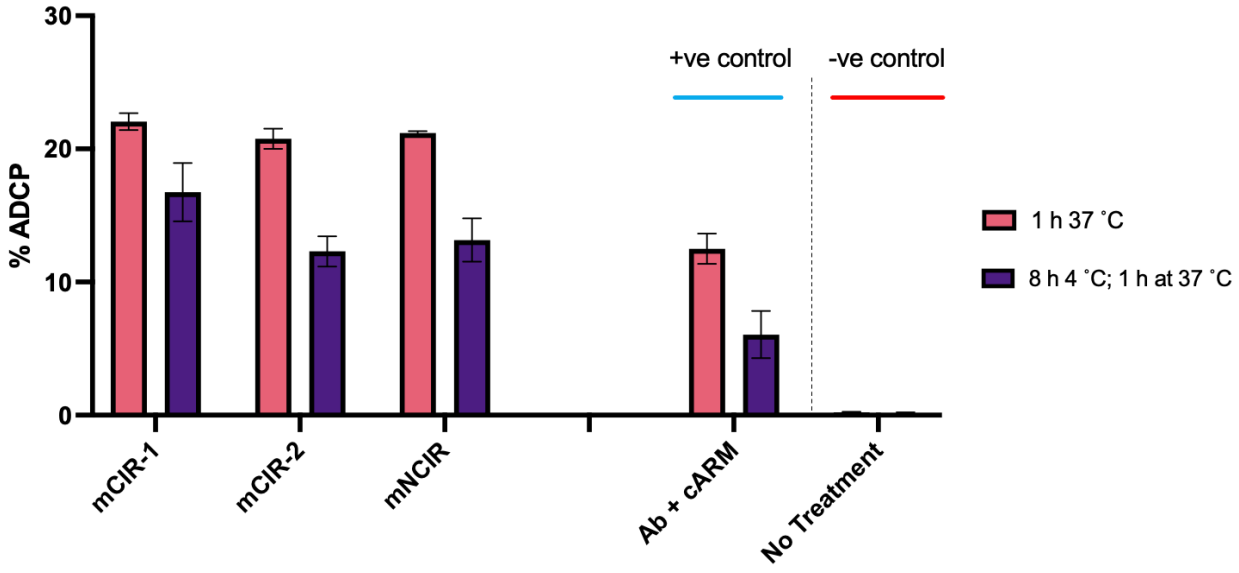

Figure 4.13. Streptavidin-Bead ADCP using mCIR1-biotin, mCIR2-biotin, and mNCIR-biotin with and without preincubation for 8 h on ice.

This experiment was run by Sissi Yang, and used 150 000 monocytes and 150 000 beads per incubation condition. Pink bars correspond to treatment wells which had the construct-bead incubation added to cells just prior to being placed at 37 ˚C, whereas purple bars represent %ADCP for treatments which were incubated with the monocytes for 8 h on ice. The positive control for this experiment was the antibody (Ab) + cARM bars, while the negative control had no treatment and reflected background ADCP.

The 8 h incubation samples had lower ADCP values than the treatments with no prior incubation. This is likely because the monocytes were stressed by being kept on ice for 8 h without the fetal bovine serum, and did not have this media to help with recovery when brought back to 37 ˚C. The pink bars, which reflect m(N)CIR performance due to non-covalent interactions are indistinguishable from one another, which is to be expected as all these constructs have identical non-covalent properties. Notably, this data suggests that targeting the immune cell directly results in greater function in comparison to using antibody-recruiting platforms.

To gain a better understanding of ternary complex formation, a series of BLI experiments were performed in an attempt to define the composite K_D's which describe ternary complex formation. The experiments were designed to isolate individual binding interactions within the ternary complex between the m(N)CIR, PSMA, and huCD64 without confounding simultaneous interactions. These experiments attempted to probe the affinity for the mCIR-GUL moiety (both mCIR1 and mCIR2) for PSMA in the absence of CD64 (Figure 4.14), the affinity of mCIR-GUL-labelled-huCD64 for PSMA (Figure 4.15), and the affinity the mCIR-GUL•PSMA complex for huCD64 (Figure 4.16). The final experiment utilized 100 nM PSMA in the dissociation buffer, and so the dominant measured binding interaction should have been the association and dissociation of mCIR-GUL•PSMA with huCD64. However, sensograms from these experiments were unable to be fit on Prism either due to biphasic association curves, negligible dissociation curves, or a combination of the two.

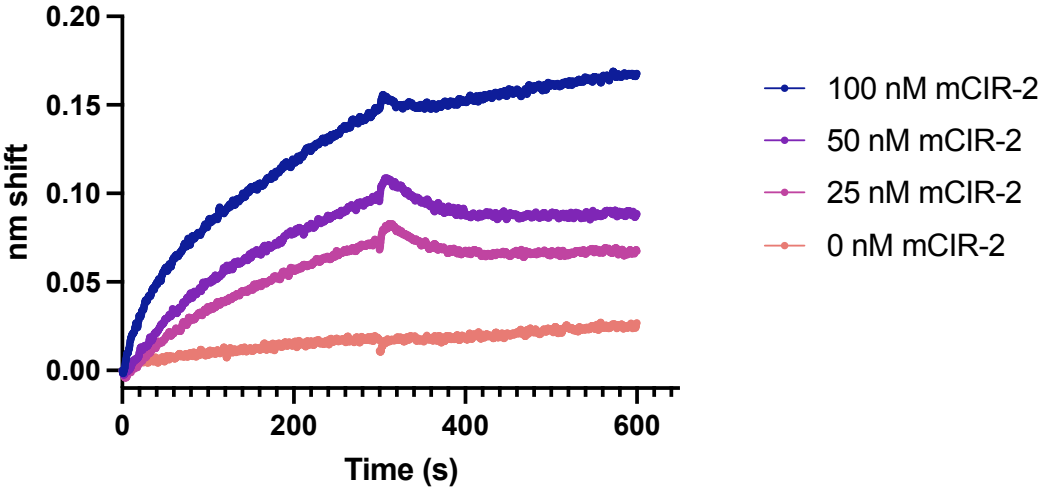

Figure 4.14. Affinity between mCIR2-GUL and Immobilized PSMA
50 nM biotinylated PSMA immobilized on the probe and associated with increasing concentrations of mCIR2-GUL. This data could not be fit due to the negligible k_{off} rate, which does indicate tight binding of our construct to PSMA.

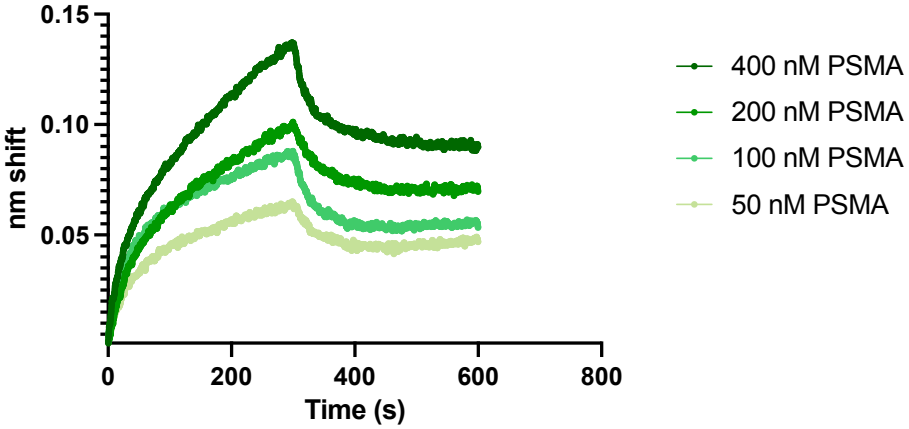

Figure 4.15. biotinylated huCD64 labelled by mCIR2-GUL associated with PSMA
Biotinylated huCD64 (50 nM) incubated with 50 nM mCIR2-GUL overnight in solution for full labelling, before being dipped into solutions with increasing concentrations of PSMA. This data could not be fit due to the biphasic association curves and negligible dissociation curves.

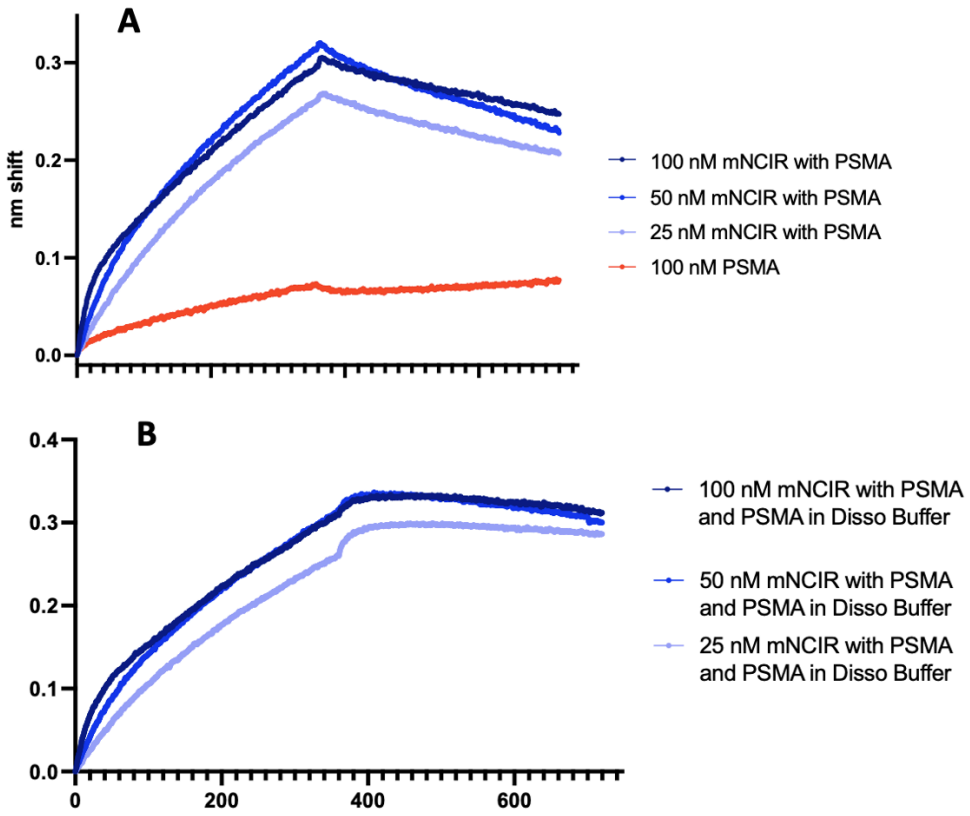

Figure 4.16. mNCIR-GUL preincubated with 100 nM PSMA and then dissociated with 100 nM PSMA or without 100 nM PSMA in the dissociation buffer

Biotinylated huCD64 (50 nM) was loaded onto the probe. Increasing concentrations of mNCIR-GUL preincubated with 100 nM PSMA and then dissociated in (A) pure dissociation buffer, 1x KB or (B) in the presence of 100 nM PSMA.

4.3. Discussion

4.3.1. SuFEx installation in peptide synthesis

For this project, the incorporation of SuFEx chemistry was attempted using 3 strategies. Initial efforts tried to install the SuFEx moiety came from reacting a Tyr residue with SuFEx containing residues. Using LCMS monitoring it appeared that the SuFEx chemistry was hydrolyzing and producing the sulfate functional group instead of the sulfonyl fluoride. The second

route for SuFEx installation came from using an Fmoc-Tyr (fluorosulfate) residue produced by Enamine for our lab. This pre-made construct enabled incorporation of the covalent chemistry at any point within the sequence and was stable to SPPS synthesis and cleavage conditions and was used to make mCIR-1. The final route for the incorporation of SuFEx chemistry was the utilization of 3-(sulfonyl fluoride) benzoic acid. This moiety only possesses a carboxylic acid and no primary amine to continue to extend the peptide chain and was thus used as a capping reagent for cp33 peptides and for mCIR-2 synthesis. Both the fluorosulfate and sulfonyl fluoride had similar efficiencies of incorporation, there were never identifiable peaks in the crude LCMS of these peptides with either moiety unincorporated with the rest of the peptide intact.

4.3.2. Properties of mCIR2 constructs

All mCIR2 constructs are equipped with a sulfonyl fluoride which proved to be significantly faster with preserved selectivity and complete labeling of huCD64 achieved within 24 h. The sulfonyl fluoride residue is a more electrophilic chemistry and enables faster reactions than the fluorosulfate. As well, the two SuFEx groups possess different chemoselectivities, and it is possible that the sulfonyl fluoride is reacting with a residue that the fluorosulfate could not. Furthermore, this more electrophilic chemistry was expected to be associated with an increased hydrolysis/degradation rate. Literature molecules equipped with sulfonyl fluorides, depending on their substituents, can have 50% degradation within 24 h or less.[45] However, this peptide showed intact chemistry for up 2 days at RT, after which its stability was not investigated further. The effect of electron donating and withdrawing groups are known to influence the stability of the sulfonyl fluoride, with electron withdrawing groups having more rapid hydrolysis rates. In the case of our peptide, the adjacent amide group likely provides the phenyl ring with electron density,

decreasing the electrophilicity of the sulfonyl fluoride functional group and increasing its stability in solution. Ultimately, the comparative labelling rates observed for the 3 successfully synthesized covalent peptides followed the order mCIR-2 (3.37×10^{-5} s^{-1}) >> mCIR-1 (1.05×10^{-7} s^{-1}) >> $L7Y_{SuFEx}L8N$ (not determined).

4.3.3. Testing the mCIRs for ternary complex formation

The first attempt to test ternary complex formation by mNCIR-GUL and mCIR1-GUL was the failed ADCP experiment using HEK PSMA+ cells and human U937 monocytes. The induction of ADCP relies on a series of factors including the number of complexes which can form, the stability of those complexes, and sterics between the two cells. The failure for the m(N)CIR system to induce ADCP was initially thought to because of a steric penalty from bridging two cells, which put too much strain on the system resulting in no ADCP. For that reason, we instead chose to test the m(N)CIR system on BLI using only the proteins of interest to eliminate any potential cell-cell effects.

Initial BLI experiments to monitor ternary complexation were carried out with mNCIR-GUL preincubated with huCD64 or PSMA in solution. The preincubation with PSMA saw greater ternary complexation form on the probe relative to preincubation with huCD64. The background loading rate of PSMA in this experiment is attributed to the fact that the PSMA was biotinylated and despite using a 500 nM biotin quench to saturate the probe, there were still unoccupied streptavidin sites which bound the PSMA. Replications of this experiment using non-biotinylated PSMA preincubated with the mCIRs demonstrated a similar binding pattern. This suggests that the binding of PSMA enforced a conformation of the m(N)CIR which enabled CD64 binding, although the inverse was not true. Additionally, the binding curves generated from these

experiments were not fit on Prism because they are the result of multiple binding interactions occurring simultaneously. As a result, any K_D fit from that data would have reflected cumulative binding interactions (Figure 4.17). A series of BLI assays were then designed in order to characterize the individual affinities of the ternary complex and to deconvolute the data from initial ternary complex BLI assays.

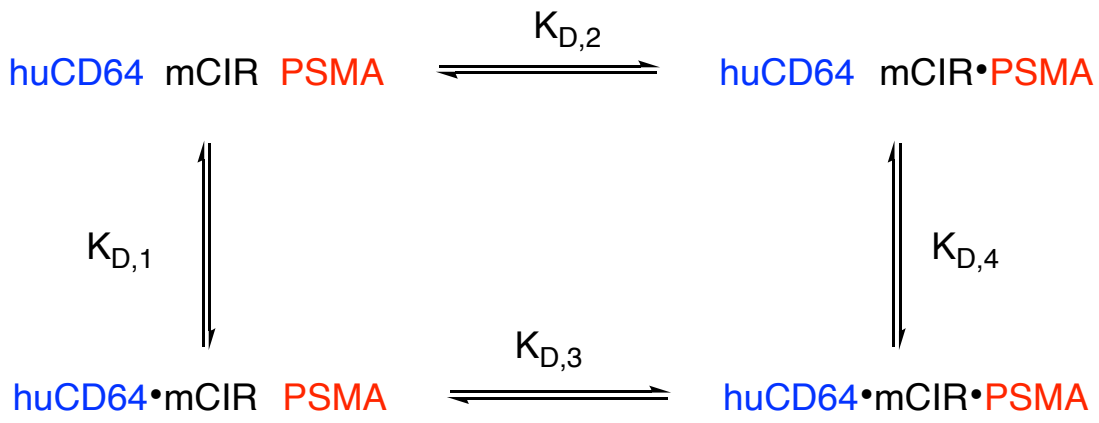

Figure 4.17. Ternary complex pathways

The BLI experiments aimed to isolate $K_{D,2}$, $K_{D,3}$, and $K_{D,4}$, as we had an estimate for $K_{D,1}$ from initial experiments with huCD64 and m(N)CIR-biotin. To isolate $K_{D,2}$, biotinylated PSMA was immobilized on super-streptavidin probes and associated with increasing concentrations of mCIR2-GUL. These super-streptavidin probes are designed to better detect small molecule binding to immobilized proteins as opposed to streptavidin probes which provide better signal for the inverse format. This experiment produced a respectable association, despite being a low nm shift, but the dissociation curves were unusually linear. The upwards drift on the highest concentration mCIR well (and the 0 nM mCIR well) have previously been attributed to evaporation of the well-volume.[46] However, the two other mCIR concentrations have no discernible

dissociation from the probe –this lack of dissociation suggests binding much tighter than literature values for the K_D of GUL and could be the result of multimeric-complexing between mCIR constructs resulting in an avidity enhanced interaction.

To isolate $K_{D,3}$, biotinylated huCD64 was incubated with mCIR2-GUL for 24 h (RT, in solution) and then associated with increasing concentrations of PSMA. Sensograms for this experiment displayed biphasic association curves. This was particularly unexpected for the experiments for $K_{D,3}$ because following the 24 h incubation, huCD64 should be completely labelled by mCIR2-GUL, and so the only measurable binding interaction is between GUL and PSMA. Biphasic binding curves indicate two binding populations – one with a fast association and a second slower association. This in turn suggests the existence of two mCIR populations.[47] The reason for such populations is unclear, but it could be due to conformational changes in the whole mCIR structure, potentially a result of one of the peptide synthesis issues listed prior or due to aggregation of the peptide. The alternative to the biphasic binding curves being due to mCIR populations would indicate non-specific binding interactions between huCD64 and PSMA. Where the initial portion of the association curve is attributed to specific binding, and the portion which represents slow binding is from non-specific interactions (Figure 4.18A). However, if non-specific binding was the predominant cause for the biphasic binding curve, subtraction of background interactions should have produced an ideal binding curve. When that approach was applied to the $K_{D,4}$ data, it still produced a biphasic binding curve (Figure 4.18B). As a result, it is likely that the biphasic curves seen in both the experiment to isolate $K_{D,3}$ and $K_{D,4}$ are a result of a combination of factors, including non-specific interactions between huCD64 and PSMA as well as aggregation of the peptide in solution.

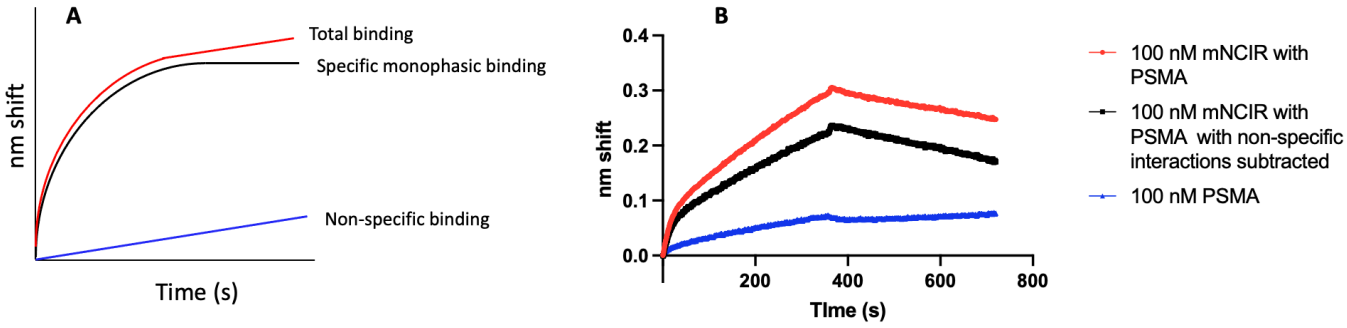

Figure 4.18. Background subtraction of PSMA association still produces biphasic binding curves **A)** Theoretical binding curves illustrating specific binding curves (black), non-specific binding curves (blue), and the representative total binding from specific and non-specific interactions (red). **B)** Data from Figure 4.15A for the greatest concentration point with the values of the non-specific binding between PSMA and huCD64 subtracted. Assay format: huCD64 immobilized on the probe and associated with 100 nM mNCIR-GUL preincubated with 100 nM PSMA.

In addition to the biphasic association, the dissociation curves exhibited incredibly slow k_{off} rates, which suggest tight binding but complicate fitting processes as there is no visible "off" rate to fit. In the experiment to obtain $K_{D,4}$ – the affinity between huCD64 and mNCIR-GUL•PSMA- excess PSMA was included in the dissociation buffer. This was done to eliminate PSMA dissociation from the probe contributing to the observed off rate. The result was an incredibly slow dissociation of the complex from the huCD64 on the probe ($k_{off} \leq 2.38 \times 10^{-7}$ s^{-1}). This pattern of little to no dissociation was seen with all the ternary complexes assessed by BLI. With the suspected multiplexing of the peptide, the slow off rate could be a result of cumulative avidity driven interactions between peptide•peptide constructs and the two terminal proteins. Ultimately, the confounding non-ideal nature of the ternary complex curves obtained via BLI prevented quantitative analysis of ternary complex formation by the m(N)CIR system. Moving forwards, BLI is unlikely to be a viable route for characterization of ternary complexes for this system.

Despite the difficulties with the kinetic approach to characterize ternary complexes, activity ADCP assays demonstrated the potential function of the mCIR system. Both bead-ADCP assays carried out for this project where the constructs were first incubated with the streptavidin beads were successful at inducing monocyte function. The first ADCP experiment which only tested mCIR1-biotin and mNCIR-biotin had respectable ADCP values with up to 46% for mCIR1. The value for mNCIR-biotin is thought to be artificially low because this stock had been used for previous experiments and had been through multiple freeze thaw cycles which has been shown to affect peptide behaviour in solution.

As a result, the second ADCP experiment utilized fresh stocks all of which were handled in the same fashion, therefore any differences in the resulting data would be due to peptide characteristics and not because of handling. The second experiment also differed in that it had two incubation periods; one where each m(N)CIR/control was incubated on ice with the cells for up to 8 h to enable labelling, and another where the treatments were added just prior to placing the cells at 37 ˚C. While on ice, all biological activity of the monocytes is suspended, with negligible ADCP or receptor turnover occurring, giving the mCIR1-biotin•bead and mCIR2-biotin•bead complexes an opportunity to label huCD64. However, due to the hydrophobic nature of the cp33 derivatives, it was a concern that the peptide would non-specifically associate with BSA in the media. To prevent this, fetal bovine serum, which is the source of BSA in the cell media, was left out of the incubations. This likely stressed the monocytes when they were moved from ice to 37 ˚C to enable ADCP. As a result, the cells for the 8 h time point had higher death counts and lower activity as seen by the lower ADCP values across all experimental and control groups.

In the same experiment, the incubations of m(N)CIR-biotin•bead which were put directly at 37 ˚C had higher ADCP values than the ones for the 8 h incubation on ice. This difference is attributed to the fact that the monocytes did not undergo a cooling and rewarming cycle, eliminating the stress that the 8 h time point cells experienced. As well, all values acquired for the treatments put directly at 37 ˚C are nearly identical to one another. Given that neither mCIR1 nor mCIR2 has rapid labelling of huCD64 within 1 h, this incubation period reflects the noncovalent activity of the m(N)CIRs. Because they have indistinguishable noncovalent binding properties, this resulted in ADCP values which closely resembled one another. Furthermore, these cell-based constructs outperformed the antibody-based cARM control, suggesting direct engagement of the monocyte is a potentially more efficacious approach. While this data is preliminary and this experiment should be repeated, but it provides a positive outlook on the immune cell recruiting platform.

5. Conclusion

This thesis has presented a new approach for covalent immune recruitment through mCIRs. In this work, the cp33 IBD has been thoroughly characterized and found to be a specific and high affinity binding peptide (K_D = 52.7 nM). A series of mutants of cp33 were created to establish viable positions to install covalent SuFEx chemistry for huCD64 labelling. From these studies, an *N*-terminal SuFEx moiety has shown the greatest promise for retaining binding capacity while enabling covalent modification of huCD64. Two SuFEx chemistries, fluorosulfates and sulfonyl fluorides, were characterized in this paper. Between the two SuFEx strategies, the sulfonyl fluoride chemistry was the faster chemistry, with complete labelling of huCD64 achieved within 24 h. BLI assays using mCIR1-GUL, mCIR2-GUL, and mNCIR-GUL demonstrated the capacity for these

structures to bridge huCD64 and PSMA simultaneously. However, BLI assays revealed an order of addition requirement for the m(N)CIR system. These BLI assays were associated with non-ideal binding curves which were unable to be fit to provide quantitative insight into ternary complex formation by the m(N)CIR constructs. Despite this, streptavidin bead ADCP experiments using m(N)CIR-biotin constructs were successfully able to induce phagocytosis, and preliminary data suggests that the cell-based immune recruiters outperform antibody-targeting systems. Ultimately, the mCIR platform has potential to provide fundamental insight into the requirements of synthetic immune recruitment, and to circumvent established limitations of small molecule immunotherapeutics.

5.1. Future Directions

This thesis has outlined the basis of the mCIR system, completing preliminary work demonstrating mCIR function and limitations. Future work on this project should focus on characterizing mCIR mediated ternary complex formation and simplification and showing mCIR function. As a kinetic based approach using BLI to gauge ternary complex stability proved to be difficult, future attempts should consider using size exclusion chromatography and isothermal titration calorimetry. Both techniques have been used previously in literature to demonstrate ternary complex engagement and stability, and isothermal titration calorimetry can be used to directly extrapolate thermodynamic constants. Furthermore, looking into the effect of linker length and rigidity on complex stability and the requirement for target-preincubation could prove to be a useful stream of research. Testing both longer PEG linkers (~ PEG12), as well as rigid linkers equivalent to the lengths tested in this work could both prove to be useful streams of knowledge. Especially because the binding pocket of GUL is so deep, by providing a longer linker, or one with

a more fixed orientation, the remainder of the linker might be better positioned to interact with CD64 preventing unwanted conformational changes leading to reduced binding.

As well, monocyte-based activity assays including ADCP assays and reactive oxygen species production assays could provide insight on mCIR function. Both ADCP and reactive oxygen species production assays are activity-based assays which depend on the stimulation of CD64 by some factor, in this case mCIRs. Finally, the streptavidin-bead ADCP assay using all the m(N)CIR constructs should be repeated, this time using fetal bovine serum to help with cell recovery to investigate the effect of covalency on huCD64 labelling and monocyte effector function. Together, these streams of research should provide a fuller picture on direct immune cell engagement and covalent labelling as a means for immune recruitment.

6. Materials and Methods

General: DBCO-PEG8-GUL, was synthesized by Ben Lake and Eden Kapcan. DBCO-PEG8-fluorescein was made by Harrison McCann.

6.1. Solid Phase Peptide Synthesis

6.1.1. Peptide Synthesis Reagents

Amino acids for SPPS, reagents were purchased from Sigma Aldrich. To minimize aspartimide formation, most peptides used a pre-made Fmoc-Asp(OtBu)-(Dmb)Gly-OH (DG) unit (EMD Millipore 8521150001). For incorporation of an azide into the peptide sequence, N alpha Fmoc, N epsilon Azido Lysine (ChemImpex 29756) was used. The Fmoc- Tyrosine (fluorosulfate) amino acid was custom made by Enamine for our lab. Peptides with sulfonyl fluorides were made using 3-(fluorosulfonyl) benzoic acid (Sigma Aldrich ALD00038-1G). All resin unless specified was 100-200 mesh rink amide resin (Sigma Aldrich 8550010005). All solvents were bought from Thermofisher.

6.1.2. Peptide Synthesis

All peptides were made using standard Fmoc SPPS procedures on a CEM Liberty Blue Peptide Synthesizer. Peptides were synthesized on a 0.1 mmol scale. Deprotection solutions were 20% piperdine (Millipore Sigma 104094) with 0.1 M oxyma (EMD Millipore 8510860100), activator for SPPS was 1 M DIC (Sigma Aldrich D125407) in DMF, and activator base was 1 M oxyma in DMF. Peptide cyclization was achieved on bead using Fmoc-Cys- (mmt)) (EMD Millipore 8.52031.0005). The mmt protecting group was selectively removed using 0.2%

trifluoroacetic acid (TFA) in DCM while the peptide was on bead, followed by oxidation with 25 mM NCS to oxidize the peptide into its cyclic structure.

6.1.3. Peptide Cleavage and Workup

Post synthesis, peptides were then cleaved and globally deprotected in a TFA cocktail (92.5% TFA, 2.5% TIPS 2.5% phenol, 2.5% H_2O) or modified TFA cocktail for SuFEx containing peptides (95% TFA 2.5% TIPS, 2.5% H_2O). For cleavage, 5 mL of cleavage cocktail was added to the beads and left to incubate at room temp for 3 h with shaking every 15-30 min. The cleaved peptide was then filtered through a glass frit to remove the beads and precipitated using 45 mL of cold diethyl ether (-20 Deg C) The beads were then washed with another 5 mL of cleavage cocktail and precipitated with 45 mL of cold diethyl ether. The crude peptide mixture was pelleted at 2700 RPM for 10 minutes and the ether supernatant was decanted. Crude peptides were then dissolved in 2:1:2 DMF:ACN, acetonitrile, :H_2O and run on LCMS, to confirm successful synthesis. LCMS used an Agilent 1290 Infinity liquid chromatography machine connected to either an LTQ Orbitrap or a MicrOTOF. LCMS samples were run through a reverse phase C18 column (Eclipse XDB-C18, 3.5 µm, 2.1 x 100 mm) using a H_2O/ACN gradient each with 0.1% formic acid (FA). Samples run on the Orbitrap were run for 5 min with a gradient of 5-90% ACN with a speed of 0.4 mL/min. Samples run on the MicrOTOF were run for 15 min with the same parameters as the Orbitrap, but the longer run times provided higher resolution. Peptides were then injected onto a reverse phase HPLC, C-18 column (Thermoscientific prep 25005-159070, 150 x 10 mm, 5 µ particle size) with an H_2O(0.1% FA)/ACN(0.1% FA) solvent system, and run using a gradient of 10-90% ACN (0.1% FA) over 24 min at a rate of 5 mL/min. Absorbance was monitored at 214 nm, 254 nm, 280 nm, and 224 nm. Peptides eluted at 60-70% ACN. Peaks with UV signals were then run on LCMS to

confirm the identity of each peak. Fractions with target masses were pooled and frozen at -80 °C for a minimum of 3 h before being lyophilized for 2 days. Lyophilized peptides were solubilized in PBS and had 0.5-4% DMSO added where necessary to enable better solubilization. Concentration of peptides without the aryl SuFEx moiety were determined using reactions with a stock solution of 13.3 mM biotin-PEG4-DBCO (Broadpharm BP-22295). Once 1:1 reaction conditions were achieved as identified through high resolution LCMS, peptide concentration was then back calculated. Peptides containing the aryl SuFEx had their concentrations determined using a calibration curve of 3-(sulfonyl fluoride) benzoic acid, using an absorbance assay at 280 nm in PBS with 0.1% DMF.

6.2. Peptide Click Reactions

All peptides were modified using strain promoted alkyne azide click reactions between the azide incorporated into each peptide and DBCO fragments on target moieties. Azide containing peptides were clicked to DBCO-PEG4-biotin 4-biotin, DBCO-PEG8-fluorescein, DBCO-AZDye 647 (a far red fluorescent probe), and DBCO- PEG8-GUL. All click reactions were done using 1:1 ratios of azide:alkyne, at 100 μM in H2O. Reactions were monitored by high-resolution LCMS. LCMS samples were run on an Agilent liquid chromatography connected to either the LQ Orbitrap or MicrOTOF mass spectrometers. Total runtime was 5 min (Orbitrap) or 15 min (MicrOTOF) with a 5-95% gradient of ACN a flow rate of 0.4 mL/min. Average time until completion was 3 h with 100% conversion to product. Reactions were then diluted with 10x KB such that the final mixtures were 10% KB. Clicked reactions put into KB were then stored at -80 °C until use.

6.3. Biolayer Interferometry Procedure

General: Generally, either 50 or 100 nM of a biotinylated construct (peptide or protein where indicated) was loaded onto streptavidin coated probes (Sartorius 18-5019) for 180 s. Probes were then moved to wells with 200 µL of 1x KB to establish a baseline. The probes were then associated with target molecules for 200 s. The assays finish by dipping the probes into 200 µL of 1x KB, where the dissociation phase is monitored for 300 s. All graphs for BLI were made on GraphPad Prism.

6.3.1. Characterizing Peptide Affinity and Specificity for HuCD64

Biotinylated peptide was diluted to 50 nM with 1x KB and loaded onto streptavidin probes. Assays for peptide affinity used increasing concentrations of huCD64, prepared from a stock of 11.6 µM huCD64 (Cedaralane Labs FCA-H52H1-100ug). while assays for binding specificity used huCD64, 100 nM muCD64 and 5 µM CD16a. Data acquired from BLI were aligned to the association phase to allow easier comparison between binding curves within experiments. Data corresponding to the dissociation and association phase were fit separately on Prism 8 using Equation 6.1 and Equation 6.2 respectively.

Equation 6.1. Dissociation Model

$$Y = (Y_0 - NS) \times e^{(-k \times x)} + NS$$

Where Y_0 is the binding at time zero, NS is the nonspecific binding at infinity times, in the units of the Y axis, and k is the rate constant in inverse units of the X axis.

Equation 6.2. Association Model

$$K_D = \frac{k_{off}}{k_{on}} \; ; \; L = Hotnm \times 1 \times 10^{-9} \; ; \; K_{ob} = k_{on} \times L + k_{off} \; ;$$

$$Occupancy = \frac{L}{L + K_D}\ ;\ Y_{max} - occupancy \times B_{max}\ ;\ Y = Y_{max} \times \left(1 - e^{(-1 \times k_{ob} \times x)}\right)$$

Hotnm is the concentration of ligand in nM, k_{off} is the dissociation rate, K_{on} is the association rate constant in the units of M^{-1} s^{-1}, K_D is the equilibrium dissociation constant in M, computed as k_{off}/k_{on}, B_{max} is the maximal binding at equilibrium, extrapolated to maximal ligand concentration in the units used to enter the y values.

6.3.2. Ternary Complex Assays on BLI

For ternary complex assays, 50 nM of biotinylated PSMA or huCD64 was loaded onto streptavidin probes. Unless otherwise specified, probes with protein loaded on them were then dipped into solutions with 200 nM huCD64 or PSMA with varying concentrations of cp33 variants modified with GUL (50-100nM). Experiments used either huCD64 or PSMA incubated with anti-PSMA mouse monoclonal IgG (sigma SAB4200257) or mNCIR modified with GUL as a positive control. Sensograms were then aligned to the association phase of the experiment and plotted on Prism 8.0 for visualization of ternary bridging.

6.4. Fluorescence Polarization Procedure

FP, fluorescence polarization, is a technique that can detect binding of small molecules (peptides) to large macromolecules (proteins). Generally, when small molecules with fluorophores are excited with polarized light, they tumble rapidly in solution and emit depolarized light. Upon binding to proteins, the rate at which they tumble is reduced and emitted light is largely polarized. Peptide constructs modified with fluorescein were diluted in 1x KB to a 5 nM solution. Incubations of huCD64 in 1x KB were prepared ranging from 5 nM to 40 nM. Peptide and protein were added together in a black flat-bottom 96-well plate and allowed to equilibrate for 15 min at RT. Following

this the equilibration period, the plate was read on a Tecan Spark plate reader using the fluorescence polarization setting with $\lambda_{excitation}$ set to 485 nm and $\lambda_{emission}$ set to 535 nm. Values for relative fluorescence units (RFU) of parallel polarization and RFU of perpendicular polarization were then put into Equation 6.3.

Equation 6.3

$$p = \frac{(I_{\parallel} - I_{\perp})}{(I_{\parallel} + I_{\perp})} \times 100$$

Where $I_{\parallel}$ is the parallel RFU, $I_{\perp}$ is the perpendicular RFU, and p is the polarization ratio in mP.

6.5. Fluorescent SDS PAGE Procedure

SDS PAGE using fluorescent reagents provided a convenient way to visualize proteins labelled by the peptide and could be used to establish the kinetics and specificity of protein labelling. Gels used for these experiments were either 14% acrylamide gels (Fisher Scientific XP00140BOX) or 4-20% gradient acrylamide gels (Thermo Scientific XP04200BOX). Unless stated otherwise, 1.6 μM peptide clicked to either fluorescein or AZ647, was incubated with 800 nM target protein for an increasing amount of time in 15 μL volumes. All protein stocks and peptide stocks were kept covered at room temperature unless otherwise noted until loading on the gel. Samples were reduced using 2x Laemmli buffer (Sigma-Aldrich S3401-10VL) and boiled for 5 min at 95 ˚C prior to beginning SDS PAGE. 15 μL of each sample was loaded into the wells. When using samples with various proteins, 15 μL of a protein ladder ranging from 10-250 kDa was run as well. (Bio-Rad1610363). All gels were first run for 15 min at 90 V, followed by 45 min at 120 V. The gel box was covered with aluminium foil at all times to reduce exposure to light. Gels were then washed 2x with H_2O and imaged on Cytiva Typhoon™ laser-scanner using the

Cy2 channel for peptides modified with fluorescein or the Cy5 channel for peptides modified with AZ647. Following fluorescent imaging, gels were again washed 2x with H_2O and then placed into 50 mL of a modified Coomassie stain (Bio-Rad5000205). Following 3 h staining, gels were placed into 50 mL of H_2O for at least 3 h, regularly changing the water every 15 min, to reduce background staining and then imaged on a Li-Cor Odyssey CLx Imager.

6.6. Flow Cytometry Procedure

General: Flow cytometry procedures for this project were carried out by Eden Kapcan on a BD LSRII flow cytometer or by Sissi Yang where indicated. All monocytes used were U937 human myeloid leukaemia cell lines provided by John Valliant.

6.6.1. Monocyte Labelling at 37 ˚C

For labelling at 37 ˚C, monocytes were first placed a clear round bottom 96-well plate (150 000 cells/well) and IFNγ (0.1 mg/mL) activated according to established protocols.[21] Simultaneously, mCIR and mNCIR constructs modified with biotin were incubated with the cells for 24 h at concentrations ranging from 5 nM-80 nM. Following the incubation period, monocytes were spun down and washed x2 with warm PBS (0.2% BSA) and resuspending in PBS (0.2% BSA). The cell-m(N)CIR incubations then had 100 µL of 18.75 nM streptavidin-PE (ThermoFisher 12-4317-87) added to all wells and was incubated for 30 min at 37 ˚C (5% CO_2). Cells were then washed and spun down and resuspended in PBS (0.2% BSA) and run on a BD LSRII flow cytometer. Monocytes populations were gated using FSC, forward scatter, and SSC, side scatter, while streptavidin-PE binding was visualized using the PE channel on the flow cytometer. Results were then analyzed on FloJo.

6.6.2. Monocyte Labelling at 4 ˚C

24 h prior to incubating monocytes with m(N)CIR constructs, 6 million U937 monocytes were seeded at 500 000 cells/mL and activated with IFNγ (0.1 mg/mL) according to established procedures.[21] Following the activation period, peptide constructs were added at varying concentrations or times (as indicated) at 4 ˚C. Following the incubation period, cells were spun down and washed 2x, and resuspended in PBS (0.2% BSA) and run on flow cytometry. Cells and constructs were identified in the same way as outlined above and then analyzed on FloJo.

6.6.3. Streptavidin Bead ADCP

For phagocytosis of streptavidin beads induced by biotin m(N)CIRs, IFNγ primed U937 cells were first stained with DiD dye (final concentration 1.9 μM) for 30 min at 37 ˚C. 150 000 streptavidin fluorobrite Microspheres (polysciences) were added to conditions consisting of either 50 nM m(N)CIR. m(N)CIR constructs were incubated with the beads for 15 min. Then, 50 μL of 1.5×10^5 U937 were added to the bead-m(N)CIR solutions and incubated at 37 ˚C for 1 h. Following incubation, the plate was put on ice to prevent more phagocytosis prior to running on flow. Bead/cell populations were gated into four quadrants using the fluorobrite microspheres and DiD stained monocytes. This enabled the differentiation of beads (top left), from monocytes (bottom right). Successful ADCP was denoted as a double positive for the two dyes (top right).

The same process was repeated for ADCP assays using the 8 h incubation on ice. The only difference being the 8 h treatment wells were incubated on ice prior being moved to 37 ˚C for 1 h to induce ADCP.

7. References

(1) Sudhakar, A. History of Cancer, Ancient and Modern Treatment Methods. https://doi.org/10.4172/1948-5956.100000e2.

(2) Bray, F.; Laversanne, M.; Weiderpass, E.; Soerjomataram, I. The Ever-Increasing Importance of Cancer as a Leading Cause of Premature Death Worldwide. *Cancer* **2021**, *127* (16), 3029–3030. https://doi.org/10.1002/CNCR.33587.

(3) Kim, R.; Emi, M.; Tanabe, K. Cancer Immunoediting from Immune Surveillance to Immune Escape. *Immunology* **2007**, *121* (1), 1. https://doi.org/10.1111/J.1365-2567.2007.02587.X.

(4) Hegde, P. S.; Karanikas, V.; Evers, S. The Where, the When, and the How of Immune Monitoring for Cancer Immunotherapies in the Era of Checkpoint Inhibition. *Clin Cancer Res* **2016**, *22* (8). https://doi.org/10.1158/1078-0432.CCR-15-1507.

(5) Bruni, D.; Angell, H. K.; Galon, J. The Immune Contexture and Immunoscore in Cancer Prognosis and Therapeutic Efficacy. *Nat. Rev. Cancer 2020 2011* **2020**, *20* (11), 662–680. https://doi.org/10.1038/s41568-020-0285-7.

(6) Liu, Y. T.; Sun, Z. J. Turning Cold Tumors into Hot Tumors by Improving T-Cell Infiltration. *Theranostics* **2021**, *11* (11), 5365. https://doi.org/10.7150/THNO.58390.

(7) Akkın, S.; Varan, G.; Bilensoy, E. A Review on Cancer Immunotherapy and Applications of Nanotechnology to Chemoimmunotherapy of Different Cancers. *Molecules* **2021**, *26* (11). https://doi.org/10.3390/MOLECULES26113382.

(8) Abass, A. K.; Lichtman, A. H.; Pillai, S. *Cellular and Molecular Immunology,* 9th ed.; Elsevier: Philadelphia, 2018.

(9) Nimmerjahn, F.; Ravetch, J. V. Fcγ Receptors: Old Friends and New Family Members. *Immunity* **2006**, *24* (1), 19–28. https://doi.org/10.1016/j.immuni.2005.11.010.

(10) Li, T.; DiLillo, D. J.; Bournazos, S.; Giddens, J. P.; Ravetch, J. V.; Wang, L. X. Modulating IgG Effector Function by Fc Glycan Engineering. *Proc. Natl. Acad. Sci. U. S. A.* **2017**, *114* (13), 3485–3490. https://doi.org/10.1073/PNAS.1702173114/SUPPL_FILE/PNAS.201702173SI.PDF.

(11) Karlmark, K. R.; Tacke, F.; Dunay, I. R. Monocytes in Health and Disease – Minireview. *Eur. J. Microbiol. Immunol. (Bp).* **2012**, *2* (2), 97. https://doi.org/10.1556/EUJMI.2.2012.2.1.

(12) Richards, D. M.; Hettinger, J.; Feuerer, M. Monocytes and Macrophages in Cancer: Development and Functions. *Cancer Microenviron.* **2013**, 179–191. https://doi.org/10.1007/s12307-012-0123-x.

(13) Grugan, K. D.; McCabe, F. L.; Kinder, M.; Greenplate, A. R.; Harman, B. C.; Ekert, J. E.; van Rooijen, N.; Anderson, G. M.; Nemeth, J. A.; Strohl, W. R.; et al. Tumor-Associated Macrophages Promote Invasion While Retaining Fc-Dependent Anti-Tumor Function. *J. Immunol.* **2012**, *189* (11), 5457–5466. https://doi.org/10.4049/jimmunol.1201889.

(14) Esfahani, K.; Roudaia, L.; Buhlaiga, N.; Del Rincon, S. V.; Papneja, N.; Miller, W. H. A Review of Cancer Immunotherapy: From the Past, to the Present, to the Future. *Curr. Oncol.* **2020**, *27* (Suppl 2), S87. https://doi.org/10.3747/CO.27.5223.

(15) Lu, R. M.; Hwang, Y. C.; Liu, I. J.; Lee, C. C.; Tsai, H. Z.; Li, H. J.; Wu, H. C. Development of Therapeutic Antibodies for the Treatment of Diseases. *J. Biomed. Sci. 2020 271* **2020**, *27* (1), 1–30. https://doi.org/10.1186/S12929-019-0592-Z.

(16) Dekkers, G.; Bentlage, A. E. H.; Stegmann, T. C.; Howie, H. L.; Lissenberg-Thunnissen, S.; Zimring, J.; Rispens, T.; Vidarsson, G. MAbs Affinity of Human IgG Subclasses to Mouse Fc Gamma Receptors Affinity of Human IgG Subclasses to Mouse Fc Gamma Receptors. **2017**. https://doi.org/10.1080/19420862.2017.1323159.

(17) Chames, P.; Van Regenmortel, M.; Weiss, E.; Baty, D. Therapeutic Antibodies: Successes, Limitations and Hopes for the Future. *Br. J. Pharmacol.* **2009**, *157* (2), 220. https://doi.org/10.1111/J.1476-5381.2009.00190.X.

(18) Liu, X.; Zhang, B.; Wang, Y.; Haymour, H. S.; Zhang, F.; Xu, L. cun; Srinivasarao, M.; Low, P. S. A Universal Dual Mechanism Immunotherapy for the Treatment of Influenza Virus Infections. *Nat. Commun.* **2020**, *11* (1), 1–14. https://doi.org/10.1038/s41467-020-19386-5.

(19) Rullo, A. F.; Fitzgerald, K. J.; Muthusamy, V.; Liu, M.; Yuan, C.; Huang, M.; Kim, M.; Cho, A. E.; Spiegel, D. A. Re-Engineering the Immune Response to Metastatic Cancer: Antibody-Recruiting Small Molecules Targeting the Urokinase Receptor. *Angew. Chemie* **2016**, *128* (11), 3706–3710. https://doi.org/10.1002/ange.201510866.

(20) McEnaney, P. J.; Parker, C. G.; Zhang, A. X.; Spiegel, D. A. Antibody-Recruiting Molecules: An Emerging Paradigm for Engaging Immune Function in Treating Human Disease. *ACS Chem. Biol.* **2012**, *7* (7), 1139. https://doi.org/10.1021/CB300119G.

(21) Lake, B.; Serniuck, N.; Kapcan, E.; Wang, A.; Rullo, A. F. Covalent Immune Recruiters: Tools to Gain Chemical Control Over Immune Recognition. *ACS Chem Bio* **2020**. https://doi.org/10.1021/acschembio.0c00112.

(22) Kapcan, E.; Lake, B.; Yang, Z.; Zhang, A.; Miller, M. S.; Rullo, A. F. Covalent Stabilization of Antibody Recruitment Enhances Immune Recognition of Cancer Targets. **2021**. https://doi.org/10.1021/acs.biochem.1c00127.

(23) Douglass, E. F.; Miller, C. J.; Sparer, G.; Shapiro, H.; Spiegel, D. A. A Comprehensive Mathematical Model for Three-Body Binding Equilibria. *J. Am. Chem. Soc.* **2013**, *135* (16), 6092–6099. https://doi.org/10.1021/ja311795d.

(24) Fujishima, S.-H.; Yasui, R.; Miki, T.; Ojida, A.; Hamachi, I. Ligand-Directed Acyl Imidazole Chemistry for Labeling of Membrane-Bound Proteins on Live Cells. *J. Am. Chem. Soc* **2012**, *134*, 32. https://doi.org/10.1021/ja2108855.

(25) Mino, T.; Sakamoto, S.; Hamachi, I. Recent Applications of N-Acyl Imidazole Chemistry in Chemical Biology. *Biosci. Biotechnol. Biochem.* **2021**, *85* (1), 53–60. https://doi.org/10.1093/BBB/ZBAA026.

(26) Narayanan, A.; Jones, L. H. Sulfonyl Fluorides as Privileged Warheads in Chemical Biology. *Chemical Science*. Royal Society of Chemistry May 1, 2015, pp 2650–2659. https://doi.org/10.1039/c5sc00408j.

(27) Martín-Gago, P. D. P.; Olsen, P. D. C. A. Arylfluorosulfate-Based Electrophiles for Covalent Protein Labeling: A New Addition to the Arsenal. *Angew. Chem. Int. Ed. Engl.* **2019**, *58* (4), 957. https://doi.org/10.1002/ANIE.201806037.

(28) Dong, J.; Krasnova, L.; Finn, M. G.; Sharpless, K. B. Sulfur(VI) Fluoride Exchange (SuFEx): Another Good Reaction for Click Chemistry. *Angew. Chemie Int. Ed.* **2014**, *53* (36), 9430–9448. https://doi.org/10.1002/anie.201309399.

(29) Guo, T.; Meng, G.; Zhan, X.; Yang, Q.; Ma, T.; Xu, L.; Sharpless, K. B.; Dong, J. A New Portal to SuFEx Click Chemistry: A Stable Fluorosulfuryl Imidazolium Salt Emerging as an "F−SO_2+" Donor of Unprecedented Reactivity, Selectivity, and Scope. *Angew. Chemie* **2018**, *130* (10), 2635–2640. https://doi.org/10.1002/ange.201712429.

(30) Jones, L. H. Emerging Utility of Fluorosulfate Chemical Probes. *ACS Med. Chem. Lett.* **2018**, *9* (7), 584. https://doi.org/10.1021/ACSMEDCHEMLETT.8B00276.

(31) Luy, J. N.; Tonner, R. Complementary Base Lowers the Barrier in SuFEx Click Chemistry for Primary Amine Nucleophiles. *ACS Omega* **2020**, *5* (48), 31432–31439. https://doi.org/10.1021/ACSOMEGA.0C05049/SUPPL_FILE/AO0C05049_SI_001.PDF.

(32) Narayanan, A.; Jones, L. H. Sulfonyl Fluorides as Privileged Warheads in Chemical Biology. *Chem. Sci.* **2015**, *6* (5), 2650. https://doi.org/10.1039/C5SC00408J.

(33) Bonetto, S.; Spadola, L.; Buchanan, A. G.; Jermutus, L.; Lund, J. Identification of Cyclic Peptides Able to Mimic the Functional Epitope of IgG1-Fc for Human FcyRI. *FASEB J.* **2009**, *23* (2), 575–585. https://doi.org/10.1096/fj.08-117069.

(34) Mcenaney, P. J.; Fitzgerald, K. J.; Zhang, A. X.; Douglass, E. F.; Shan, W.; Balog, A.; Kolesnikova, M. D.; Spiegel, D. A. Chemically Synthesized Molecules with the Targeting and Effector Functions of Antibodies. **2014**. https://doi.org/10.1021/ja509513c.

(35) Montalbetti, C. A. G. N.; Falque, V. Amide Bond Formation and Peptide Coupling. *Tetrahedron* **2005**, *61* (46), 10827–10852. https://doi.org/10.1016/j.tet.2005.08.031.

(36) Manne, S. R.; Sharma, A.; Sazonovas, A.; El-Faham, A.; de la Torre, B. G.; Albericio, F. Understanding OxymaPure as a Peptide Coupling Additive: A Guide to New Oxyma Derivatives. *ACS Omega* **2022**, *7* (7), 6007–6023. https://doi.org/10.1021/ACSOMEGA.1C06342/ASSET/IMAGES/ACSOMEGA.1C06342.SOCIAL.JPEG_V03.

(37) Subirós-Funosas, R.; Prohens, R.; Barbas, R.; El-Faham, A.; Albericio, F. Oxyma: An Efficient Additive for Peptide Synthesis to Replace the Benzotriazole-Based HOBt and HOAt with a Lower Risk of Explosion[1]. *Chem. – A Eur. J.* **2009**, *15* (37), 9394–9403. https://doi.org/10.1002/CHEM.200900614.

(38) Radkiewicz, J. L.; Zipse, H.; Clarke, S.; Houk, K. N. Accelerated Racemization of Aspartic Acid and Asparagine Residues via Succinimide Intermediates: An Ab Initio Theoretical Exploration of Mechanism. *J. Am. Chem. Soc.* **1996**, *118* (38), 9148–9155. https://doi.org/10.1021/JA953505B.

(39) Subirós-Funosas, R.; El-Faham, A.; Albericio, F. Use of Oxyma as PH Modulatory Agent to Be Used in the Prevention of Base-Driven Side Reactions and Its Effect on 2-Chlorotrityl Chloride Resin. *Pept. Sci.* **2012**, *98* (2), 89–97. https://doi.org/10.1002/BIP.21713.

(40) Concepcion, J.; Witte, K.; Wartchow, C.; Choo, S.; Yao, D.; Persson, H.; Wei, J.; Li, P.; Heidecker, B.; Ma, W.; et al. Label-Free Detection of Biomolecular Interactions Using BioLayer Interferometry for Kinetic Characterization. *Comb. Chem. High Throughput*

Screen. **2009**, *12*, 791–800.

(41) Petersen, R. L. Strategies Using Bio-Layer Interferometry Biosensor Technology for Vaccine Research and Development. *Biosens. 2017, Vol. 7, Page 49* **2017**, *7* (4), 49. https://doi.org/10.3390/BIOS7040049.

(42) Mancardi, D. A.; Albanesi, M.; Jönsson, F.; Iannascoli, B.; Van Rooijen, N.; Kang, X.; England, P.; Daëron, M.; Bruhns, P. The High-Affinity Human IgG Receptor FcγRI (CD64) Promotes IgG-Mediated Inflammation, Anaphylaxis, and Antitumor Immunotherapy. *Blood* **2013**, *121* (9), 1563–1573. https://doi.org/10.1182/BLOOD-2012-07-442541.

(43) Temming, A. R.; Bentlage, A. E. H.; de Taeye, S. W.; Bosman, G. P.; Lissenberg-Thunnissen, S. N.; Derksen, N. I. L.; Brasser, G.; Mok, J. Y.; van Esch, W. J. E.; Howie, H. L.; et al. Cross-Reactivity of Mouse IgG Subclasses to Human Fc Gamma Receptors: Antibody Deglycosylation Only Eliminates IgG2b Binding. *Mol. Immunol.* **2020**, *127*, 79–86. https://doi.org/10.1016/J.MOLIMM.2020.08.015.

(44) Prabhu, N.; Sharp, K. Protein-Solvent Interactions. *Chem. Rev.* **2006**, *106* (5), 1616. https://doi.org/10.1021/CR040437F.

(45) Mukherjee, H.; Debreczeni, J.; Breed, J.; Tentarelli, S.; Aquila, B.; Dowling, J. E.; Whitty, A.; Grimster, N. P. A Study of the Reactivity of S(VI)–F Containing Warheads with Nucleophilic Amino-Acid Side Chains under Physiological Conditions. *Org. Biomol. Chem.* **2017**, *15* (45), 9685–9695. https://doi.org/10.1039/C7OB02028G.

(46) Yang, D.; Singh, A.; Wu, H.; Kroe-Barrett, R. Determination of High-Affinity Antibody-Antigen Binding Kinetics Using Four Biosensor Platforms. *JoVE (Journal Vis. Exp.* **2017**,

2017 (122), e55659. https://doi.org/10.3791/55659.

(47) Sultana, A.; Lee, J. E. Measuring Protein-Protein and Protein-Nucleic Acid Interactions by Biolayer Interferometry. *Curr. Protoc. Protein Sci* **2015**, *79*. https://doi.org/10.1002/0471140864.ps1925s79.

8. Appendix

Table 2. Summary of attempted cp33 variants and synthesis

Peptide	GD fragment	Enamine Y_{SuFEx} or 3 (sulfonyl fluoride) benzoic acid	Notes	Sequence
cp33	Y	NA	Successfully made	Ac-Kazido-V-N-S-C-L-L-L-P-N-L-L-G-C-D-G-D-CONH2
cp33 (SyAM)	N	NA	Successfully made. This peptide had the K_{azido} at the C-terminus	Ac-V-N-S-C-L-L-L-P-N-L-L-G-C-G-D-D-Kazido-CONH2
cp33 -Nt-Y	Y/N	NA	Successfully made – lower yields when made without GD fragment	Ac-Kazido-Y-V-N-S-C-L-L-L-P-N-L-L-G-C-D-G-D-CONH2
cp33 -Ct-Y	Y	NA	Successfully made	Ac-Kazido-V-N-S-C-L-L-L-P-N-L-L-G-C-D-G-D-Y-CONH2
cp33 -G13Y	Y	NA	Successfully made	Ac-Kazido-V-N-S-C-L-L-L-P-N-L-L-Y-C-D-G-D-CONH2
cp33 -G13Y SuFEx	Y	Attempted to install through imidazolium fluorosulfonate	Unable to install the SuFEx moiety – saw premature hydrolysis in solution.	Ac-Kazido-V-N-S-C-L-L-L-P-N-L-L-Y_{SuFEX}-C-D-G-D-CONH2
cp33 -Nt-Y_{SuFEx}	Y/N	Enamine Tyr	Successfully made – lower yields when made without GD fragment	Ac-Kazido-G-Y_{SuFEx}-V-N-S-C-L-L-L-P-N-L-L-G-C-D-G-D-CONH2

cp33 -Nt-Gly_7	Y	N/A	No azido lysine or acetylation of the n-terminal Glycine residue. Designed to be amide coupled to acid-containing fragments. Was never able to successfully synthesize.	NH2-G-G-G-G-G-G-G-V-N-S-C-L-L-L-P-N-L-L-G-C-D-G-D-CONH2
cp33 -Ct-Y_{SuFEx}	Y	Enamine Tyr	Poor solubility prior to purification, no yield post HPLC	Ac-Kazido-V-N-S-C-L-L-L-P-N-L-L-G-C-D-G-D-Y_{SUFEX}-CONH2
cp33 -GSG-Y_{SuFEx}	Y	Enamine Tyr	GSG was inserted into the peptide sequence before the Y_{SuFEx} residue. Unable to find target mass post synthesis.	Ac-Kazido-G-Y_{SUFEX}-G-S-G-V-N-S-C-L-L-L-P-N-L-L-G-C-D-G-D-CONH2
cp33 -Hexanoic Acid-Y_{SuFEx}	Y	Enamine Tyr	Hexanoic acid was coupled prior to the Y_{SuFEx} residue, but target mass was not found post synthesis. Repeated synthesis using high swelling resin but was unsuccessful.	Ac-Kazido-G-Y_{SUFEX}-Hexanoic Acid-V-N-S-C-L-L-L-P-N-L-L-G-C-D-G-D-CONH2
cp33 -ct K_{azido} Nt Y_{SuFEx}	Y	Enamine Tyr	Successfully made. This peptide had the K_{azido} at the C-terminus. Only tested for non-covalent behaviour – no difference from mCIR-1	Ac-Y_{SUFEX}-V-N-S-C-L-L-L-P-N-L-L-G-C-D-G-D-Kazido-CONH2
cp33 -Nt Y_{SuFEx}*	Y	Enamine Tyr	Made with cyst trt and in-solution cyclization – found peptide dimers and trimers	Ac-Kazido-G-Y_{SuFEx}-V-N-S-C-L-L-L-P-N-L-L-G-C-D-G-D-CONH2
cp33 Nt- Y_{SuFEx},R	Y	NA	Made with an arginine reside at the N-terminus. Unstable in solution – prone to rapid degradation	Ac-Kazido-R-G-Y_{SuFEx}-V-N-S-C-L-L-L-P-N-L-L-G-C-D-G-D-CONH2
cp33 Nt-benzoic sulfonyl fluoride	Y/N	Aryl SuFEx	Successfully made	SUFEX-Kazido- V-N-S-C-L-L-L-P-N-L-L-G-C-D-G-D-CONH2
cp33 S4Y	Y	NA	Successfully made – unstable in solution	Ac-Kazido-V-N-Y-C-L-L-L-P-N-L-L-G-C-D-G-D-CONH2
cp33 D15Y	N	NA	Could not find target mass post synthesis	Ac-Kazido-V-N-S-C-L-L-L-P-N-L-L-G-C-Y-G-D-CONH2
cp33 G Nt-Y_{SuFEx}	N	Enamine Tyr	Could not find target mass post synthesis	Ac-Kazido-G-Y_{SUFEX}-G-V-N-S-C-L-L-L-P-

				N-L-L-G-C-D-G-D-CONH2
cp33 L7YL8N	N	NA	Successfully made	Ac-Kazido-V-N-S-C-L-Y-N-P-N-L-L-G-C-D-G-D-CONH2
cp33 L7Y$_{SuFEx}$L8N	Y/N	Enamine Tyr	Successfully made	Ac-Kazido-V-N-S-C-L-Y$_{SUFEX}$-N-P-N-L-L-G-C-D-G-D-CONH2
cp33 L7YL8N Nt-Aryl SuFEx	Y/N	Aryl SuFEx	Poor solubility of crude pellet. Isolated mass post HPLC displayed aspartimide formation	SuFEx-Kazido-V-N-S-C-L-Y-N-P-N-L-L-G-C-D-G-D-CONH2

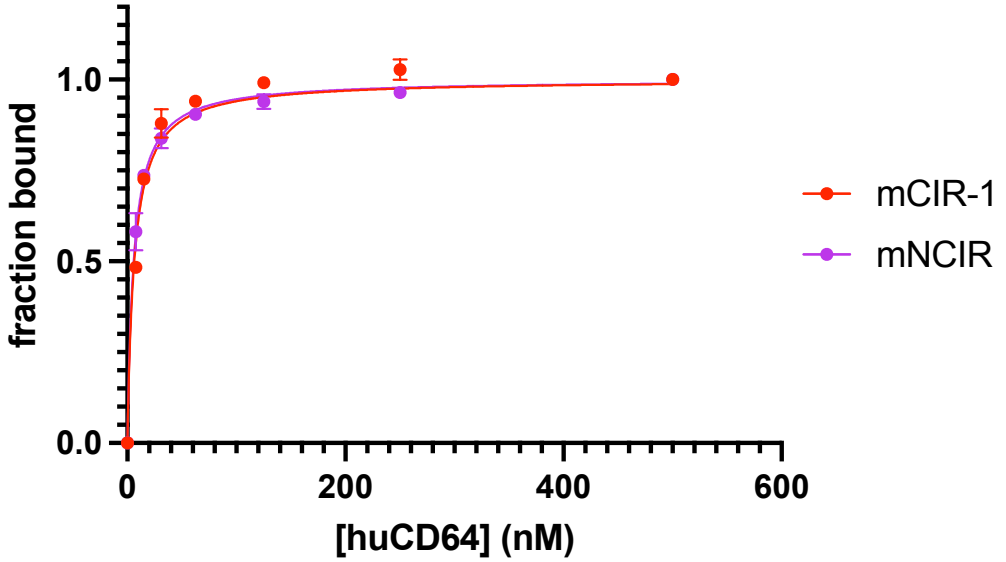

Figure 8.1. Saturated FP of mCIR-1 and mNCIR fluorescein 20 nM construct incubated with up to 500 nM huCD64.

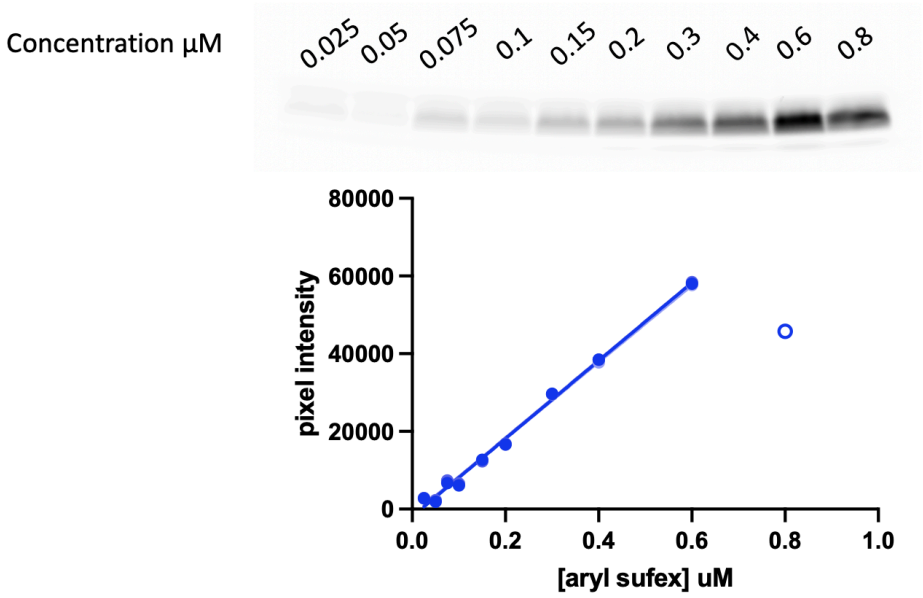

Figure 8.2. Aryl SuFex calibration curve
Empty circle was not included in the fit. This point is artificially low because the bands at the edge of the gel are subject to more diffusion than surrounding points.